NASA Technical Memorandum 86296

Aeroacoustic Data for High Reynolds Number Supersonic Axisymmetric Jets

John M. Seiner and Michael K. Ponton

JANUARY 1985

NASA

NASA Technical Memorandum 86296

Aeroacoustic Data for High Reynolds Number Supersonic Axisymmetric Jets

John M. Seiner
Langley Research Center
Hampton, Virginia

Michael K. Ponton
Kentron International, Inc.
Hampton, Virginia

National Aeronautics
and Space Administration

Scientific and Technical Information Branch

1985

SUMMARY

Both aerodynamic and near-field acoustic data are reported for an axisymmetric shock-free supersonic jet produced by a convergent-divergent nozzle designed for an exit Mach number of 2. Near-field acoustic data are also reported for two other shock-free supersonic jets produced by convergent-divergent nozzles with design exit Mach numbers of 1.5 and 2.5 and by a convergent nozzle operating at a Mach number of 0.9 and at two shock-containing underexpanded conditions. The purpose of this report is to provide a data base for which comparisons can be made to analytical prediction models. In general, the results indicate a close coupling between Strouhal components in the aerodynamic and acoustic fields; the spectrum peak value in the principal direction of acoustic radiation is observed in the aerodynamic field where this component has achieved maximum growth and the acoustic radiation appears to originate. Shock noise appears to originate from this same region but is directed more upstream.

INTRODUCTION

In this report, both aerodynamic and near-field acoustic data are presented for several shock-free axisymmetric supersonic jets whose Reynolds numbers based on nozzle exit diameter exceed 10^6. The motivation for documenting these results is to provide information that may prove useful to theoretical efforts that predict supersonic jet noise. Of particular interest are those analytical formulations (for example, refs. 1 to 4) that model the sound generation process by instability waves and require experimental data of the mean flow, axial growth and decay of any organized turbulent structure, and near-field acoustic properties for comparative purposes.

To enhance the overall comparison between this type of analysis and observation requires that both the aerodynamic and near-field acoustic data be acquired from the same nozzle. Surprisingly most prior research that has been reported on high Reynolds number supersonic jets present either aerodynamic or far-field acoustic data. Of the limited high Reynolds number near-field acoustic data, the results reported by Yu and Dosanjh (ref. 5) have provided a cornerstone for early comparisons to the developing instability analysis. More recently Seiner, McLaughlin, and Liu (ref. 6) reported both aerodynamic and near-field acoustic data for supersonic jets at various Reynolds numbers at a single nominal exit Mach number near 2. The near-field acoustic data gathered for the present study included several other high Reynolds number jets with exit Mach numbers ranging from 0.9 to 2.5. This report then presents acoustic results obtained from this study and provides a more comprehensive set of aerodynamic and acoustic data for the nozzle with an exhaust exit Mach number near 2 than is given in reference 6.

The data presented in this report were obtained on unheated static (no external flow) jets and are organized in the following fashion. The results for the mean flow are first presented for a nozzle designed for an exhaust Mach number of 2 at its fully expanded condition. Next the turbulence data obtained by using a wedge hot-film probe in the $M_d = 2$ jet plume are provided to demonstrate the universal velocity spectrum in the initial mixing region as well as the growth and decay of various spectral components in the shear layer that are integrally related to the jet noise spectrum peak value. The remainder of the report is used to show associated

near-field acoustic properties for this aerodynamic condition, as well as that obtained from the other nozzles. The acoustic near-field properties are presented in terms of narrow-band acoustic spectra, directivity for several spectral components, and contour plots of the same spectral components using one-third-octave filters.

One consistent overall feature evident from the contoured acoustic data and aerodynamic results is that the noise energy associated with the spectrum peak value in the principal direction of radiation emanates from a region slightly beyond the end of the potential core. This result for supersonic jets has previously been reported by Laufer, Schlinker and Kaplan (ref. 7) with a far-field directional mirror. Since all full-scale supersonic engines will most likely also contain a weak shock-wave field in their plume, several acoustic near-field contour plots have been included from the convergent nozzle when shocks were present in its plume. In this way, a more realistic presentation is achieved of what one is likely to see when operating a nozzle designed within the practical constraints of full-scale engine technology.

SYMBOLS

A	area
b	velocity half-width of annular mixing region, $r_{.5} - h$
c_o	ambient sound speed
D	nozzle exit diameter
$\tilde{e}, E_b$	fluctuating and mean anemometer voltages
f	frequency
h	radius of potential core
k_o	thermal conductivity of air at stagnation conditions
L	width of probe wedge element
L_s	length of supersonic section
m_o	constant equal to 0.765
M	Mach number
Nu_o	Nusselt modulus
P_a, P_o	ambient and stagnation supply pressures
$r, r_{.5}$	radial coordinate and radius to half-velocity point
R	radial coordinate
Re	Reynolds number based on nozzle exit diameter
R_j	nozzle exit radius

St Strouhal number, fD/U

S_u anemometer sensitivity to velocity

$\tilde{u}$,U axial turbulent and mean velocities

x axial coordinate

x_o axial location of reference microphone

y vertical distance from nozzle exit

α anemometer temperature resistance coefficient

γ ratio of specific heats taken equal to 1.4

η nondimensional radial coordinate (eq. (2))

θ angle to jet axis

τ anemometer temperature overheat ratio or time delay

Subscripts:

c centerline value

d nozzle design condition

e jet exit condition

j fully expanded condition

ℓ local region of flow measurement

o reference quantity

t throat condition of nozzle

∞ free-stream conditions

EXPERIMENTAL METHODOLOGY

The aerodynamic plume measurements shown in this paper were acquired in the Langley Jet-Noise Laboratory (LJNL). The near-field acoustic measurements were acquired in the Langley Anechoic Noise Facility (LANF), whose interior dimensions from wedge tip to wedge tip are 6.7 by 8.4 by 7.2 m. Both the LJNL and LANF utilized the same air supply and were capable of supplying a maximum continuous flow rate of 4.1 kg/s of unheated dry air. Desired nozzle pressure ratios were maintained to within 0.3 percent by electronically controlled valves.

Four nozzles were tested; the exit design and operational parameters under which the nozzles were tested are given in table I. The Reynolds number based on exit conditions exceeded 10^6 for all nozzles examined. As can be observed from table I, the convergent nozzle was examined at two underexpanded conditions. The

fully expanded plume Mach number M_j for these two shock-containing plumes were selected to match the design Mach numbers M_d of two supersonic convergent-divergent nozzles. The fully expanded plume Mach number M_j is calculated directly from the isentropic equation relating the nozzle stagnation-ambient pressure ratio to Mach number. The contraction section of the convergent nozzle was designed by a procedure based on the transonic flow solution of reference 8. The solution was optimized to produce the most uniform sonic surface at the nozzle exit consistent with the desire to achieve a thin throat boundary layer. The supersonic sections of the $M_d = 1.5$ and 2.0 nozzles were designed by using the method of characteristics solution of reference 9 to produce an exhaust flow which is parallel to the jet axis at the nozzle exit plane. The contraction section for these two supersonic nozzles was obtained from the transonic flow solution with a radius of curvature of the nozzle throat selected to match the predicted radius of curvature of the supersonic section. The design of the Mach 2.5 supersonic section is believed to be based on a method-of-characteristics solution; however, the design procedure used to derive its contraction section is unknown. Figure 1 shows the general geometry associated with both convergent and convergent-divergent nozzles.

Determination of local jet Mach number was accomplished by using the Rayleigh supersonic pitot-tube formula, which requires a measure of local static and total pressures. A schematic of the static-pressure probe is shown in figure 2. The total-pressure tube was of the standard supersonic type: a square-end tube with a concentric sensing port diameter one-third of the outside diameter of the tube. The static-pressure probe was designed to provide a rapid recovery to free-stream static pressure to minimize errors in interpreting the data in the presence of large pressure gradients. The static probe was designed by Pinckney (ref. 10). Both the total-pressure tube and the static-pressure probe were mounted in a low drag supersonic wing as shown in figure 3 to minimize undesirable probe vibration. A remotely controlled computerized three-axis digital traverse mechanism positioned the wing and its probe to desired locations in the jet plume. The spatial accuracy of the traverse was ±0.0254 mm.

The total temperature of the flow was always within ±2°C of ambient so that the local sound speed and, consequently, the mean axial velocity could be determined from the pitot-tube measurements and isentropic relations. The resulting mean velocity radial profiles presented in this report appear in the following nondimensional form:

$$U/U_c = \begin{cases} U(\eta) & (r > h) \\ 1 & (r \leq h) \end{cases} \tag{1}$$

where h is the radius of the potential core. The nondimensional coordinate η is given by

$$\eta = \frac{r - h}{b} \tag{2}$$

where b is the velocity half-width of the mixing layer. Designating $r_{.5}$ as the radial distance to where the axial velocity is one-half that of its centerline value, the velocity half-width can be expressed as

$$b = r_{.5} - h \tag{3}$$

The shape function customarily chosen to represent $U(\eta)$ is the half-Gaussian as given by

$$U/U_c = \exp[-(\ln 2)\eta^2] \tag{4}$$

which describes the axial mean profiles in the annular mixing region and beyond the end of the potential core for high Reynolds number jet plumes.

The supersonic turbulence data were obtained with a wedge hot-film probe. Its behavioral response has been found to differ from that of hot wires in the transonic and supersonic regimes. A profile view of the commercial wedge probe is shown in figure 4 which provides all relevant dimensions. A complete analysis of the operational characteristics of this probe has been recently published in reference 11. However, since only one temperature overheat was used to acquire the data, the approximate procedure used in reference 6 has been used to interpret the turbulence data. This procedure is based on the observation in reference 11 that measured bridge voltage fluctuations with high film probe temperature loadings and free-stream Mach numbers exceeding 1.3 will primarily vary with velocity fluctuations. The turbulence data presented in this report satisfy both conditions.

Using this approximate procedure, local longitudinal turbulence intensity is related to bridge voltage fluctuations by

$$\frac{\tilde{u}}{U_\ell} \approx \frac{1}{S_u}\frac{\tilde{e}}{E_b} \tag{5}$$

where the velocity sensitivity, as derived from the calibration data of figure 5 and reference 11, provides

$$S_u = 0.25[1 + m_o(\gamma - 1)M^2]\left(1 - \frac{B}{Nu_o}\right) \tag{6}$$

In equation (6), the data intercept B from figure 5 gives $B = 15.3$, and the Nusselt modulus Nu_o is computed from bridge voltage measurements through the relation

$$Nu_o = \frac{\alpha E_b^2}{2k_o L}\frac{\tau + 1}{\tau}\frac{R_r}{[R_r(\tau + 1) + R_L + 50]^2} \tag{7}$$

where R_r is probe recovery resistance and R_L is probe lead resistance. Figure 6 shows the wedge hot-film probe mounted in its low drag supersonic wing. The probe

was positioned by the same three-axis traverse mechanism as used in the pitot surveys.

Near-field acoustic measurements were acquired by using a single microphone with a polar traverse mechanism and a nine-microphone linear array. The polar traverse used a 0.25-in. free-field microphone, whereas the linear array elements were composed of 0.25-in. pressure microphones. The polar traverse mechanism, shown in figure 7, had a range of travel from $R/D = 5$ to 40 with angles to the jet axis ranging from 15° to 90°. The positional accuracy of the polar traverse was determined to be ±0.01R/D and ±0.5°. All nozzles were tested by using the polar traverse, each run being composed of 108 spatial locations. The linear microphone array, shown in figure 8, was previously used in reference 12 to examine near-field acoustic properties associated with shock-containing jet plumes. The measurements of shock-free jet plumes associated with the $M_d = 2$ supersonic nozzle with this array are reported at this time. The linear array was located along a line parallel to the jet axis at a distance of $R/D = 2.3$ for the $M_d = 2$ nozzle. The locations for the microphones are listed in table II. These results are presented in terms of the cross-correlation coefficient between microphone pairs.

The near-field acoustic data were recorded on magnetic tape with a frequency response from dc to 80 kHz. The data were later analyzed in one-third-octave and 20-Hz narrow bands. The format chosen for data presentation was narrow-band spectra, directivity, and near-field contours of one-third-octave-band data, and nonfiltered cross-correlation coefficient of microphone pairs. The center frequencies chosen for presentation were based on integral values associated with the far-field spectrum peak value at 30° to the jet axis relative to each nozzle examined. The center frequencies are given in terms of the Strouhal number $St = fD/U_j$. All nozzles were treated with fiberglass during the acoustic studies to minimize sound reflections from the exterior wall of each nozzle.

AERODYNAMIC RESULTS

Mean Flow

The centerline Mach number and velocity variation for the perfectly expanded $M_d = 2$ nozzle is shown in figure 9. The data field consists of 703 data points, which is sufficient to show that, with even the most ideal experimental conditions, the plume is composed of a weak wave system. The measured exit Mach number at $x/R_j = 0$ is 1.99. Downstream of the annular mixing region, the centerline flow follows, as expected, a decay rate proportional to x^{-1}. (See fig. 9(c).)

The measured axial variation of the parameters $r_{.5}$ and b, associated with the plume-spread rate, are shown in figure 10. These parameters appear in equations (2) and (3), and are used in equation (4) to demonstrate that the mean flow can be described by a half-Gaussian shape. This is shown in figure 11, which involves the use of 27 measured radial profiles whose axial stations range from $x/R_j = 0.98$ to 66.76, as indicated in figure 10. It is apparent from these data that the measured mean velocity profiles are well represented by the half-Gaussian shape. The results in figures 9, 10, and 11 completely specify the mean axial flow state of the $M_d = 2$ nozzle when operated at its design Mach number.

Turbulent Flow

The mean flow results clearly demonstrate that the jet plume spreads linearly in the annular mixing region. To establish the operational frequency response of the anemometer in supersonic flow, this property can be put to use. Longitudinal turbulent velocity spectra are shown in figure 12(a) that correspond to measurements obtained at various axial stations in the annular mixing region and along the jet lipline $R/R_j = 1$. These spectra are presented in terms of Strouhal number St based on nozzle exit conditions. The spectral amplitudes are normalized on an absolute basis by the jet exit velocity. Because of the linear-spread rate, one anticipates the existence of a universal turbulent velocity spectrum for the annular mixing region. As previously reported in reference 6, figure 12(b) shows that this is indeed true. The universal spectrum in figure 12(b) is composed of all the data used in figure 12(a) and is presented on the basis of a local Strouhal number $St = fx/U_\ell$, where U_ℓ is the local mean flow velocity and x is the axial location in the annular mixing region. The spectral amplitudes are appropriately normalized to properly account for spectral band compression due to the use of the local Strouhal number. It is evident from figure 12 that the frequency response of the hot-film probe is entirely adequate for this aerodynamic condition. A better collapse to a universal spectral shape could have, of course, been achieved if the measurements were taken along the $r_{.5}$ line of figure 10 or any η = Constant line rather than along the jet lipline ($R/R_j = 1$).

Of importance to an instability wave analysis is the axial growth and decay of any organized structure in a supersonic jet plume. The axial variation of both voltage and turbulent velocity fluctuations along the jet lipline are shown in figure 13. The turbulent velocity fluctuations $\tilde{u}$ have been decomposed from voltage fluctuations $\tilde{e}$ according to equation (5). The data of figure 13 have been further decomposed into select spectral bands that are shown later to match those found in the acoustic field. A narrow-band filter width of 20 Hz was used to obtain the spectral components in figure 13, and the data are normalized at $x/D = 2$ (as represented by U_o) since greater confidence is placed on this location than at $x/D = 0.5$ due to the thin initial annular mixing layer.

The data presented in figure 13, although showing the growth and decay of selected Strouhal number components, do not represent distributions that can be associated directly with organized structure. These hot-film spectral component data were acquired without using a conditional sampling method, a necessary requirement for uncovering any wavelike structure. Nevertheless the data of figure 13 do show that higher frequency components reach their maximum growth nearer the nozzle exit than do lower frequency components and that they typically achieve a smaller growth. The selection of the various Strouhal numbers in figure 13 is apparent in the next section after examining narrow-band acoustic spectra. The Strouhal number component $St = 0.158$ represents the spectrum peak value for acoustic radiation in the principal direction. This component achieves a maximum growth near $x/D = 12$, which from the mean aerodynamic results of figure 10 is just beyond the axial region where the potential core terminates (i.e., $x/R_j \approx 22$). The importance of this behavior becomes more clear as acoustic results are presented.

ACOUSTIC RESULTS

Narrow-Band Spectra

Narrow-band acoustic spectra are used in this report to identify the Strouhal number of the spectrum peak value for acoustic radiation in the principal direction and at 90° to the jet axis. The narrow-band spectra for the six nozzle operating conditions of table I are shown in figure 14. They are presented on a linear scale to enhance location of the spectrum peak value. The data at $R/D = 40$ were acquired by using a constant 20-Hz band. Since jet noise is generated on a distributed basis in the jet plume, the spectra are presented by using results obtained at $R/D = 40$ with the polar traverse and at a larger value of R/D. The larger value of R/D is obtained from a far-field microphone array similar to what is described in reference 6, and its data were analyzed by using a constant 40-Hz band. The angle selected for the larger R/D value represents the direction for maximum sound energy radiation, and because of the distributive nature of jet noise, the angle for the smaller R/D value is chosen slightly different to account for this feature and align the spectrum peak values. For acoustic radiation in the principal direction this change in angle can be readily calculated by assuming that peak acoustic energy emanates from the region slightly beyond the end of the potential core of the plume. The Strouhal numbers (fD/U_j) associated with the spectrum peak value in the principal radiation direction are listed in table I. From figure 14, shock-associated noise is clearly manifested for the two underexpanded cases involving the convergent nozzle. No screech suppression device was used while acquiring these data, but the nozzles were always treated with sound absorbent material. The 90° data for the $M_d = 1.5$ nozzle also exhibits shock noise in its spectrum. While this nozzle was designed to produce an exhaust Mach number of 1.5 at its exit plane, subsequent plume aerodynamic measurements revealed that the exhaust Mach number was closer to 1.46. Figure 14 also shows for each nozzle the measured or inferred (table I) exit Mach number M_e and the Mach number M_j that corresponds to the actual test nozzle pressure ratio.

Directivity

Directivity plots are used to display the peak radiation direction. Figures 15, 16, and 17 provide those results obtained at $R/D = 40$ for each nozzle pressure ratio listed in table I. The results are presented in terms of one-third-octave-band levels centered around various frequencies that are distributed about the spectrum peak value obtained from the narrow-band data in the principal radiation direction. The directivity of the overall sound pressure level is also included. Figure 15 shows the overall level and Strouhal number associated with the peak spectrum value, figure 16 shows Strouhal number components lower than the peak value, and figure 17 shows Strouhal number values larger than the peak value.

Select directivity comparisons between the convergent nozzle with an underexpanded jet plume and two essentially shock-free jet plumes are shown in figures 18 and 19. Figure 18 shows comparisons with respect to the $M_d = 1.5$ convergent-divergent nozzle, whereas figure 19 shows similar comparisons with the $M_d = 2$ convergent-divergent nozzle. The one-third-octave-band data refer to Strouhal number components that are clearly identified with shock noise. These directivity plots clearly identify the Doppler shift associated with convective disturbances through shock waves, and it is to be noted that the data in figure 18 refer to two nozzles operating at the same ideal thrust. The throat diameters of these two nozzles are very close so that the amplitude levels indicate the increase in noise associated with a shock-containing jet plume. A similar comparison between the directivity data for the

convergent and $M_d = 2$ nozzles in figure 19 cannot be made because the ideal thrust of the convergent nozzle is much less than that of the $M_d = 2$ nozzle at this test pressure ratio and strong shocks (Mach disk) in the convergent nozzle plume at this pressure ratio lead to shock strength reductions in downstream shocks and consequently in shock noise emission. Far-field directivities of the overall sound pressure level and the 40-Hz narrow-band level centered around the spectrum peak in the principal direction of radiation for each of the six nozzles studied are shown in figure 20. These data are included to show a more correct view of the directional nature of the associated acoustic field. The data also include angles of the jet inlet arc.

Near-Field Contours

Acoustic near-field contours are shown in figures 21 through 26. The acoustic pressure contour levels are expressed in dB (re 0.00002 Pa) with 2-dB-contour-level increments. These were established by using the 108 points per case from the polar traverse mechanism. The values of Strouhal number correspond to those used in the directivity plots and the aerodynamic data. They are obtained from the one-third-octave-band anaysis. Figures 21, 22, and 23 refer to the convergent nozzle at a high subsonic Mach number and the two underexpanded cases listed in table I. The shock-containing conditions clearly exhibit the presence of both jet and shock noise. Each component originates from near the end of the potential core but with different directional behavior. The peak spectrum value of the jet noise component is directed downstream with a lower Strouhal number than shock noise which appears directed more upstream. The acoustic near-field contours for the convergent-divergent supersonic nozzles appear in figures 24, 25, and 26. In each figure, the component of the spectrum peak value in the principal radiation direction appears to emanate from a region just beyond the end of the potential core. Even though each convergent-divergent nozzle was operated near its design point, shock noise, not necessarily evident in narrow-band spectral data, can be visualized in the outer radial regions near 90° to the jet axis.

Near-Field Microphone Correlations

Near-field covariance results obtained from the linear microphone array shown in figure 8 are presented in figure 27 and are for unfiltered data. Each figure shows the measured cross-correlation coefficient between a reference microphone in ascending order and all other microphones in the array. The time axis is normalized by the distance between the reference microphone at x_o and the variable microphone at x with sign being preserved and by ambient sound speed. Thus, a value of unity would indicate that the pressure wave is traveling parallel to the linear array at sonic speed. To aid in interpretation of these results a microphone covariance between the reference and a downstream microphone appears positive with pressure waves traveling in the downstream direction. For this same type of microphone covariance, a negative peak indicates that the pressure waves are traveling in the upstream direction. The opposite is of course true for covariance between the reference and upstream microphones.

The data of figure 27 indicate that noise is convected upstream past the first several microphones, and pressure waves from the hydrodynamic field are convected downstream supersonically. The demarcation between upstream sound and downstream pressure waves appears to occur in the vicinity of microphone 3 at $x/D = 2.60$, where both phenomena are present. The covariance amplitude of the correlations increases

with downstream location, indicating at least an increase in pressure field wavelength, which is consistent with the aerodynamic results of figure 13.

CONCLUSIONS

Both aerodynamic and near-field acoustic data are reported for a convergent-divergent nozzle designed to provide an exit Mach number of 2 and a shock-free plume when operated on design. The results show a close coupling between aerodynamic characteristics and those obtained in the near acoustic field. In general it can be stated that, when considering the Strouhal number component of the spectrum peak value, noise emanates from a region slightly beyond the end of the annular mixing region where the same Strouhal number of the flow exhibits maximum growth before decay.

The report also documents the near-field acoustics for two other convergent-divergent nozzles designed to provide exit Mach numbers of 1.5 and 2.5 when operated on design, as well as that of a convergent nozzle operated subsonically and at two underexpanded conditions. The behavior observed in the near acoustic field for these nozzles is consistent with that observed for the nozzle designed for an exit Mach number of 2. The shock-containing plume acoustic contour plots also reveal that the principal component for shock noise originates near the same region as found for jet noise but radiates with a larger angle to the jet axis than does the jet noise component.

Langley Research Center
National Aeronautics and Space Administration
Hampton, VA 23665
October 25, 1984

REFERENCES

1. Tam, Christopher K. W.; and Burton, Dale E.: Sound Generated by Instability Waves of Supersonic Flows. Part 2. Axisymmetric Jets. J. Fluid Mech., vol. 138, Jan. 1984, pp. 273-295.

2. Tam, Christopher K. W.; and Morris, Philip J.: The Radiation of Sound by the Instability Waves of a Compressible Plane Turbulent Shear Layer. J. Fluid Mech., vol. 98, pt. 2, May 29, 1980, pp. 349-381.

3. Chan, Y. Y.: Spatial Waves of Higher Order Modes in an Axisymmetric Turbulent Jet. Phys. Fluids, vol. 19, no. 12, Dec. 1976, pp. 2042-2043.

4. Liu, J. T. C.: Developing Large-Scale Wavelike Eddies and the Near Jet Noise Field. J. Fluid Mech., vol. 62, pt. 3, Feb. 11, 1974, pp. 437-464.

5. Yu, James C.; and Dosanjh, Darshan S.: Noise Field of Supersonic Mach 1.5 Cold Model Jet. J. Acoust. Soc. America, vol. 51, no. 5, pt. 1, May 1972, pp. 1400-1410.

6. Seiner, John M.; McLaughlin, Dennis K.; and Liu, C. H.: Supersonic Jet Noise Generated by Large-Scale Instabilities. NASA TP-2072, 1982.

7. Laufer, J.; Schlinker, R.; and Kaplan, R. E.: Experiments on Supersonic Jet Noise. AIAA J., vol. 14, no. 4, Apr. 1976, pp. 489-497.

8. Hopkins, D. F.; and Hill, D. E.: Effect of Small Radius of Curvature on Transonic Flow in Axisymmetric Nozzles. AIAA J., vol. 4, no. 8, Aug. 1966, pp. 1337-1343.

9. Johnson, Charles B.; and Boney, Lillian R.: A Method for Calculating a Real-Gas Two-Dimensional Nozzle Contour Including the Effects of Gamma. NASA TM X-3243, 1975.

10. Pinckney, S. Z.: A Short Static-Pressure Probe Design for Supersonic Flow. NASA TN D-7978, 1975.

11. Seiner, John M.: The Wedge Hot-Film Anemometer in Supersonic Flow. NASA TP-2134, 1983.

12. Seiner, John M.; and Yu, James C.: Acoustic Near-Field Properties Associated With Broadband Shock Noise. AIAA J., vol. 22, no. 9, Sept. 1984, pp. 1207-1215.

Table I.- PARAMETER RANGE

Nozzle	$D_{t'}$ cm	$D_{e'}$ cm	A_e/A_t	$(p_o/p_a)_d$	M_d	$(p_o/p_a)_{test}$	M_e	$U_{e'}$ m/s	M_j	Re	St_{peak}	U_j/c_o
1	3.962	3.962	1.000	1.893	1.0	1.893	0.90	285	0.9	1.02×10^6	0.174	0.84
*1	3.962	3.962	1.000	1.893	1.0	3.671	†1.00	312	1.5	2.04	.149	1.24
*1	3.962	3.962	1.000	1.893	1.0	7.825	†1.00	312	2.0	6.80	.098	1.49
2	3.935	4.267	1.176	3.671	1.5	3.671	1.46	425	1.5	2.49	.161	1.24
3	3.840	4.989	1.688	7.825	2.0	7.704	1.99	509	2.0	5.19	.158	1.49
4	3.128	5.080	2.637	17.085	2.5	17.085	2.50	569	2.5	8.84	.113	1.67

*Underexpanded plume conditions.
†Inferred exit exhaust Mach number.

TABLE II.- LINEAR MICROPHONE ARRAY POSITIONS

[R/D = 2.3]

Microphone	x/D
1	0.00
2	1.30
3	2.60
4	4.10
5	5.60
6	6.92
7	8.25
8	9.51
9	10.76

CONVERGENT NOZZLE

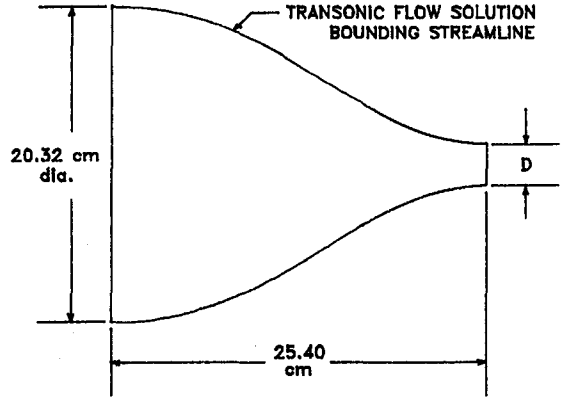

CONVERGENT–DIVERGENT NOZZLE

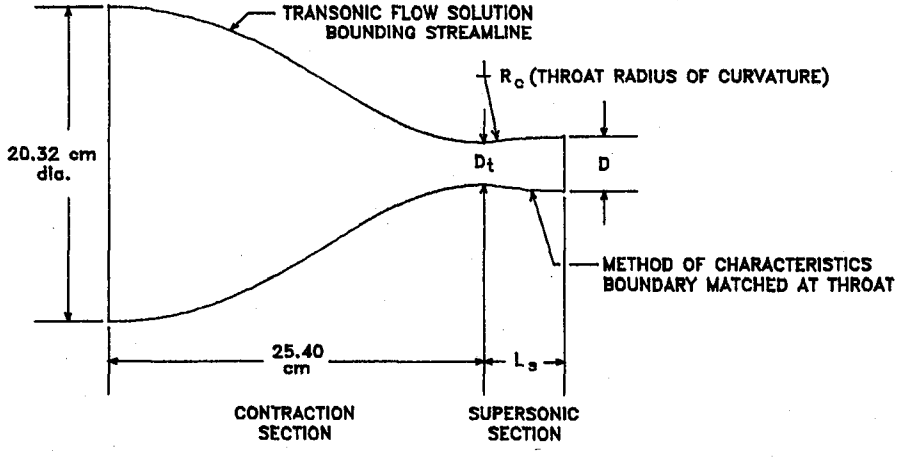

Figure 1.- General geometry for nozzles used in this study.

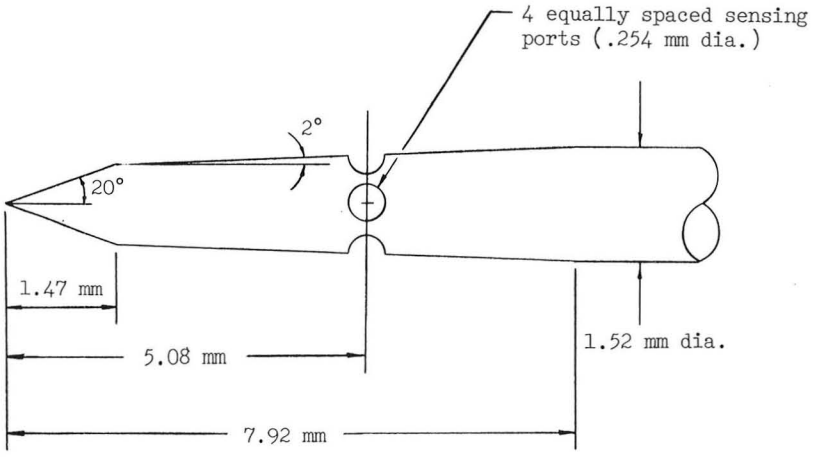

Figure 2.- Schematic presentation of static-pressure probe.

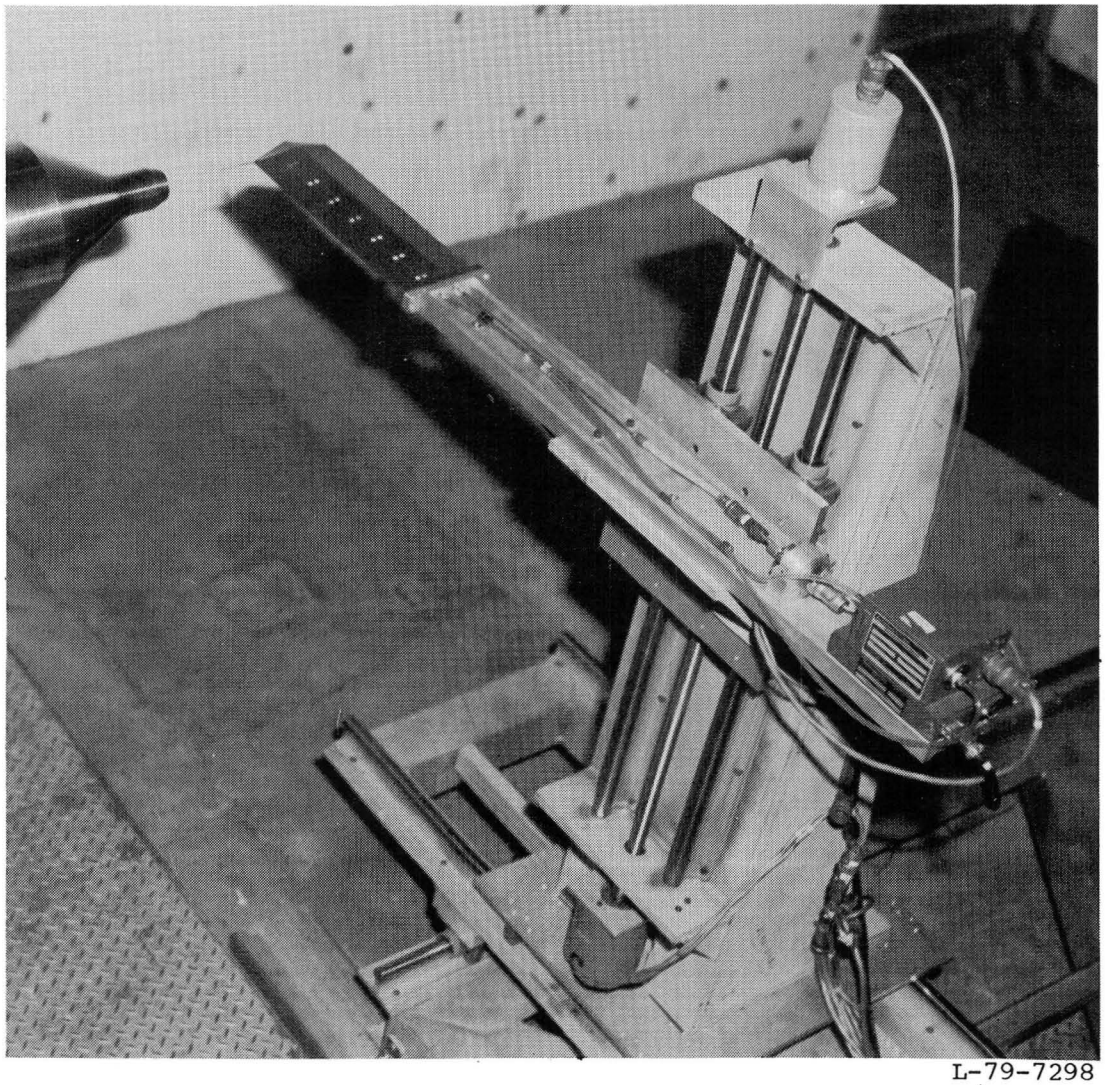

L-79-7298

Figure 3.- Nozzle and pressure drive mechanism in LJNL.

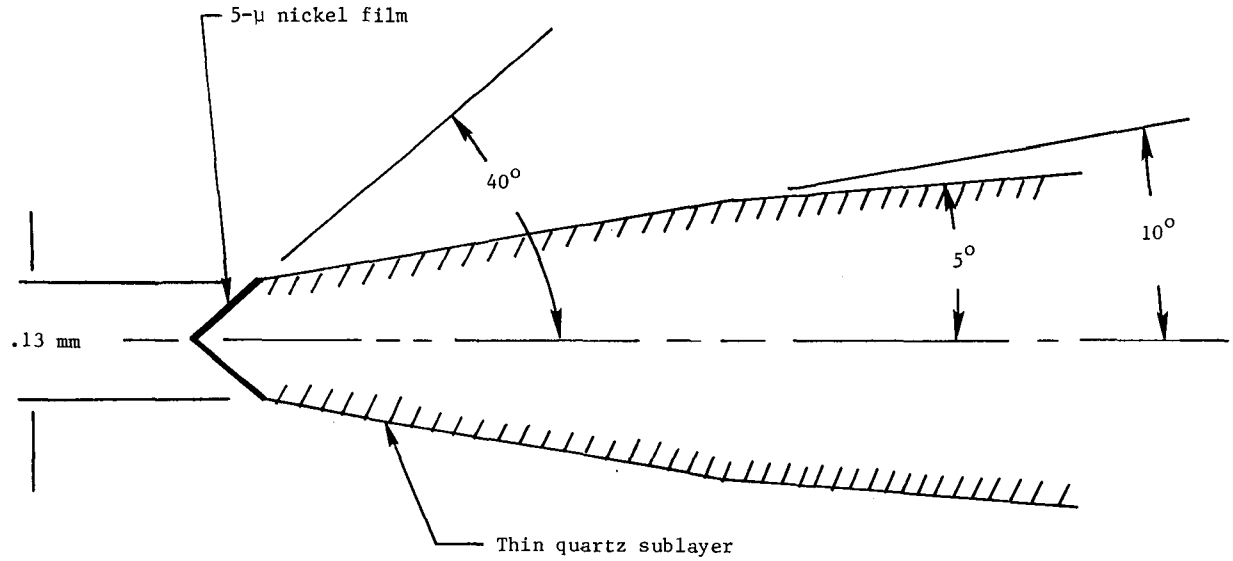

Figure 4.- Profile view of nickel-plated wedge hot-film probe.

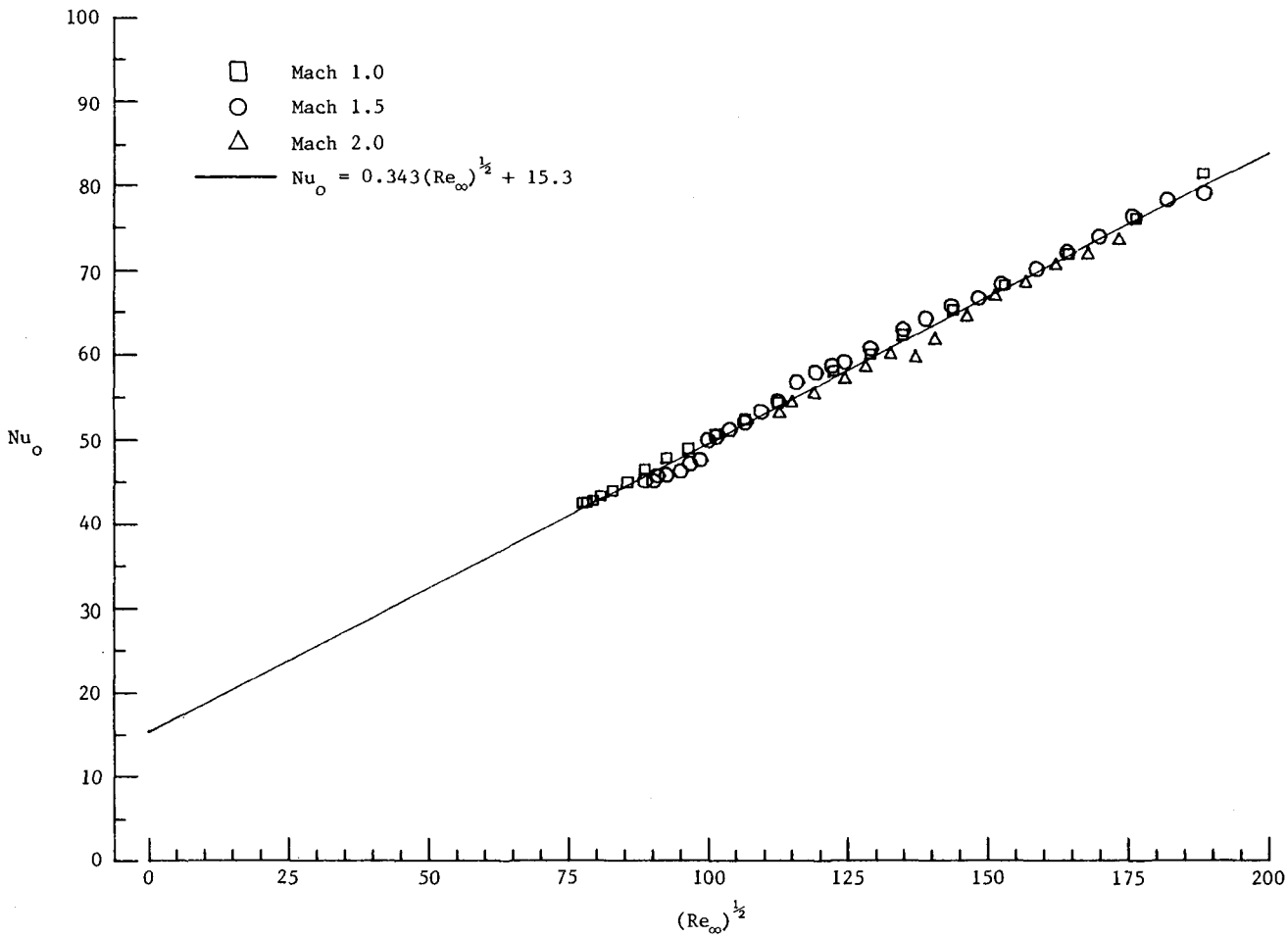

Figure 5.- Wedge hot-film calibration data.

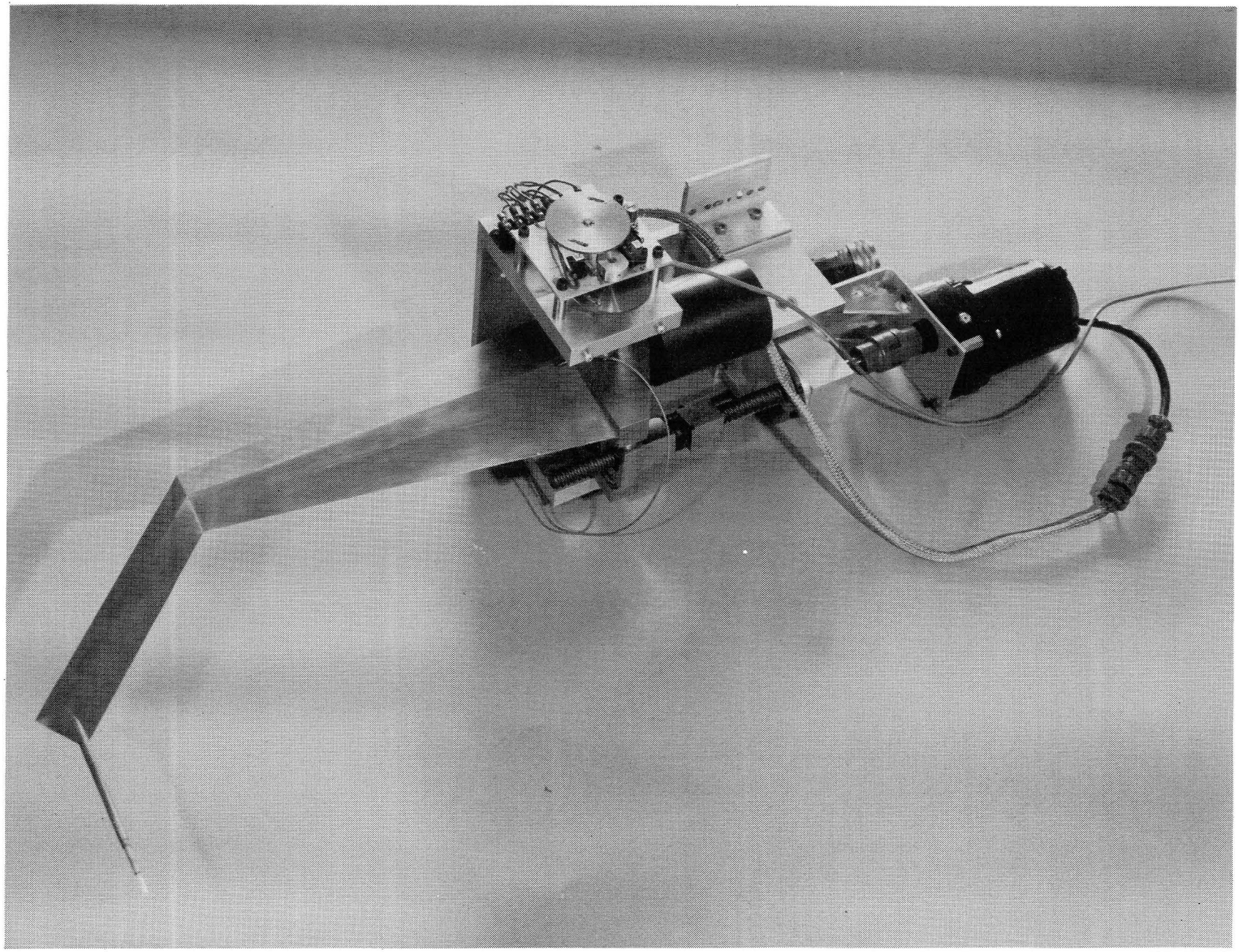

L-79-7299

Figure 6.- Hot-film supersonic wing with probe.

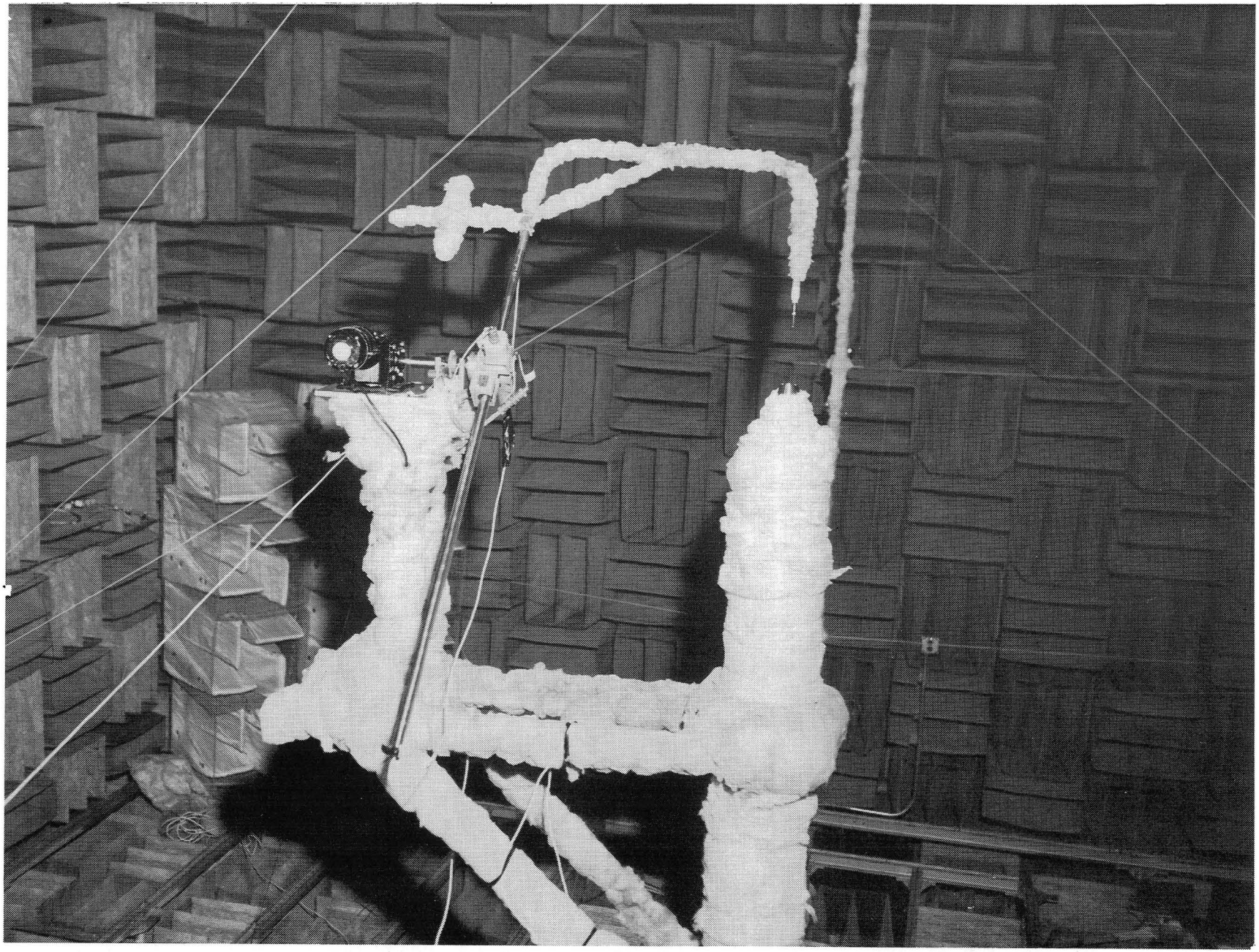

L-78-8599

Figure 7.- Near-field polar traverse mechanism.

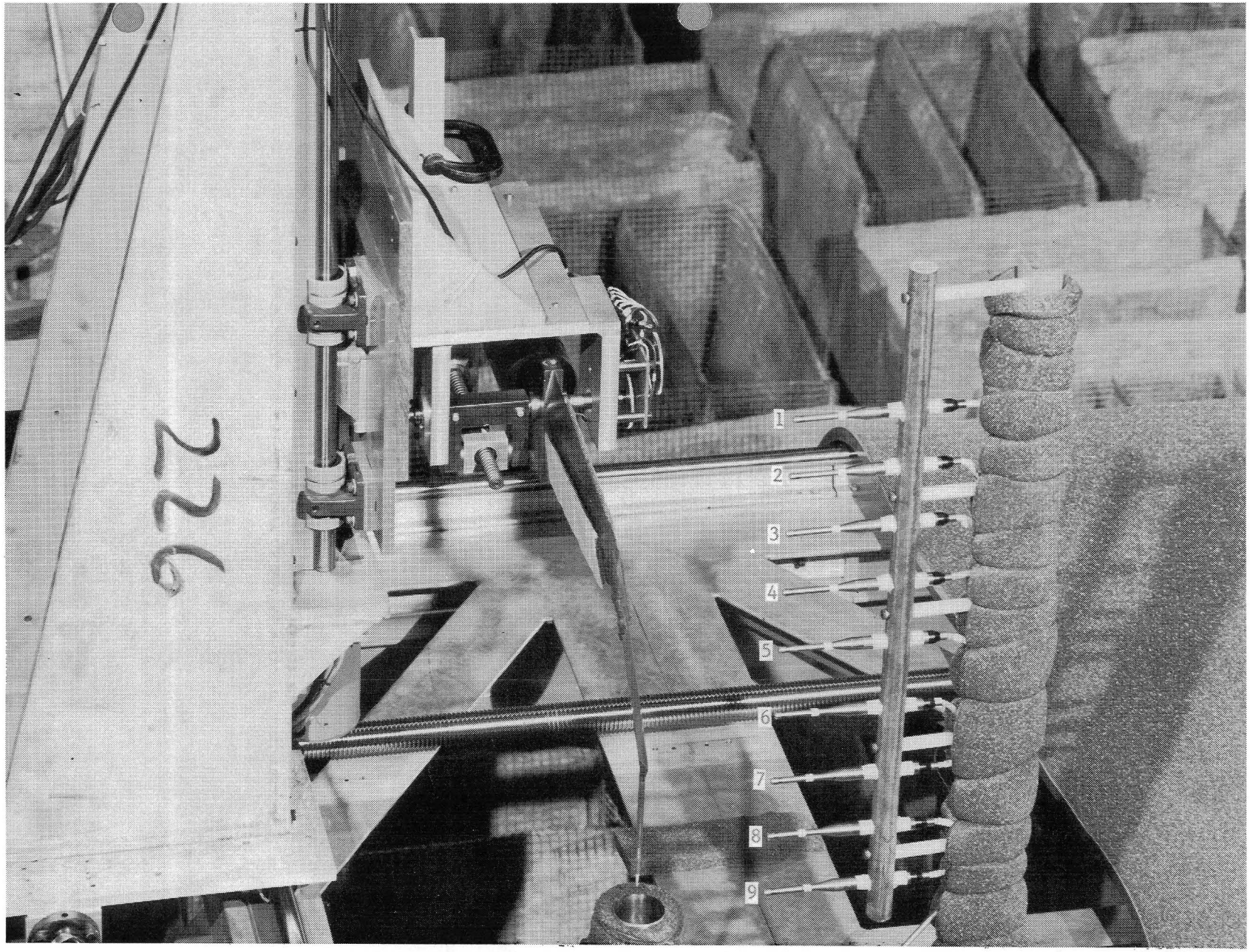

L-80-7306

Figure 8.- Near-field linear microphone array.

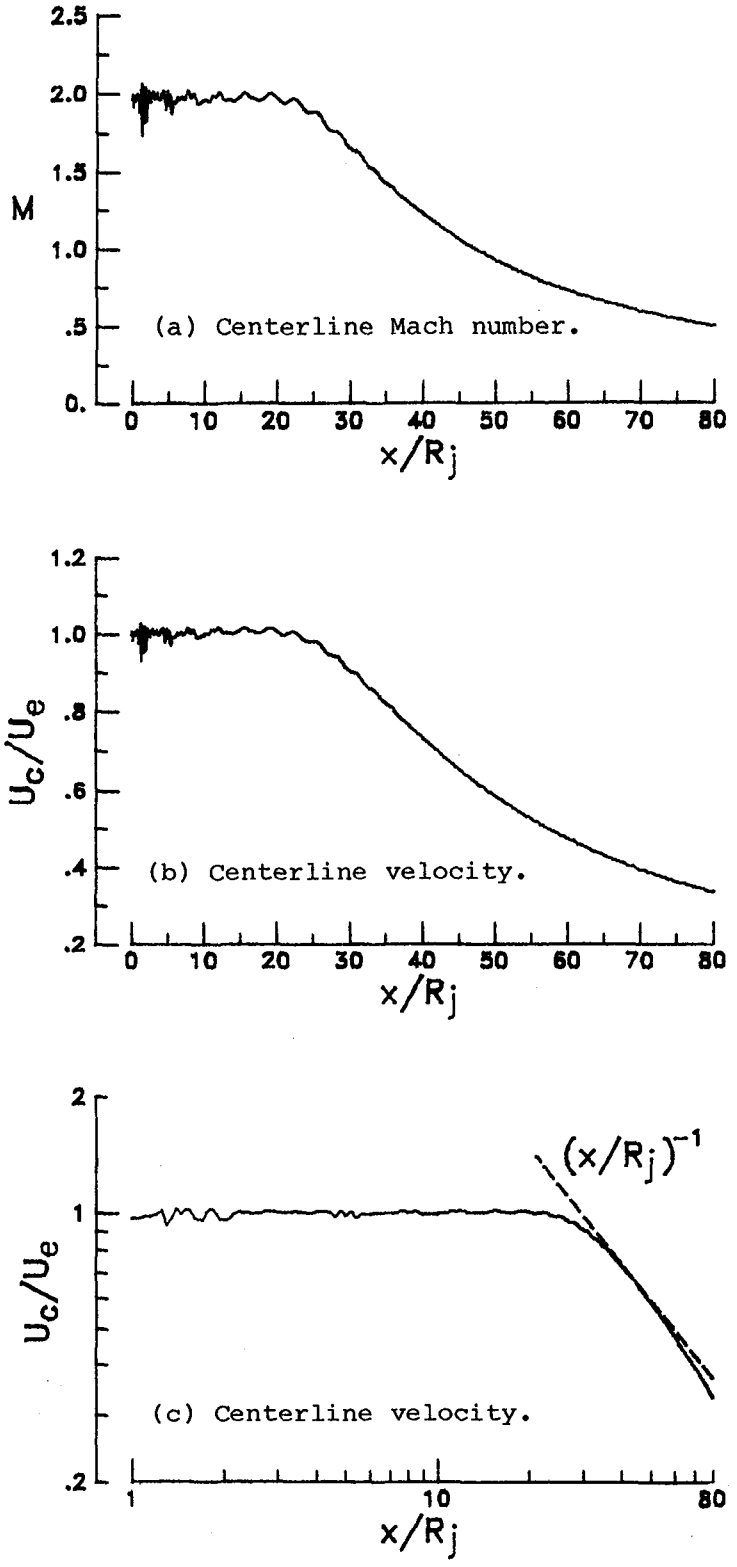

Figure 9.- Decay of centerline mean Mach number and velocity of $M_d = 2$ nozzle.

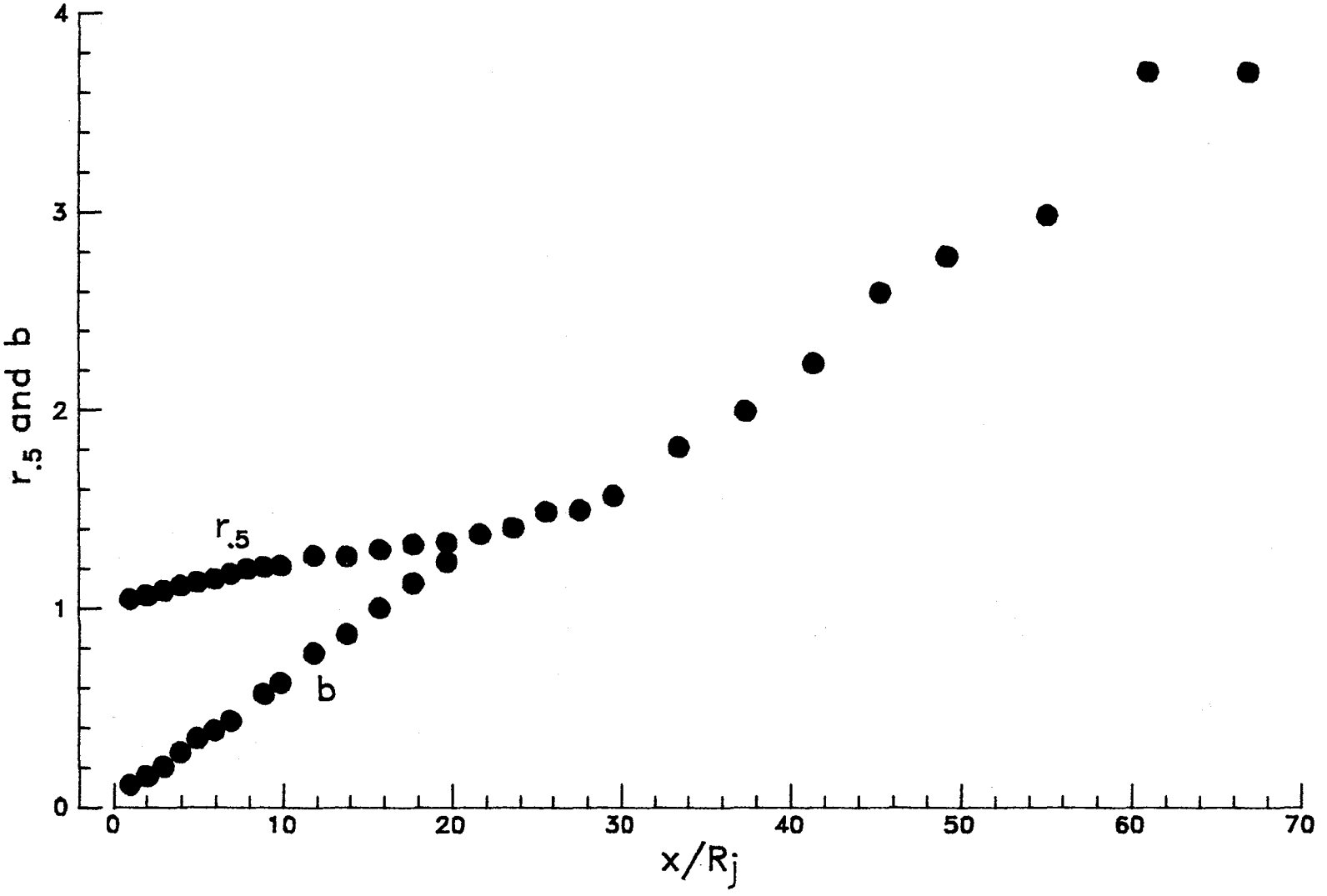

Figure 10.- Axial distribution of mean velocity profile parameters $r_{.5}$ and b.

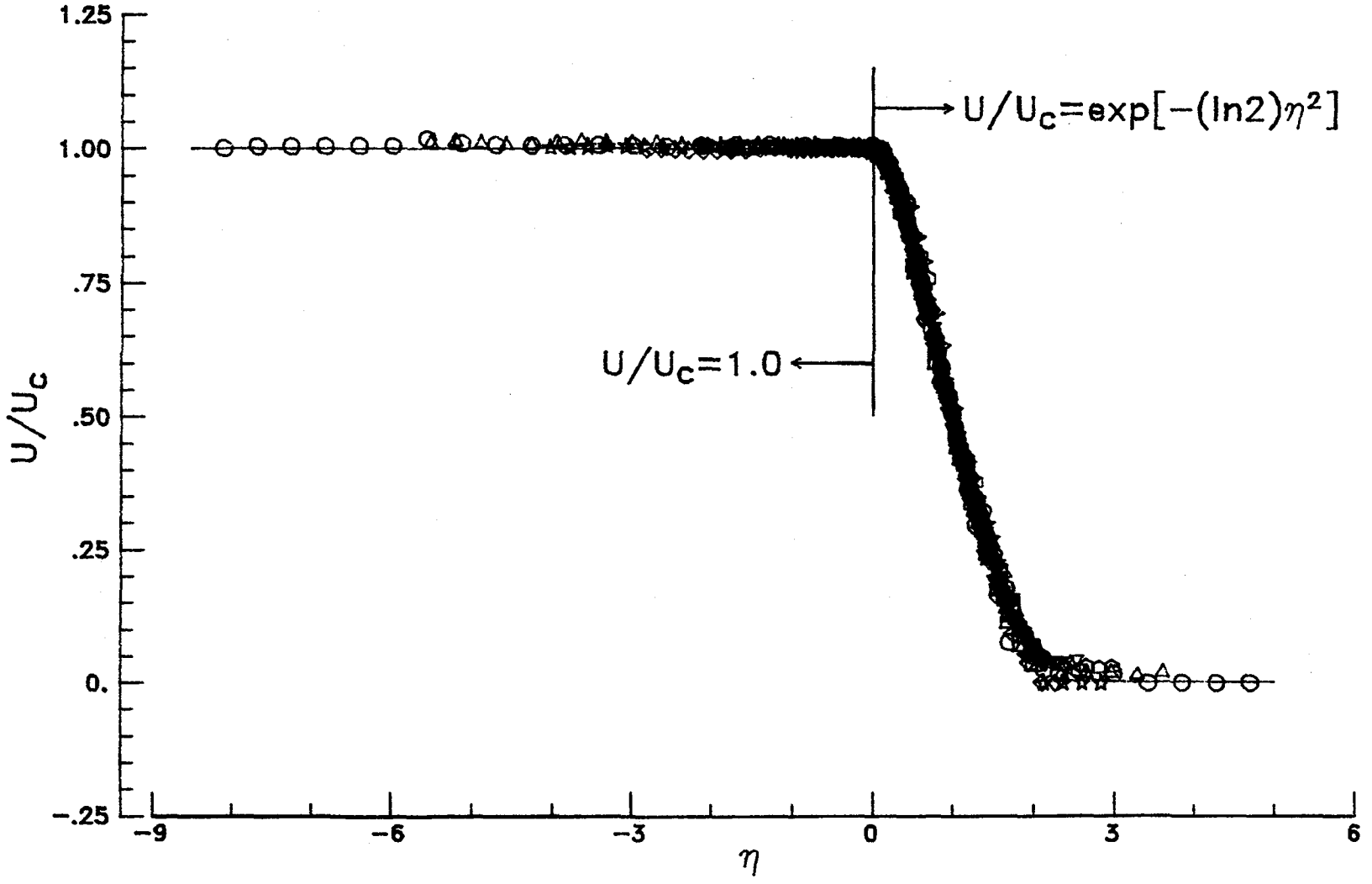

Figure 11.- Mean velocity profiles x/R_j from 0.98 to 66.76.

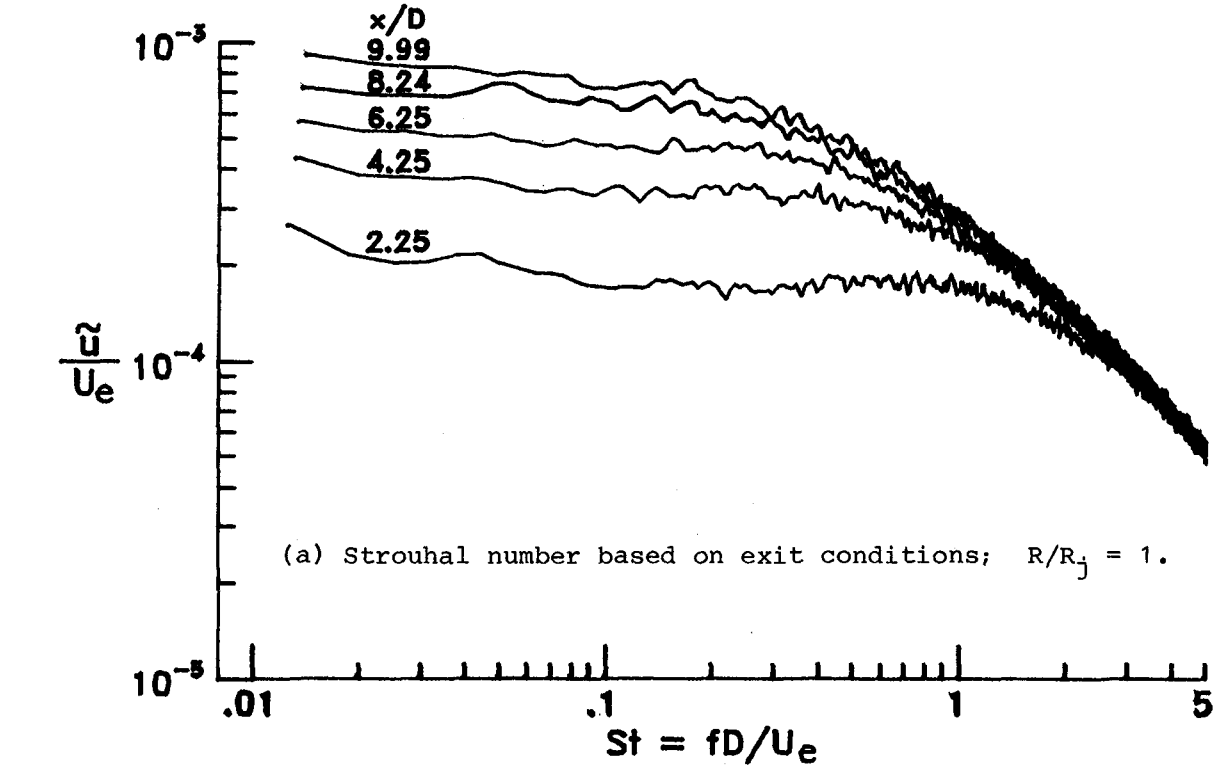

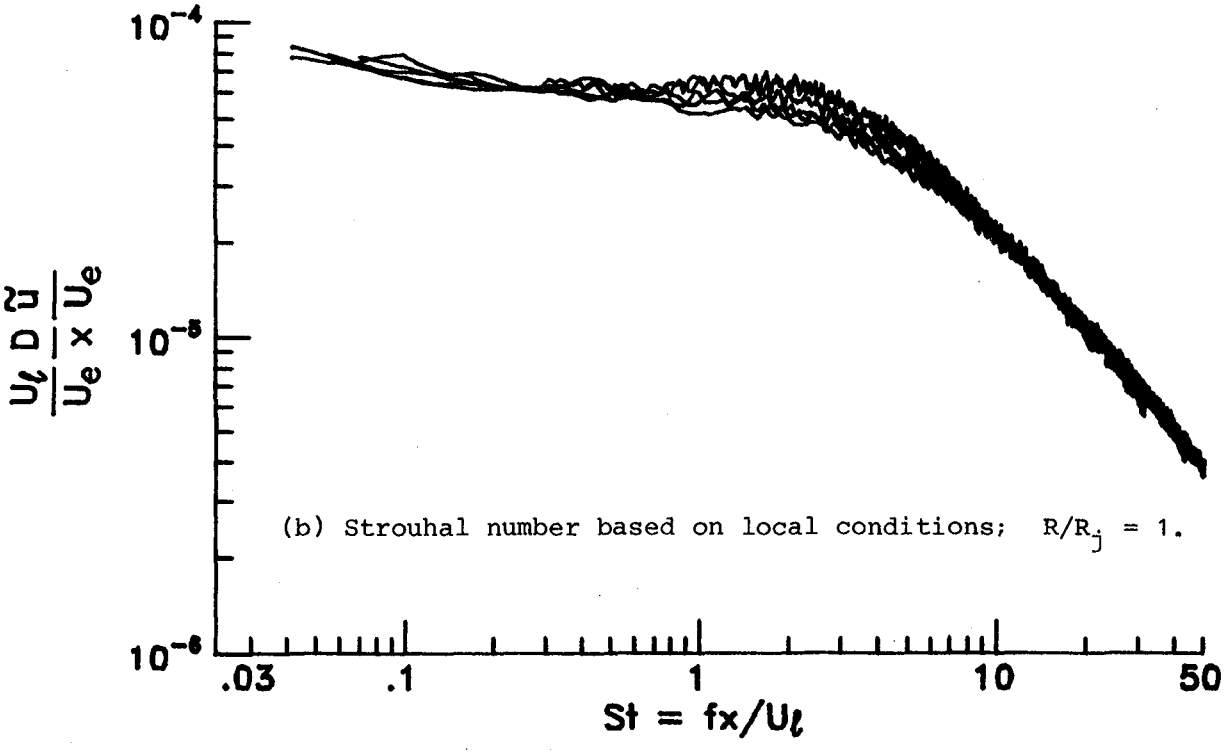

Figure 12.- Universal turbulent velocity spectra in annular mixing region.

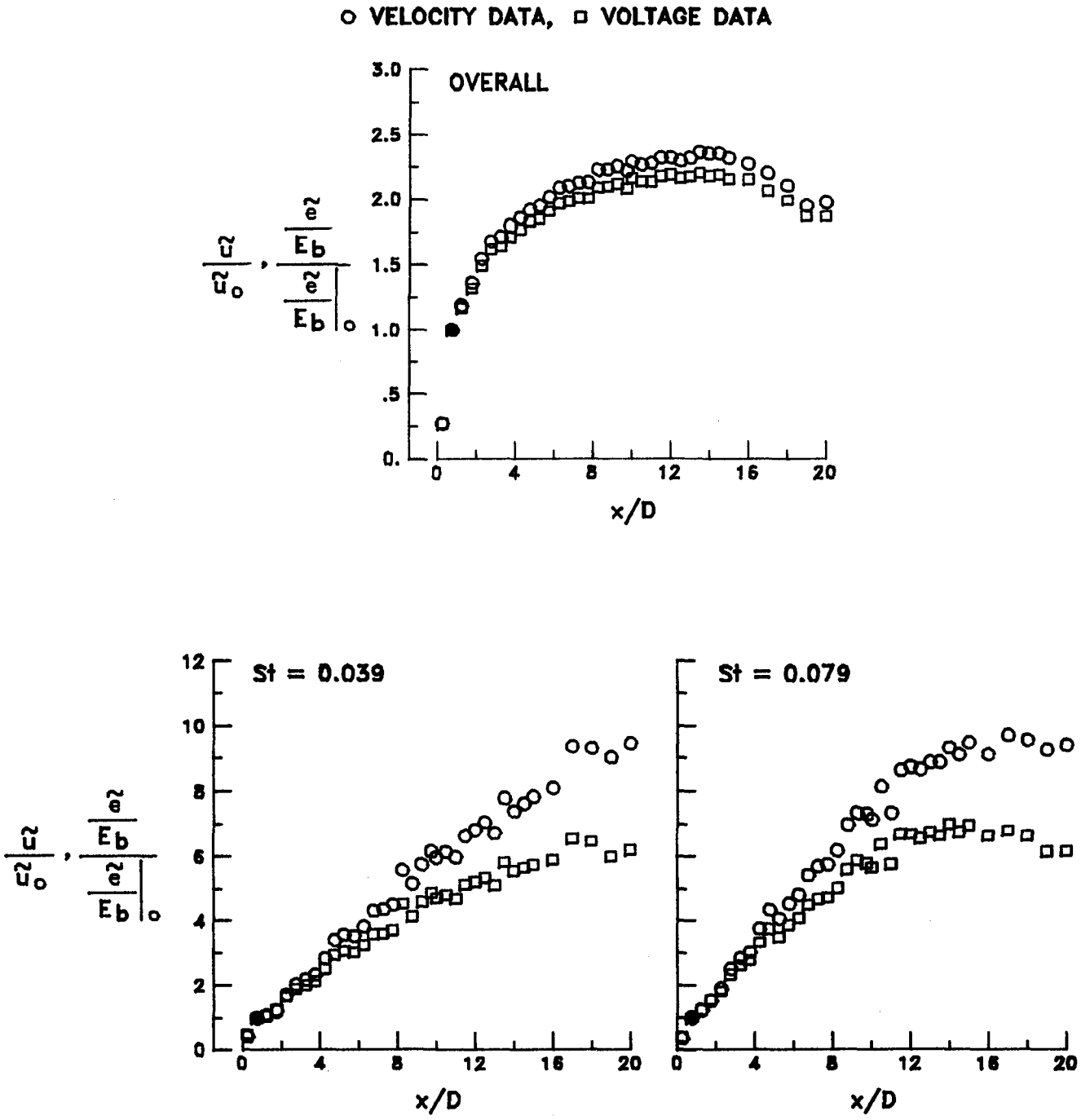

Figure 13.- Growth and decay of various narrow-band Strouhal number components in $M_d = 2$ nozzle supersonic jet plume.

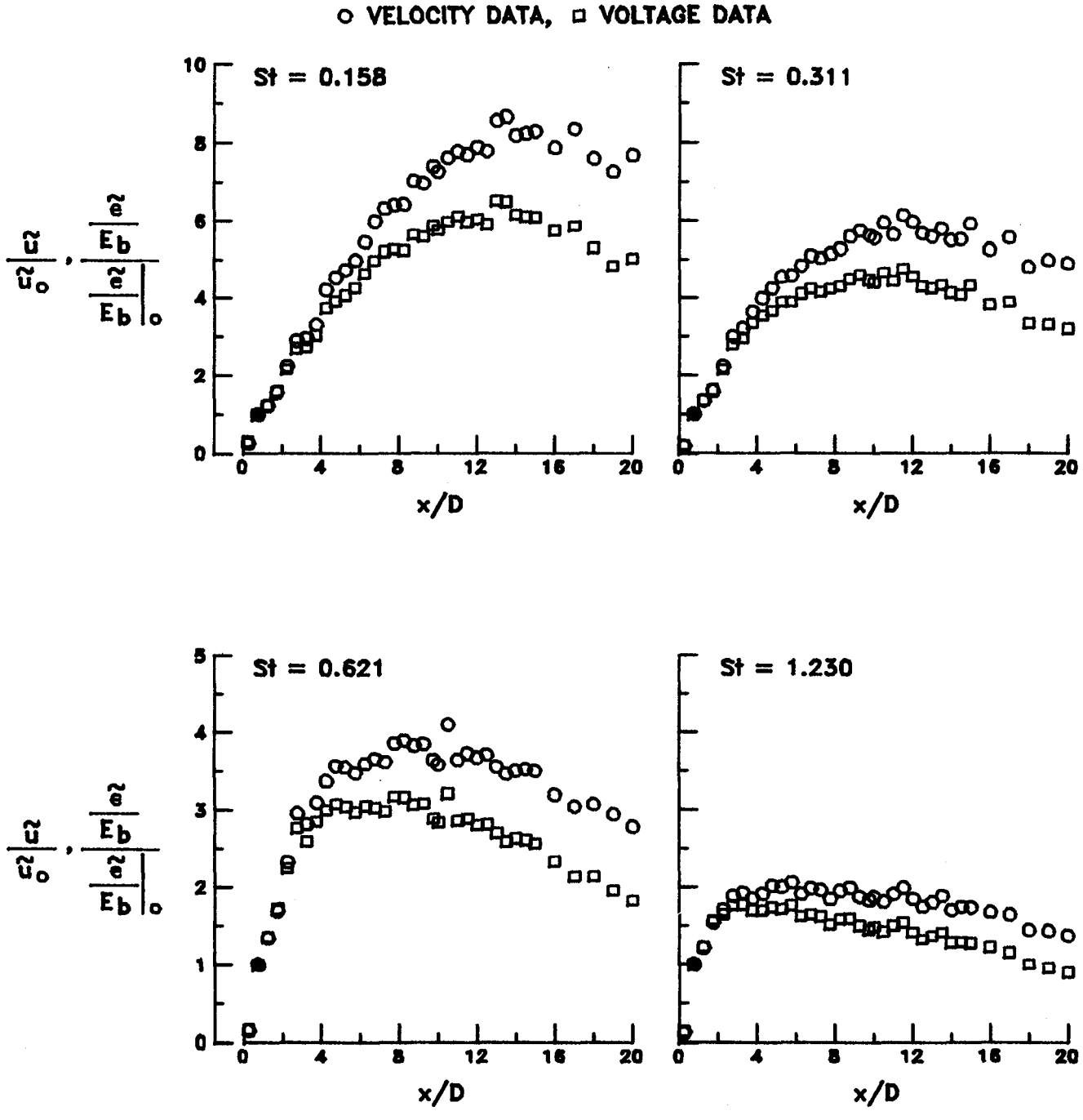

Figure 13.- Concluded.

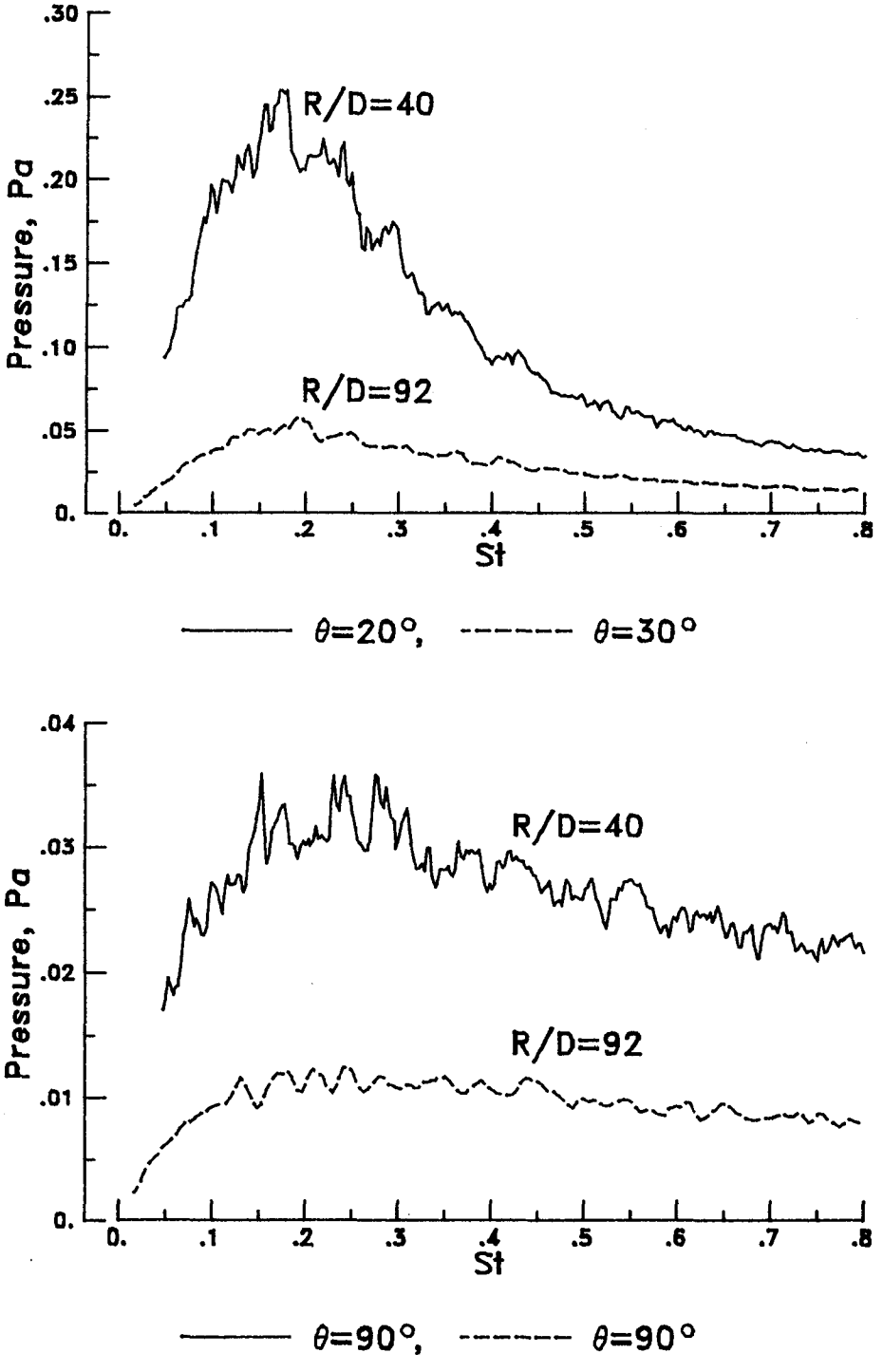

(a) Convergent nozzle; M_j = 0.90.

Figure 14.- Narrow-band near- and far-field acoustic spectra.

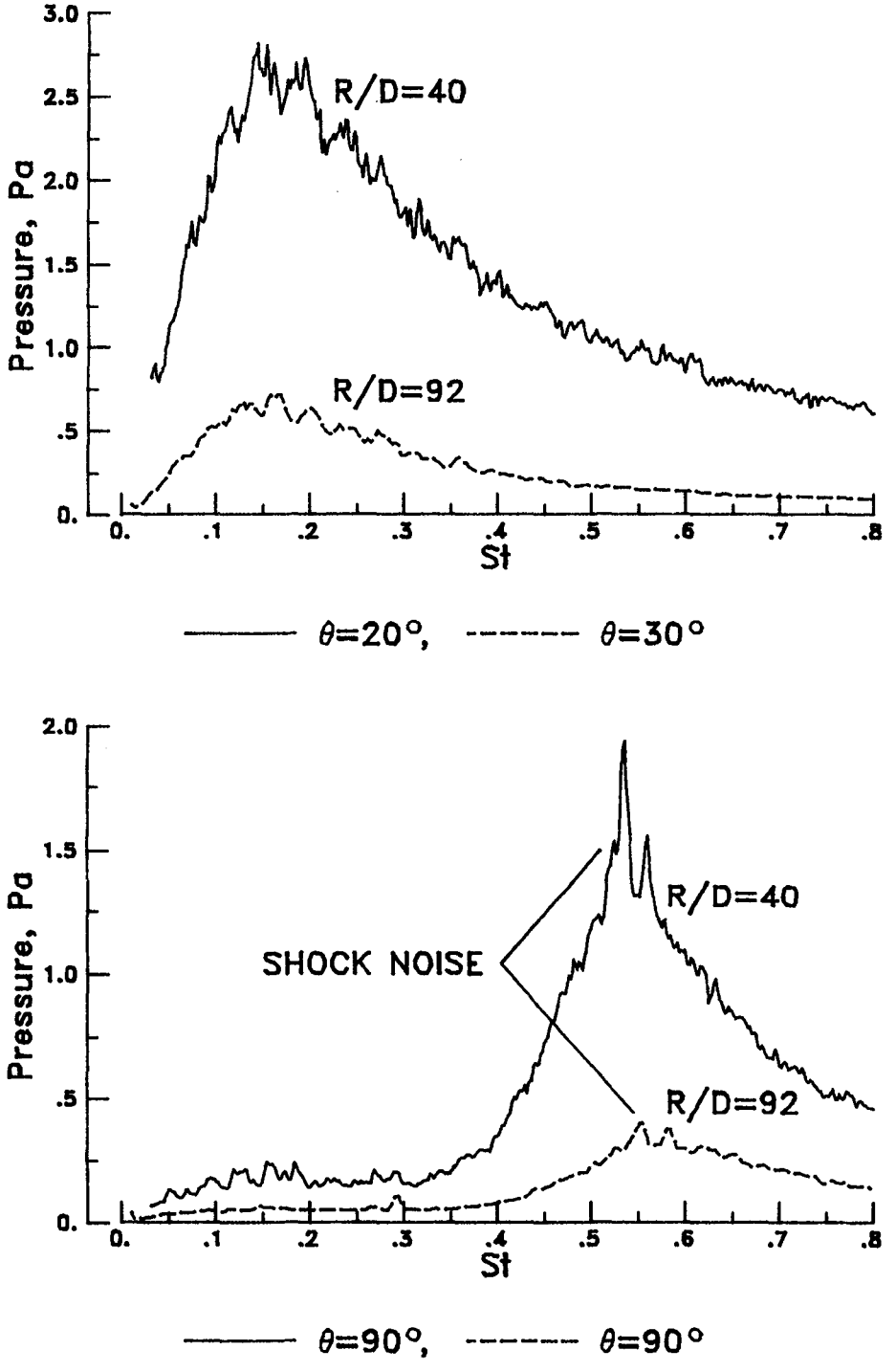

(b) Convergent nozzle; M_j = 1.50.

Figure 14.- Continued.

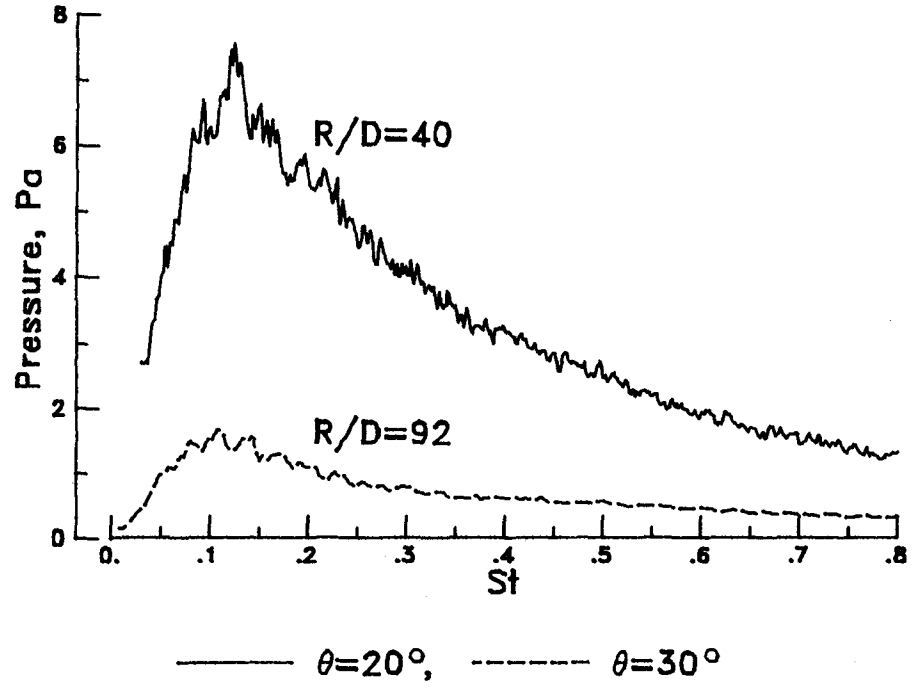

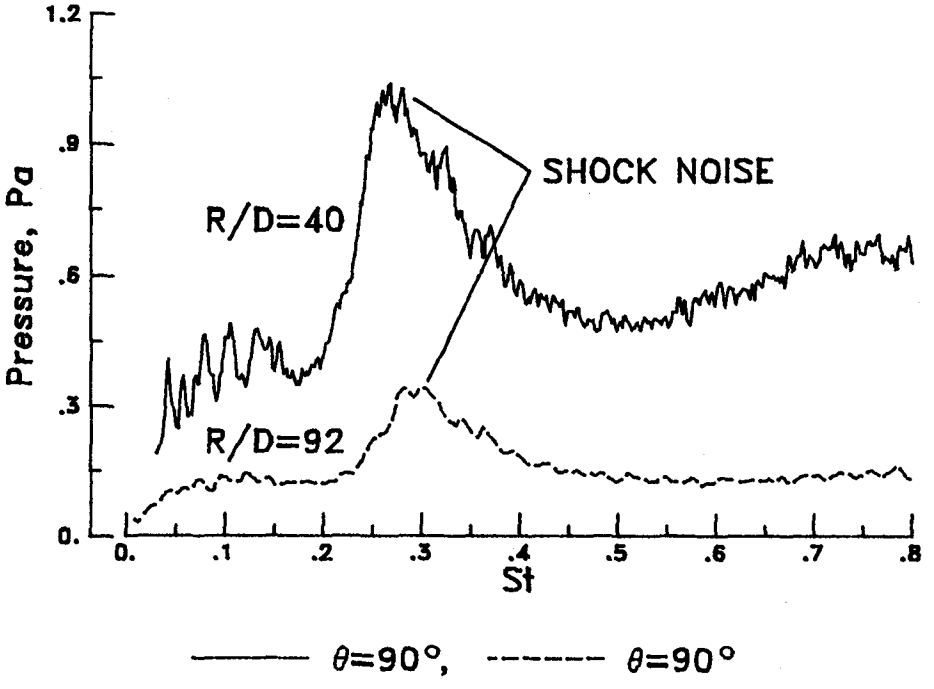

(c) Convergent nozzle; M_j = 2.00.

Figure 14.- Continued.

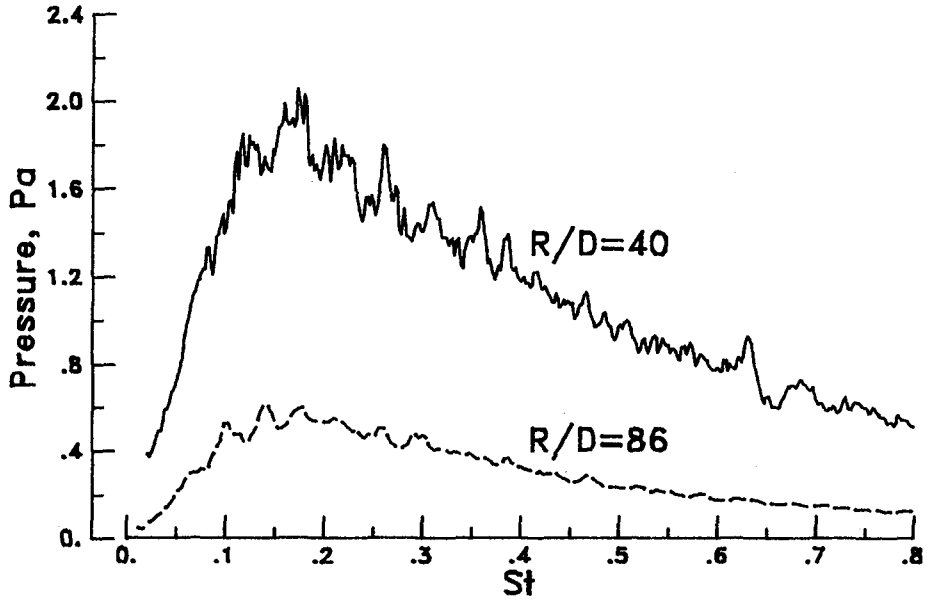

——— θ=20°, ------ θ=30°

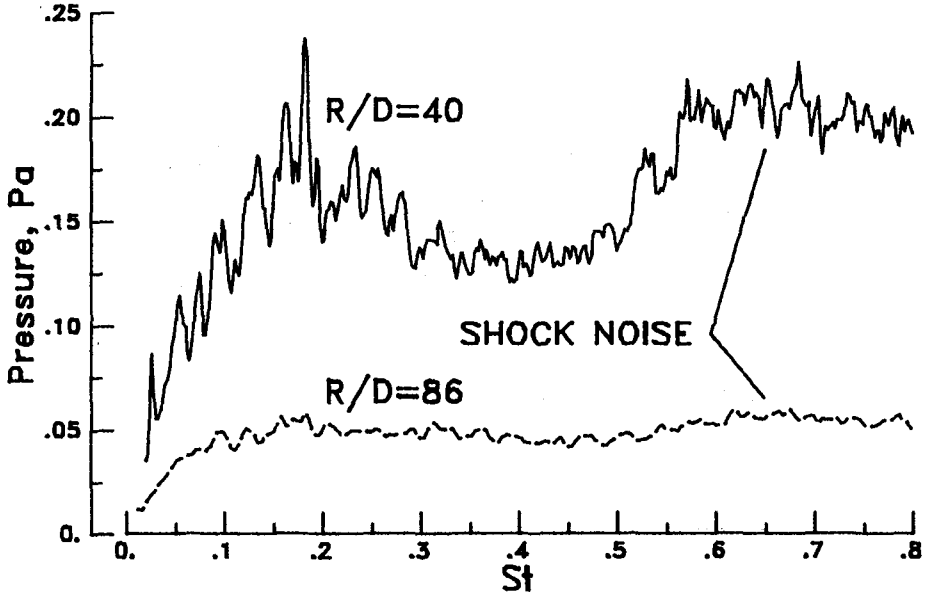

——— θ=90°, ------ θ=90°

(d) M_e = 1.46; M_j = 1.50.

Figure 14.- Continued.

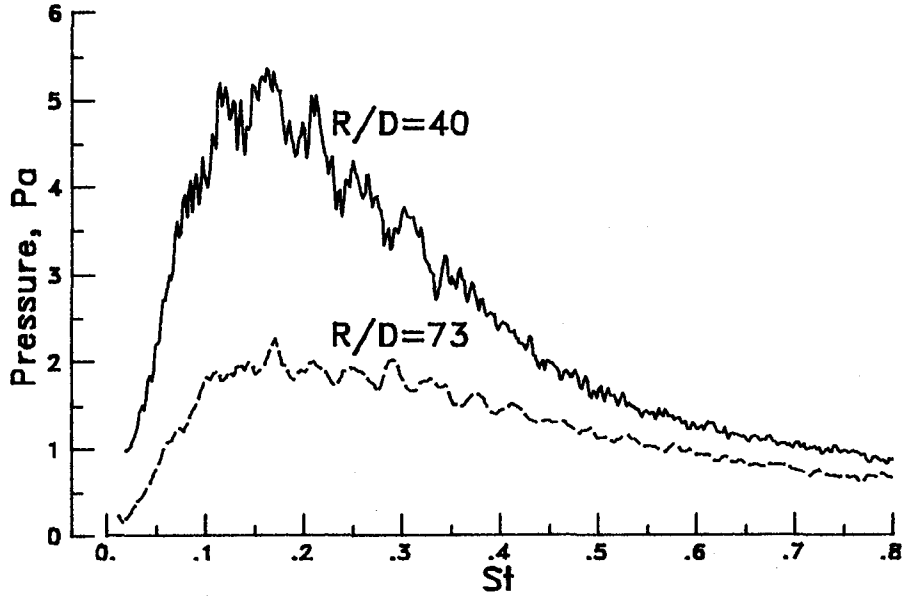

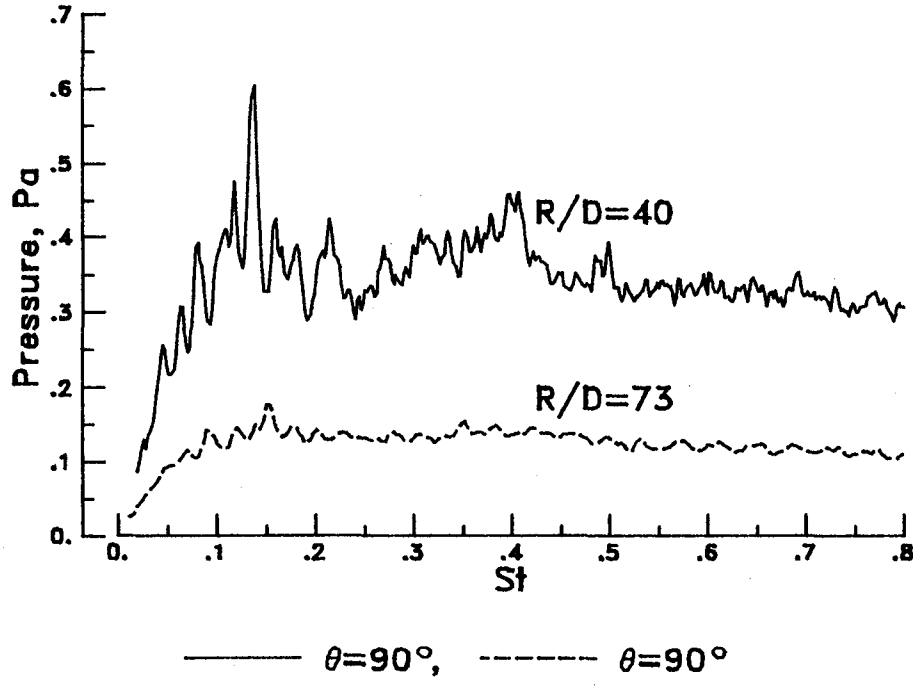

(e) M_e = 1.99; M_j = 1.99.

Figure 14.- Continued.

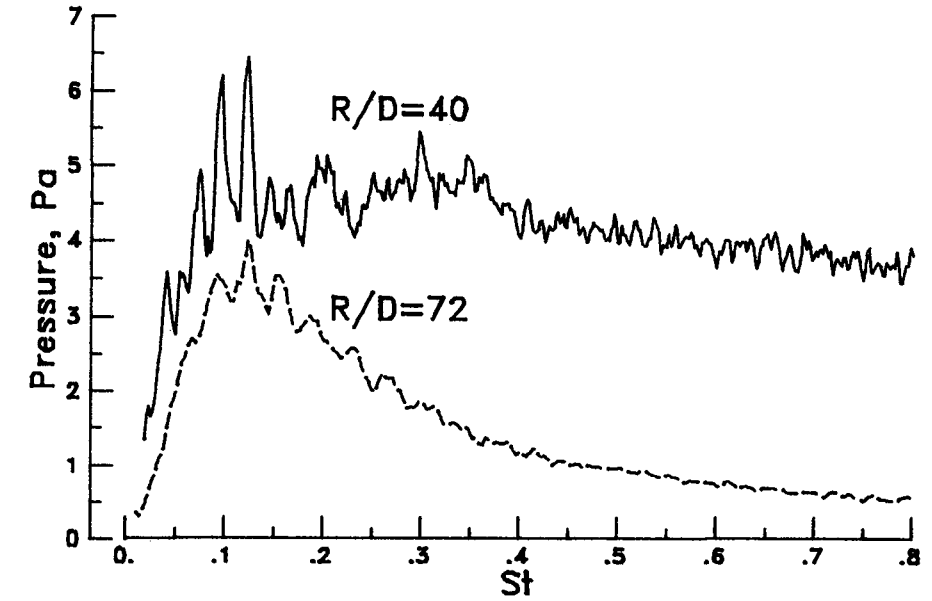

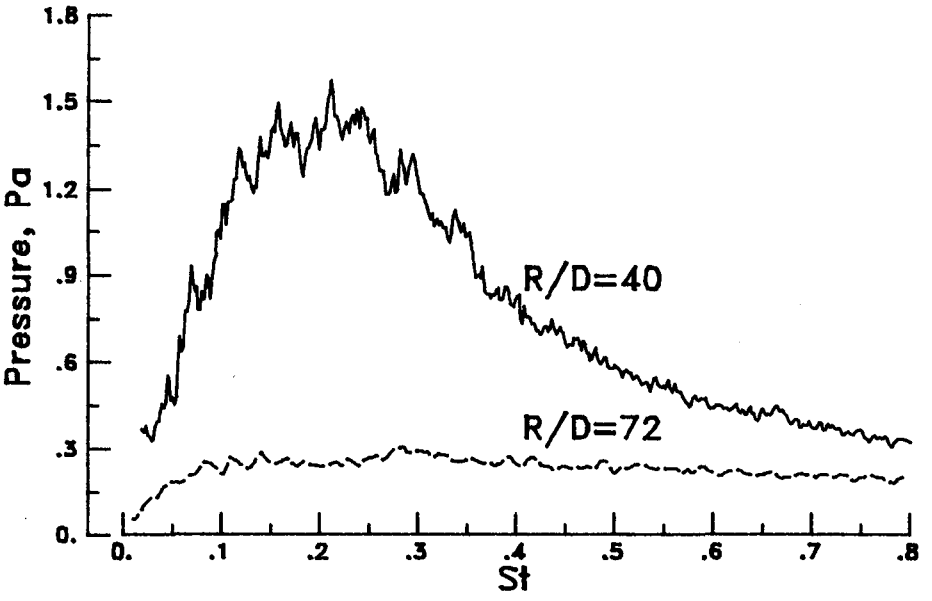

(f) M_e = 2.50; M_j = 2.50.

Figure 14.- Concluded.

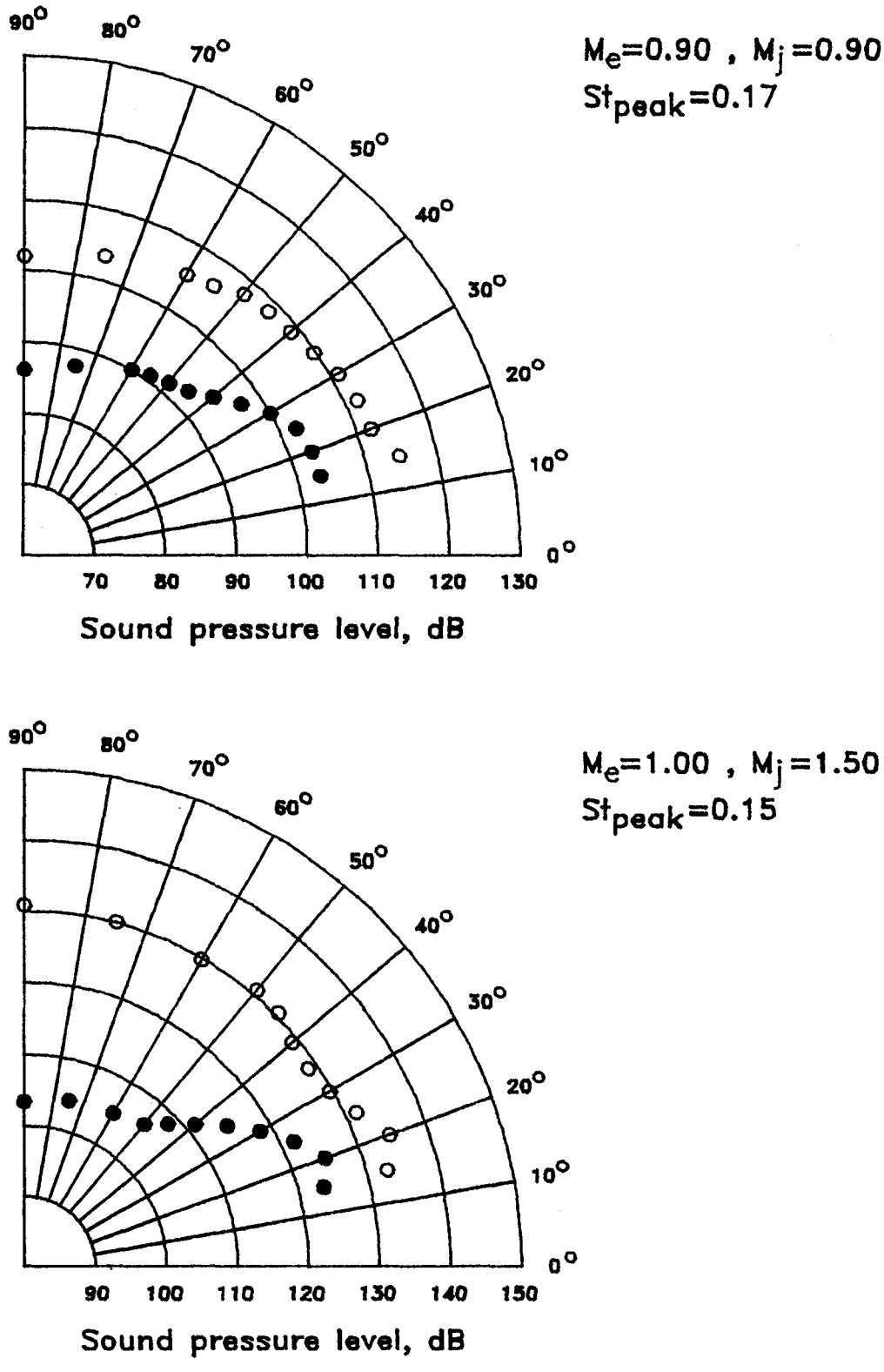

Figure 15.- Directivity of overall and one-third-octave spectrum peak value.

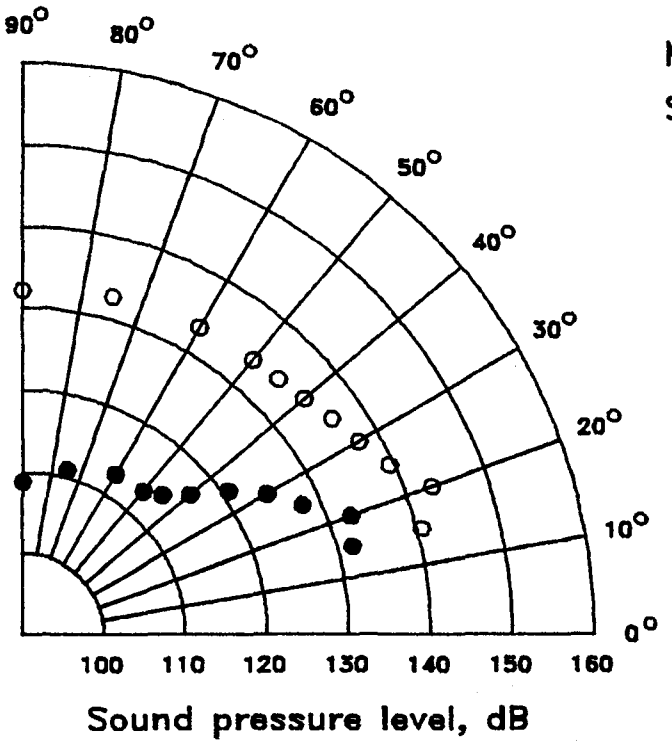

M_e=1.00 , M_j=2.00
St_{peak}=0.10

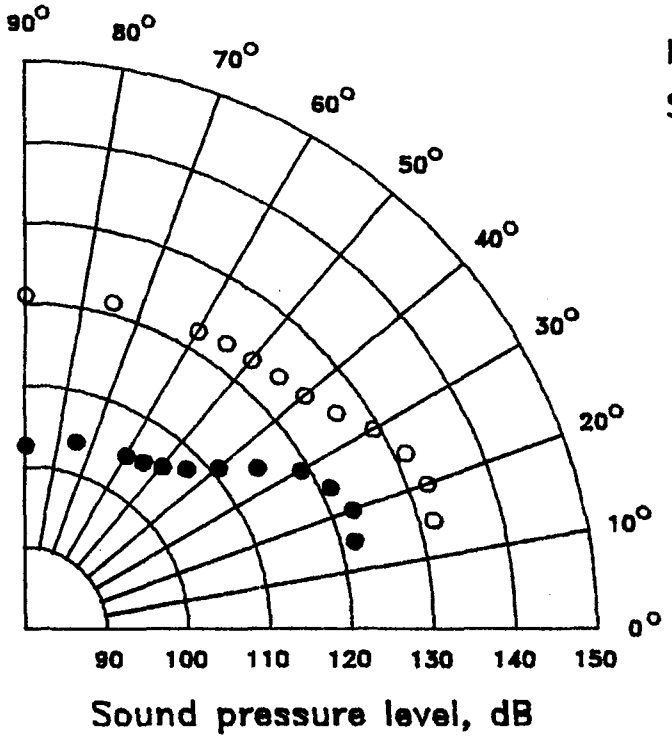

M_e=1.46 , M_j=1.50
St_{peak}=0.16

R/D=40, ○ OVERALL, ● PEAK STROUHAL NUMBER

Figure 15.- Continued.

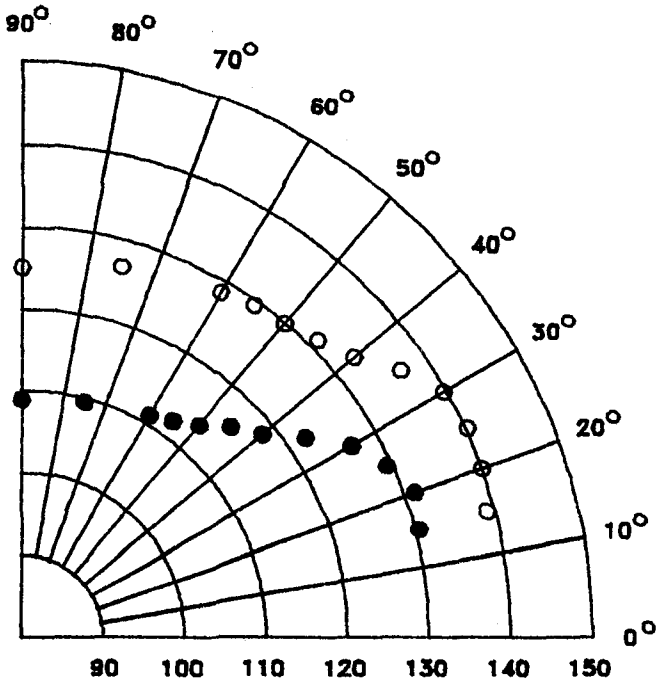

M_e=1.99 , M_j=1.99
St_{peak}=0.16

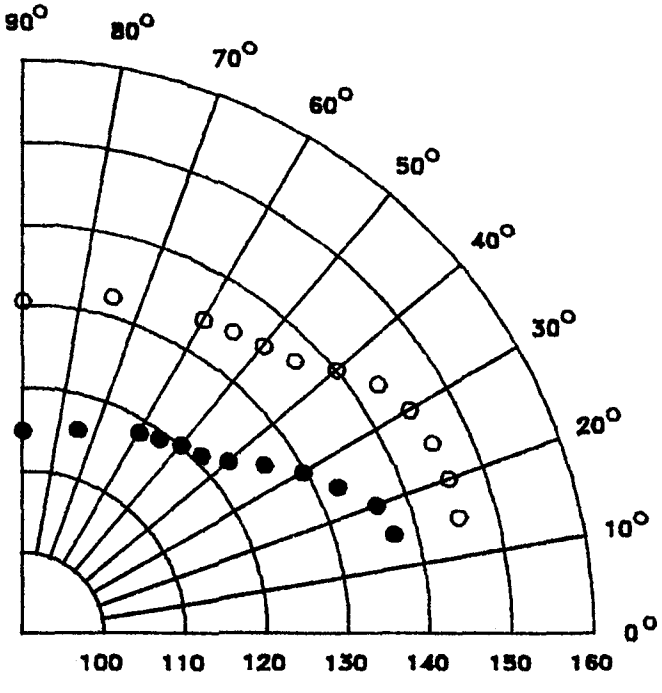

M_e=2.50 , M_j=2.50
St_{peak}=0.11

R/D=40, ○ OVERALL, ● PEAK STROUHAL NUMBER

Figure 15.- Concluded.

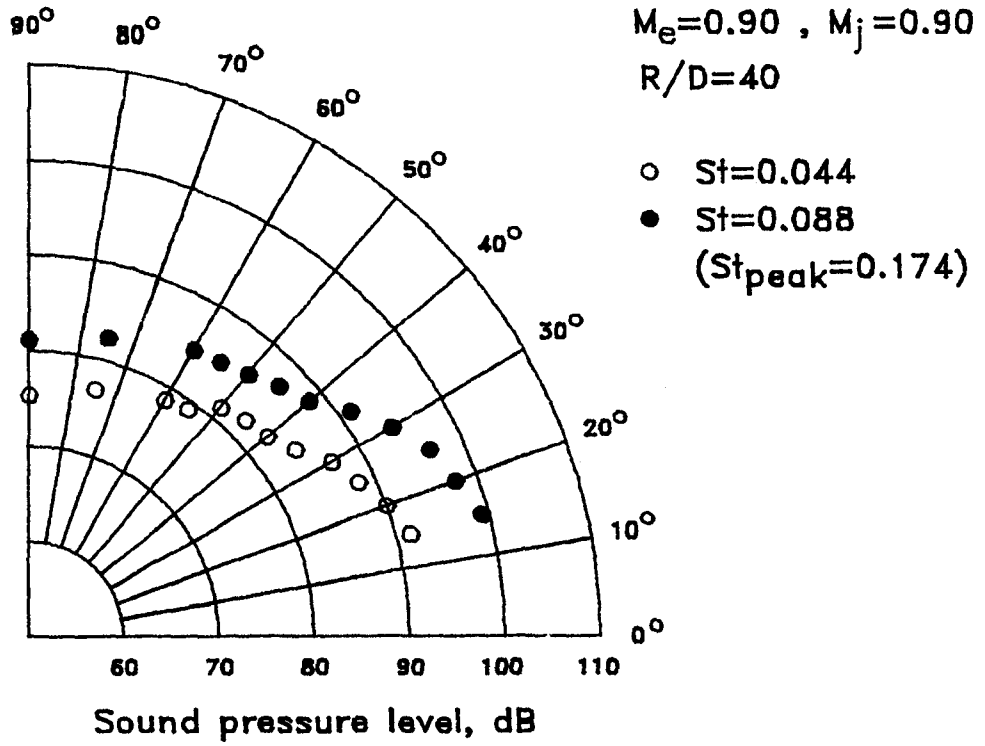

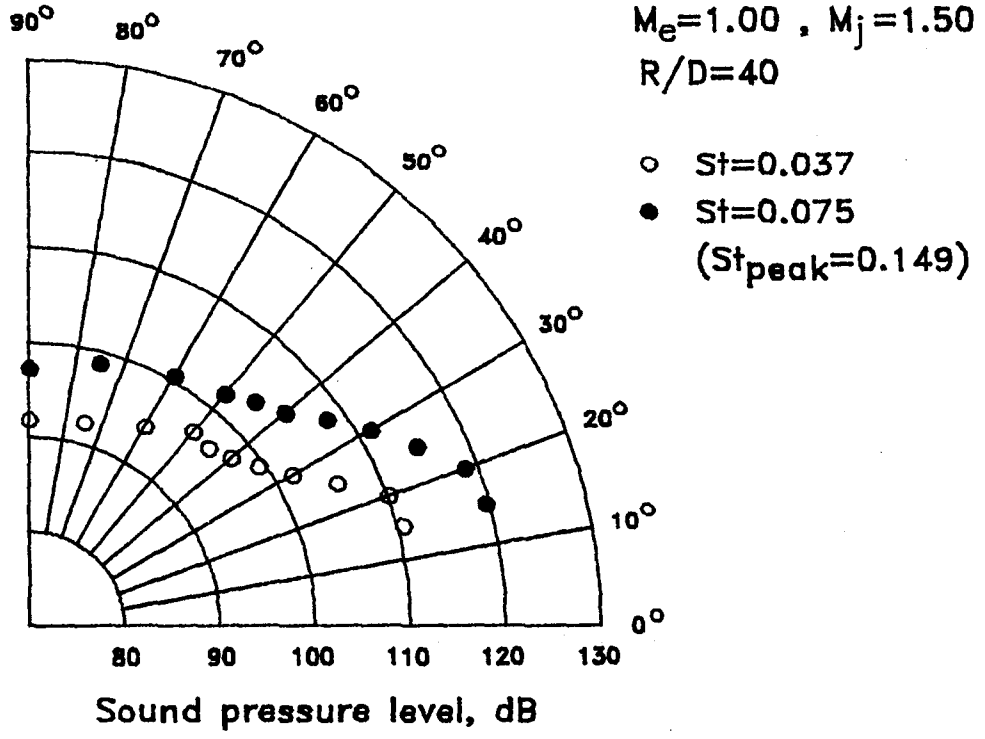

Figure 16.- Directivity of Strouhal number components lower than St_{peak}.

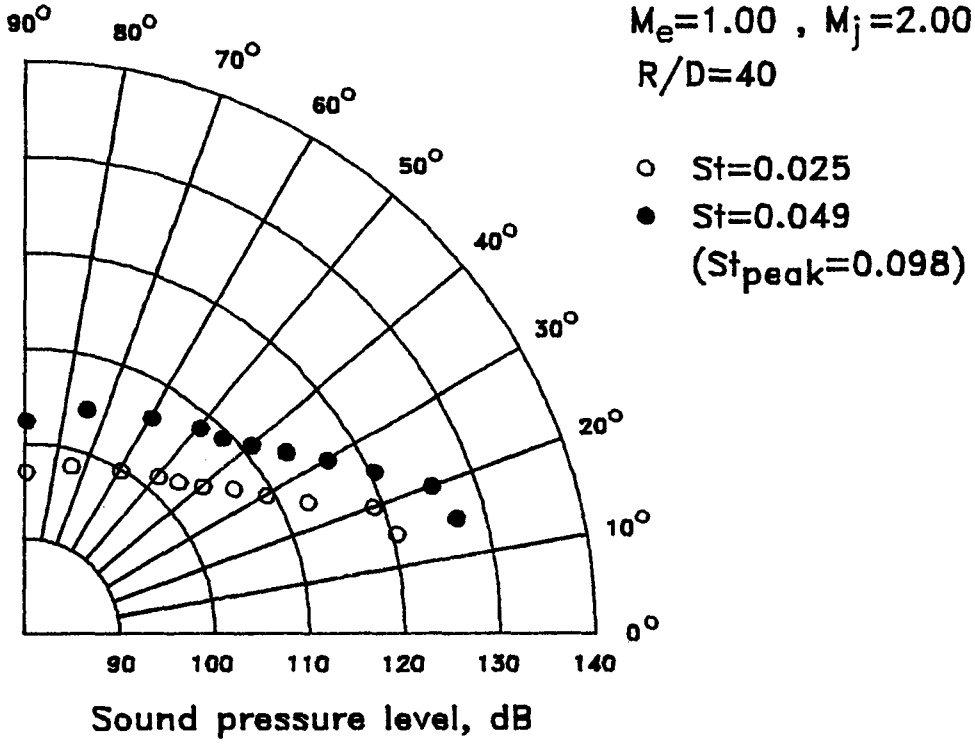

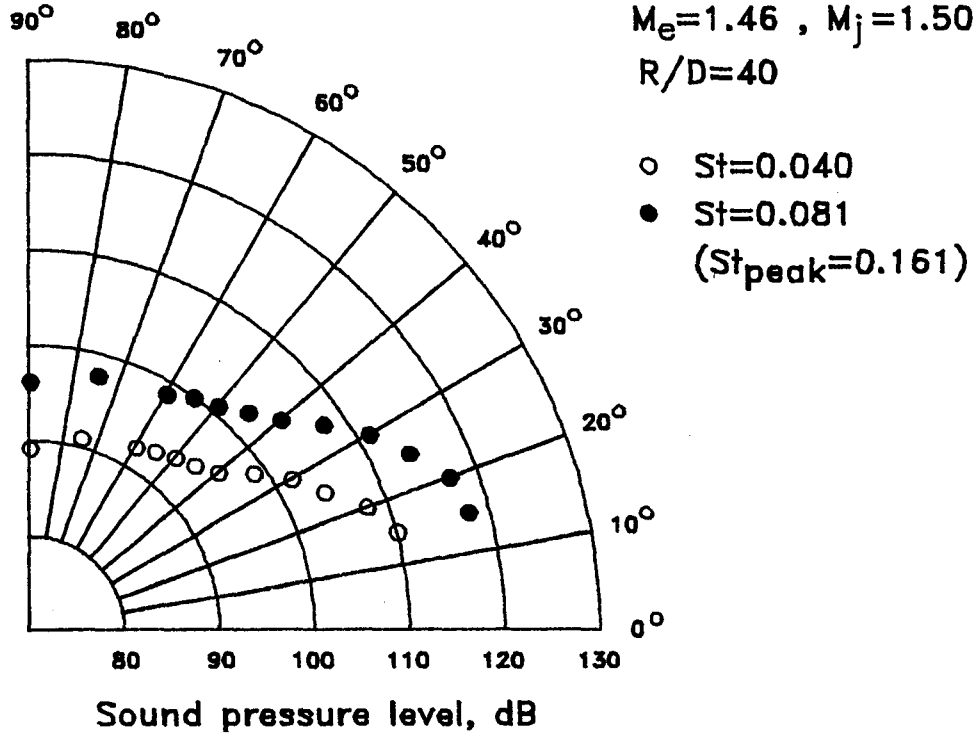

Figure 16.- Continued.

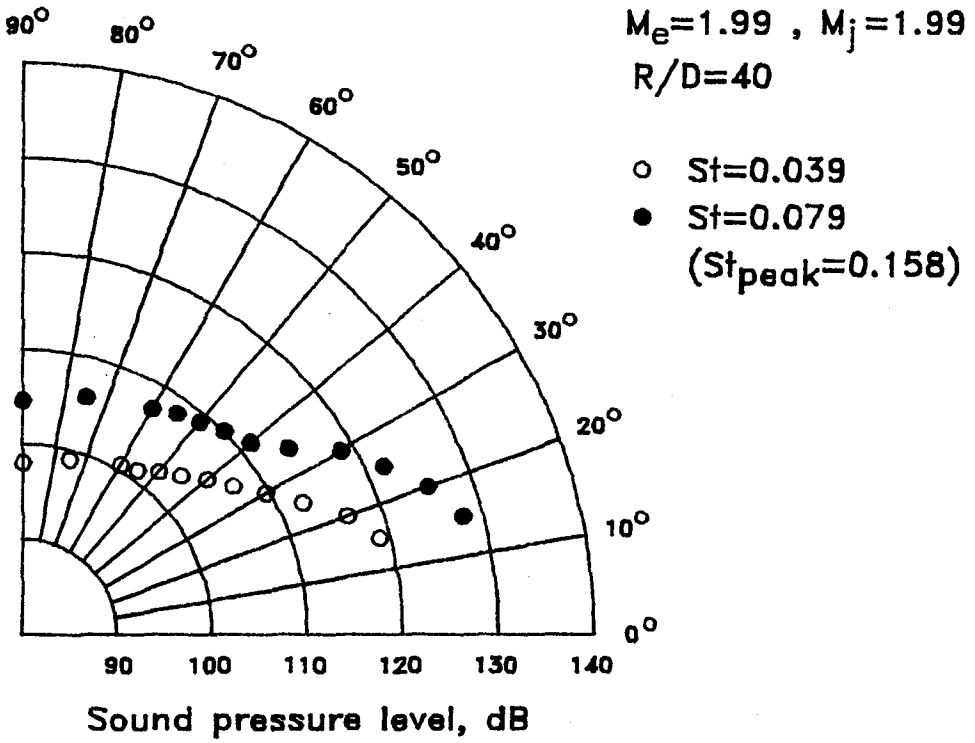

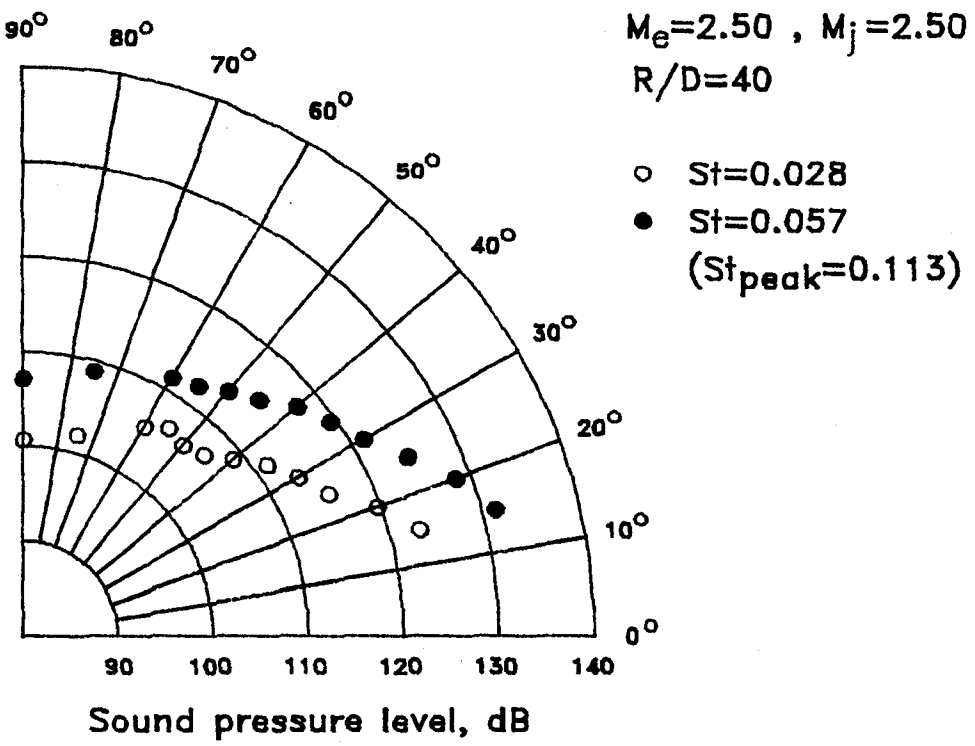

Figure 16.- Concluded.

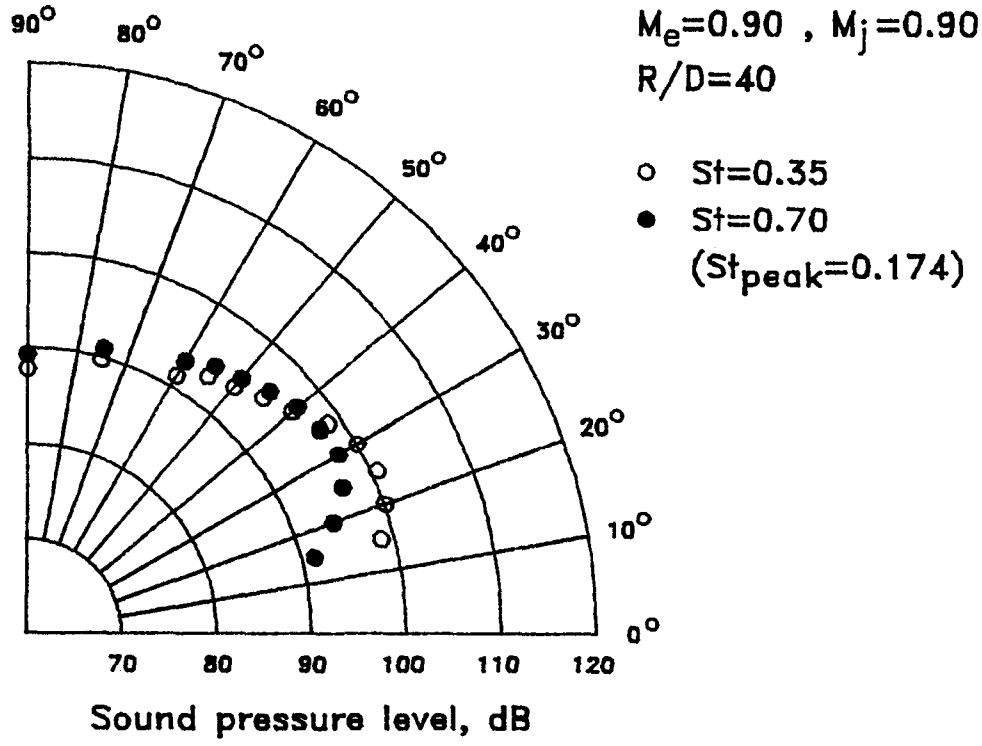

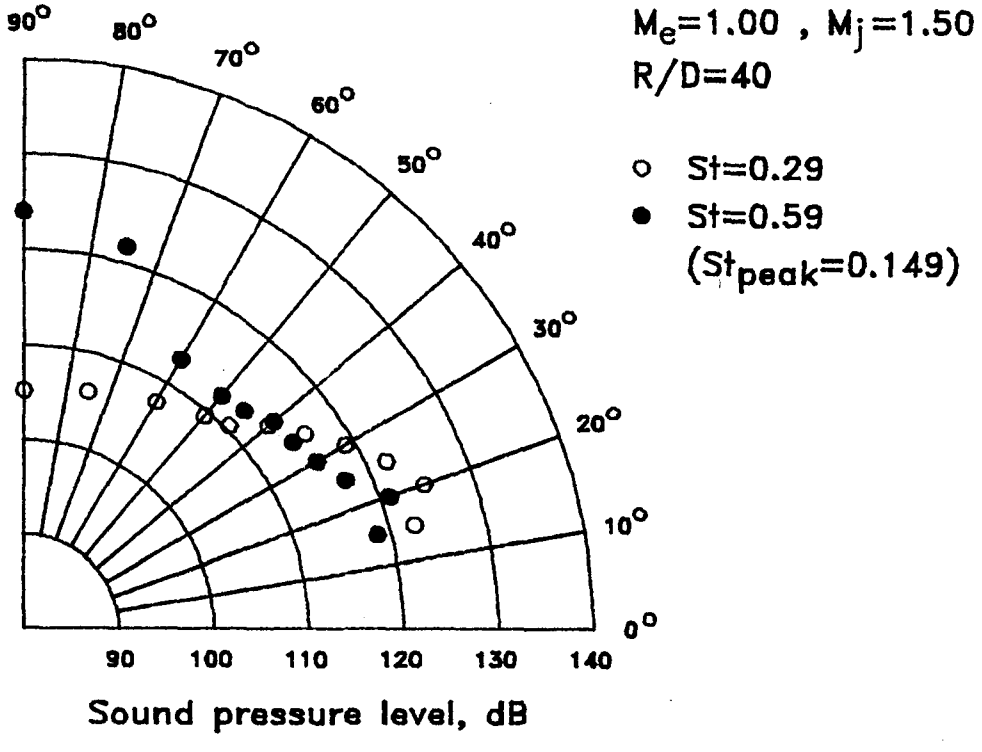

Figure 17.- Directivity of Strouhal number components higher than St_{peak}.

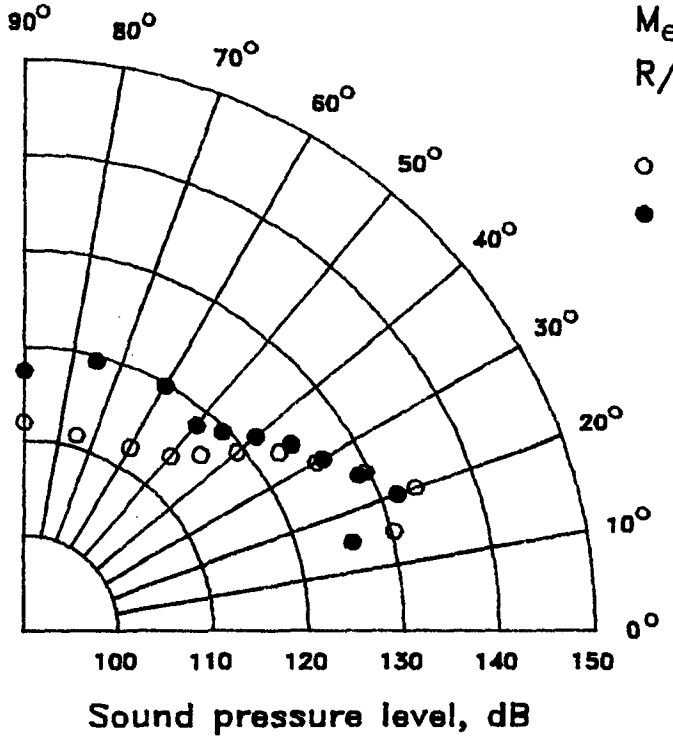

M_e=1.00 , M_j=2.00
R/D=40

○ St=0.20
● St=0.39
(St_{peak}=0.098)

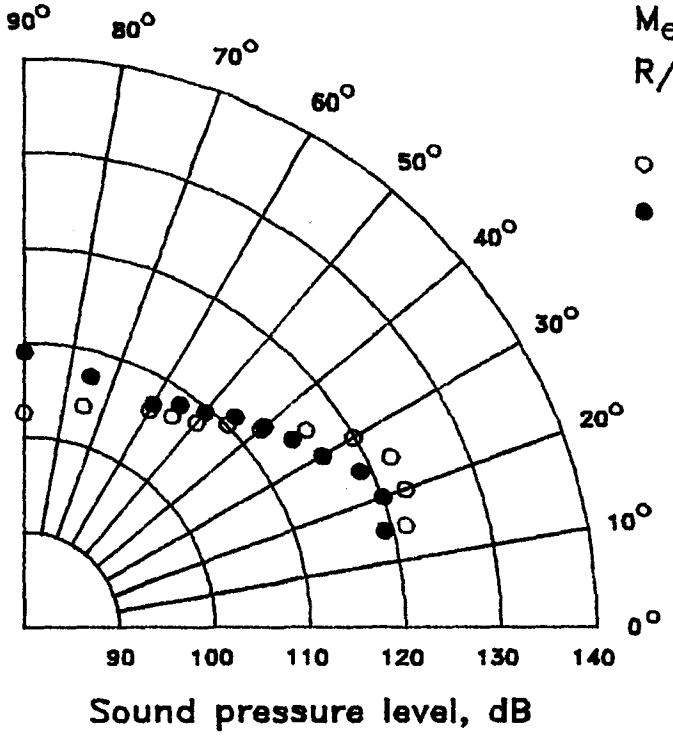

M_e=1.46 , M_j=1.50
R/D=40

○ St=0.32
● St=0.63
(St_{peak}=0.161)

Figure 17.- Continued.

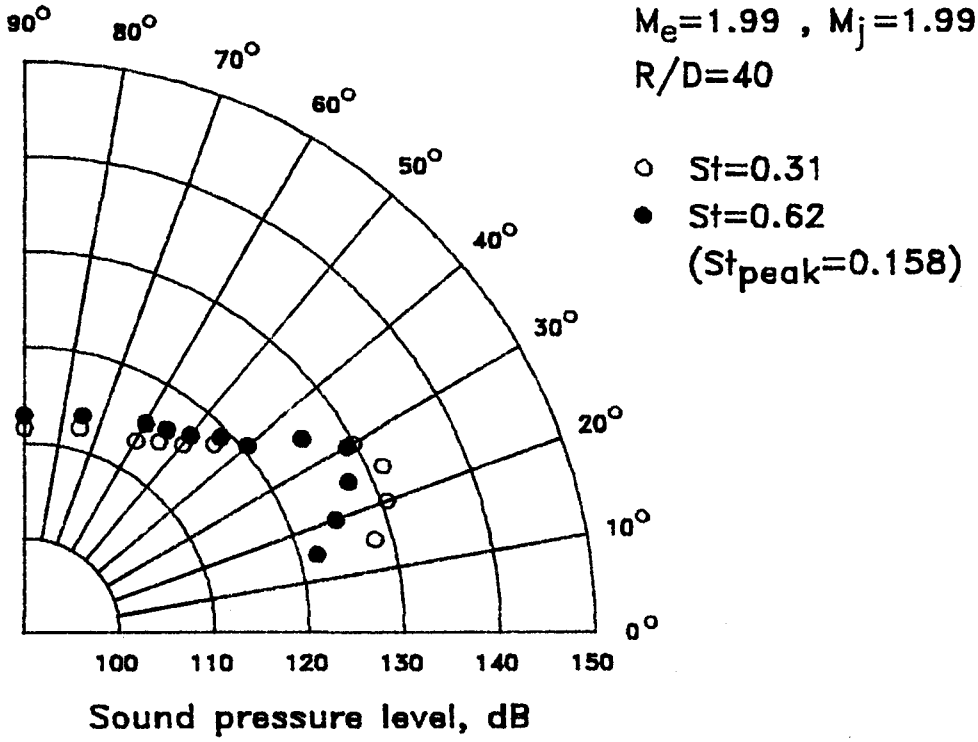

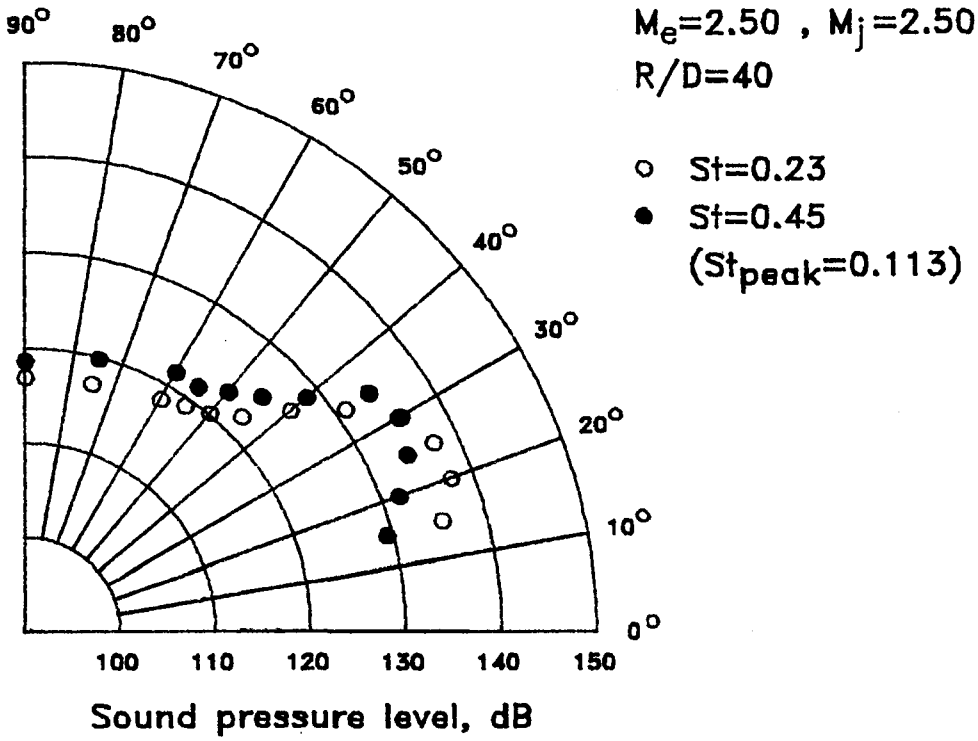

Figure 17.- Concluded.

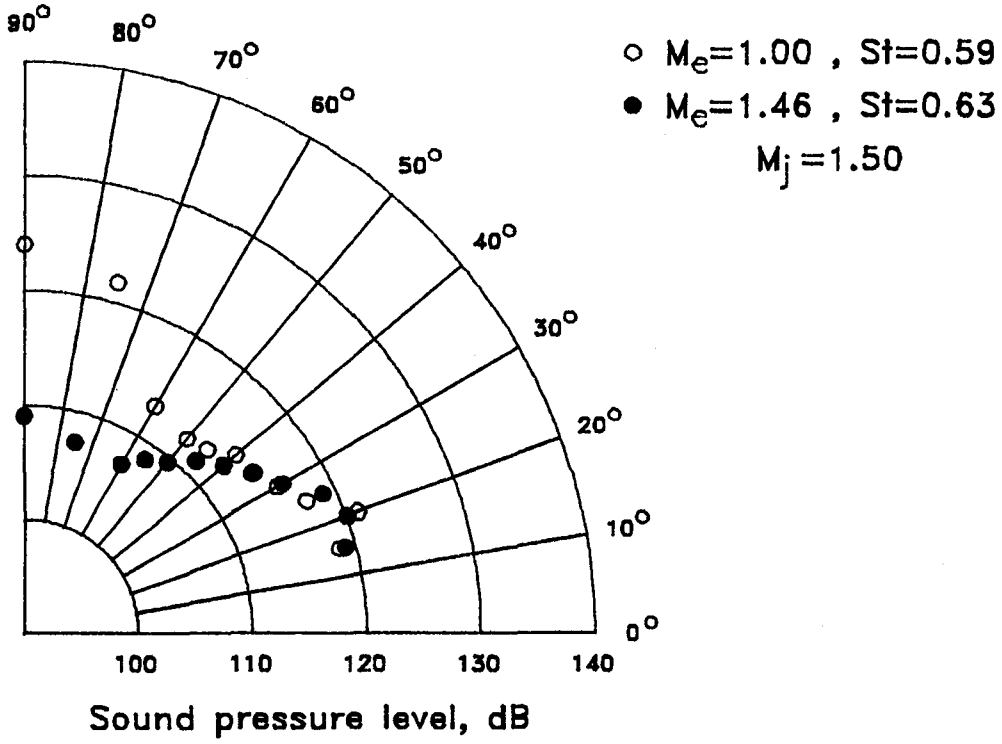

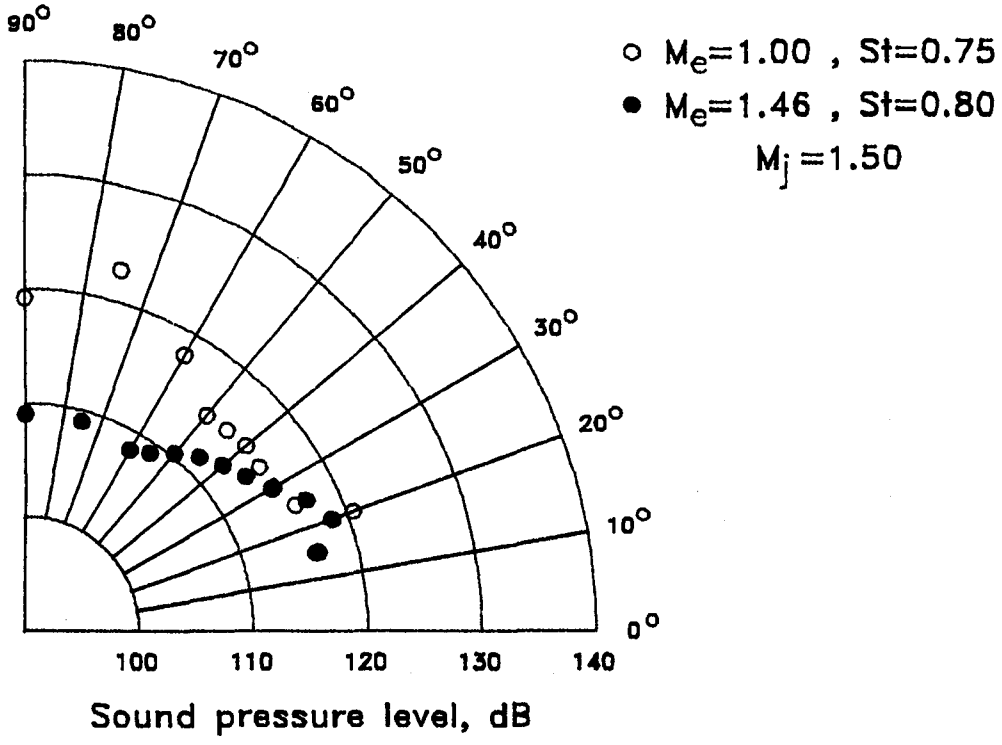

Figure 18.- Acoustic near-field directivity comparisons of underexpanded convergent nozzle plume with shocks with M_d = 1.5 shock-free plume.

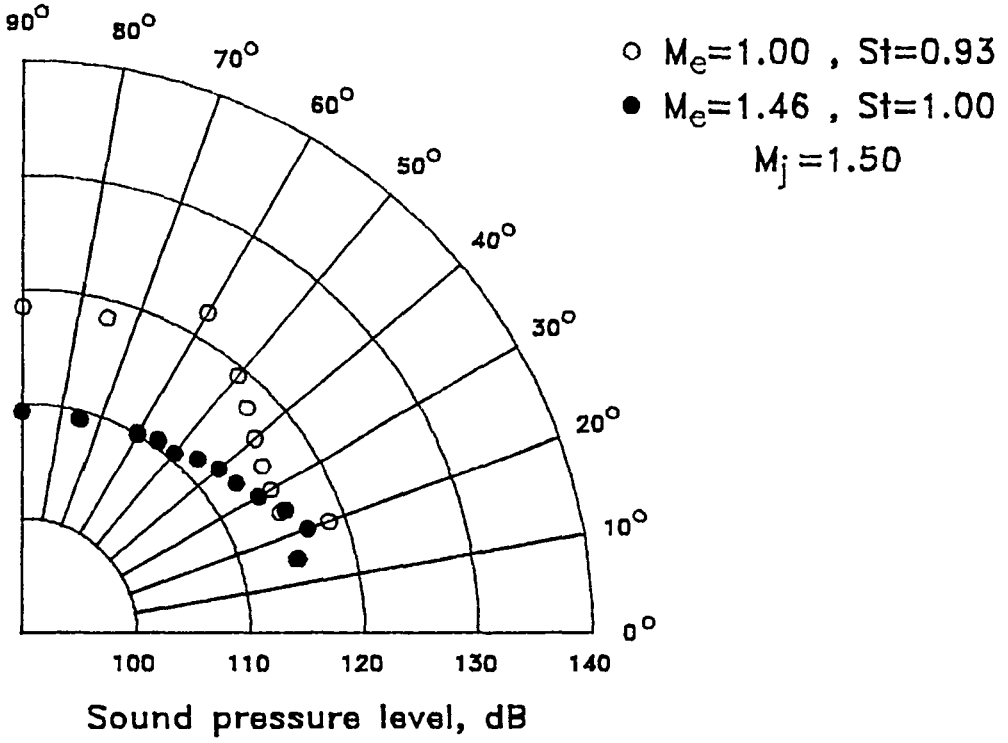

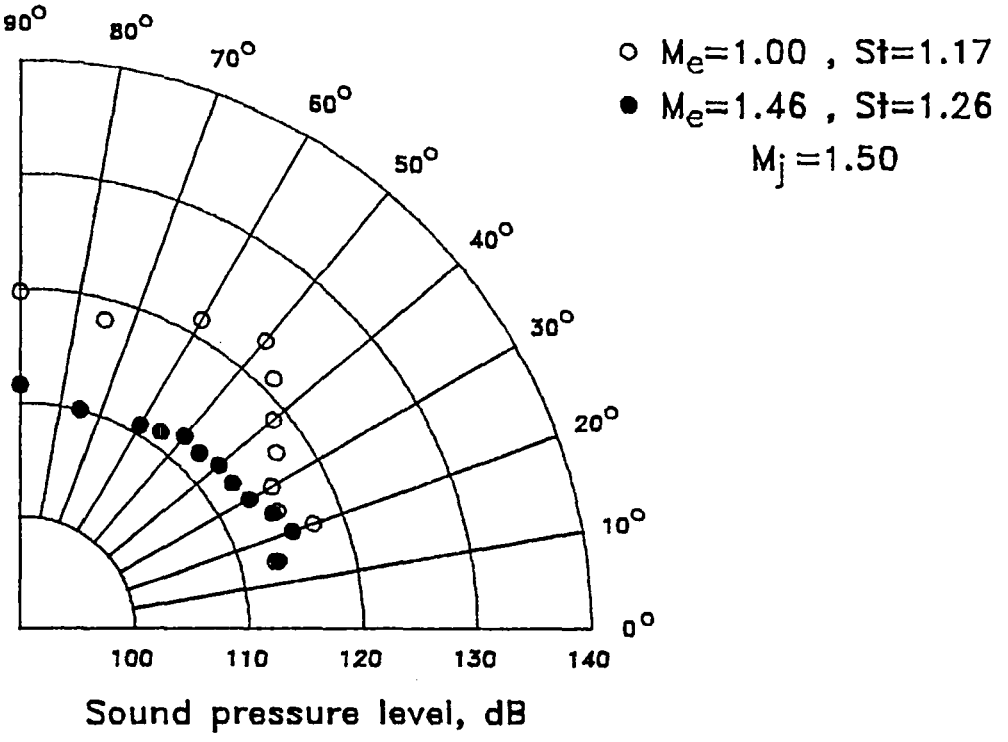

Figure 18.- Continued.

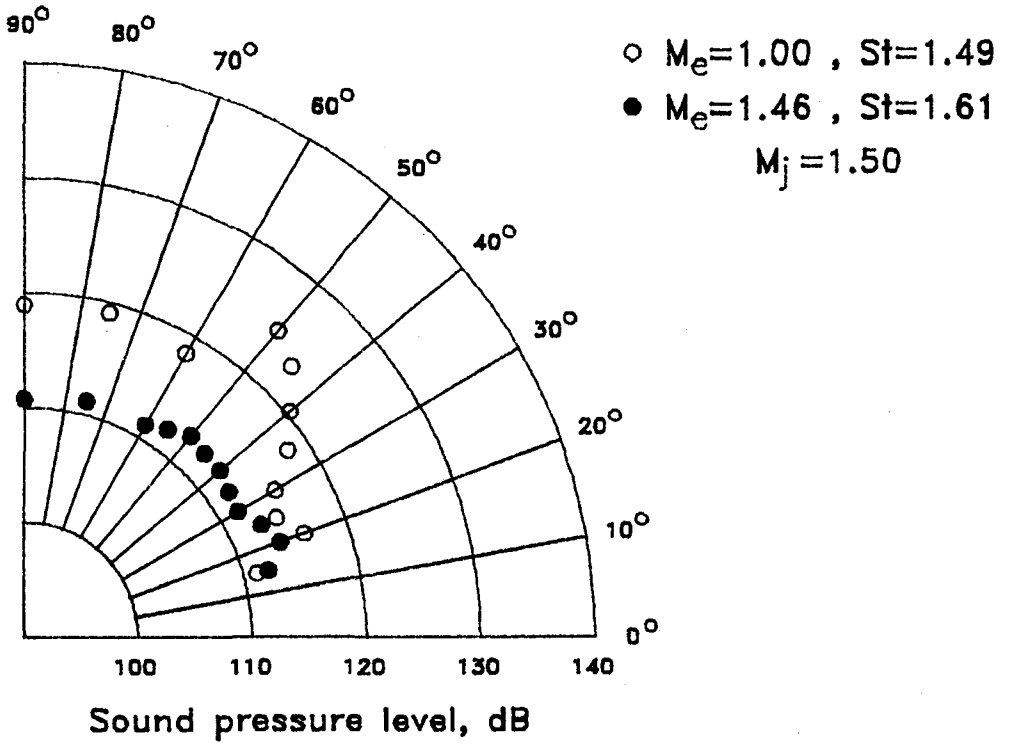

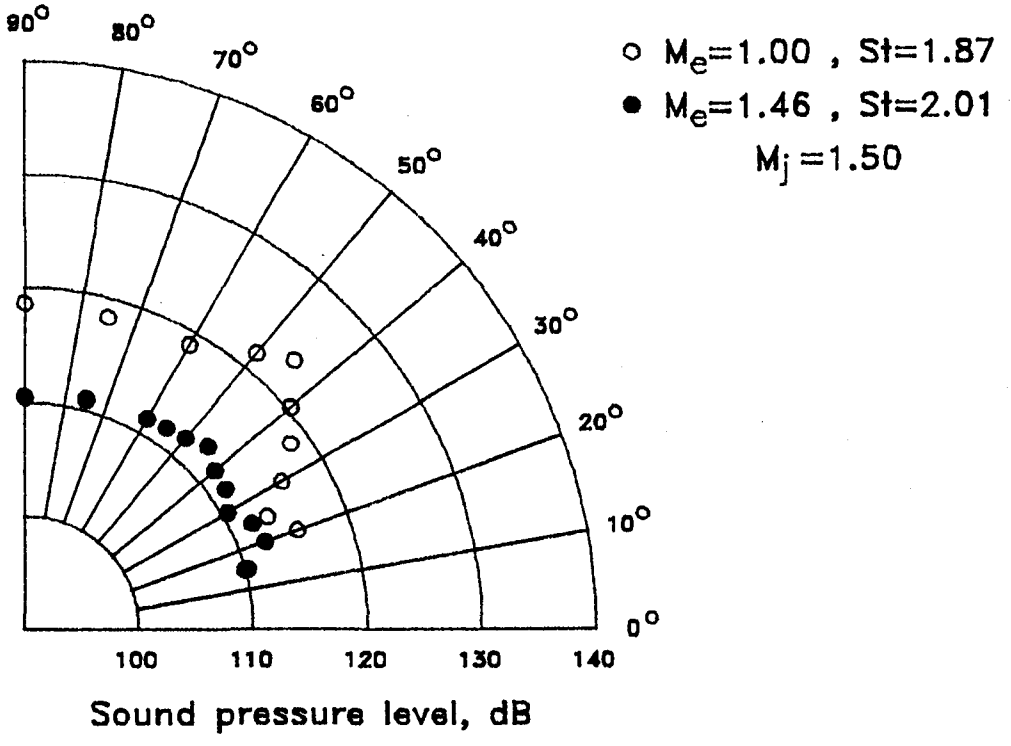

Figure 18.- Continued.

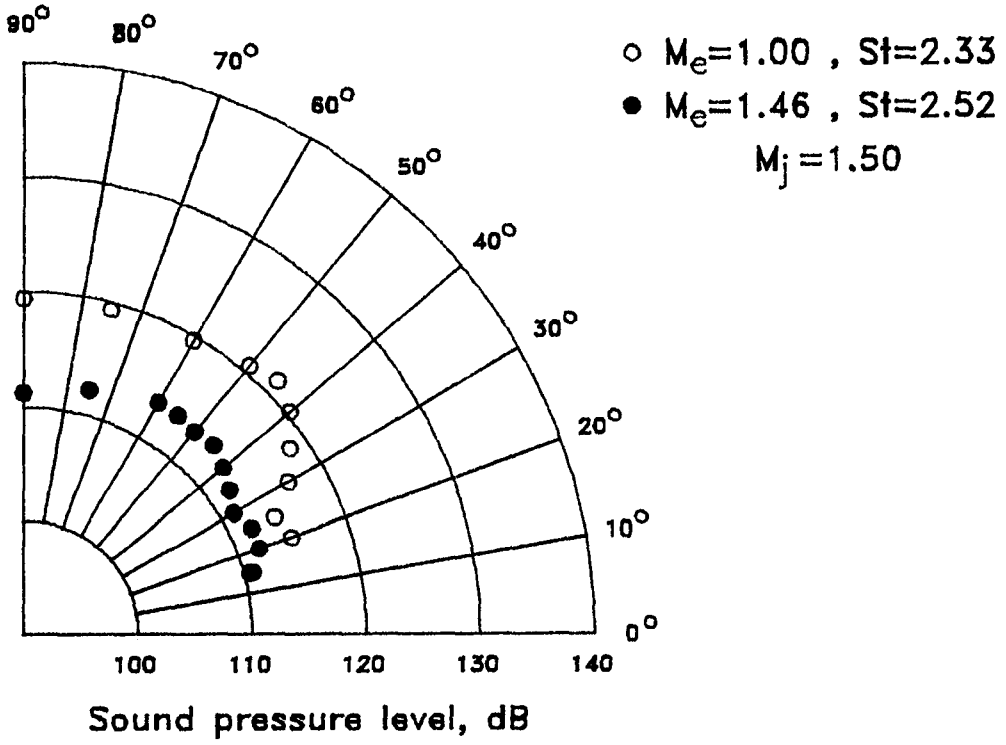

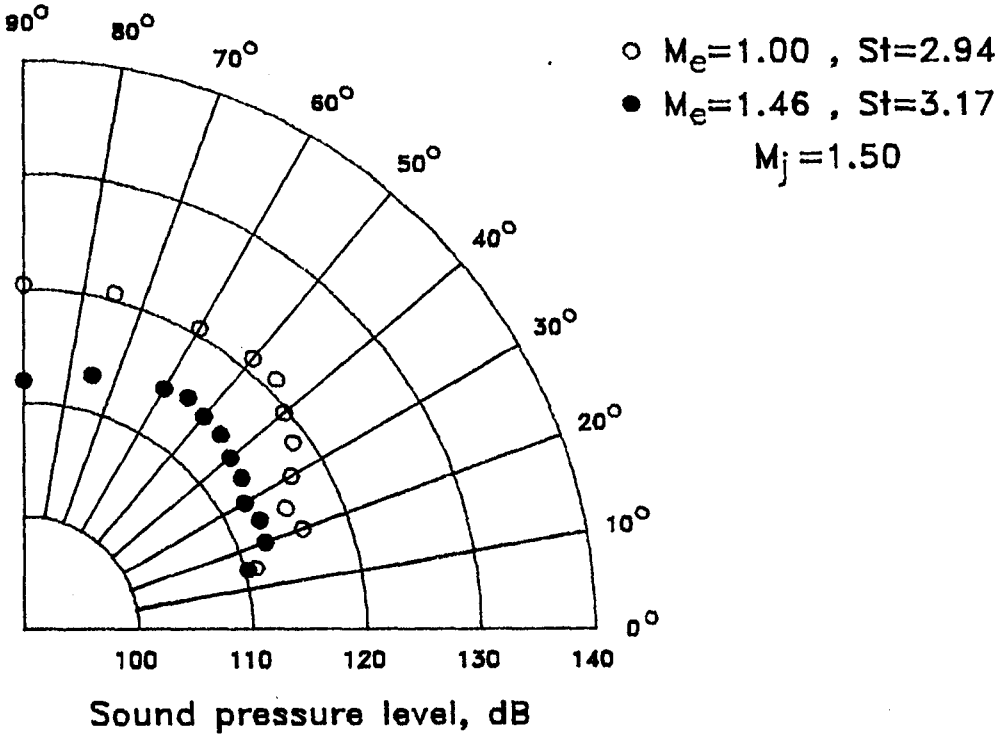

Figure 18.- Concluded.

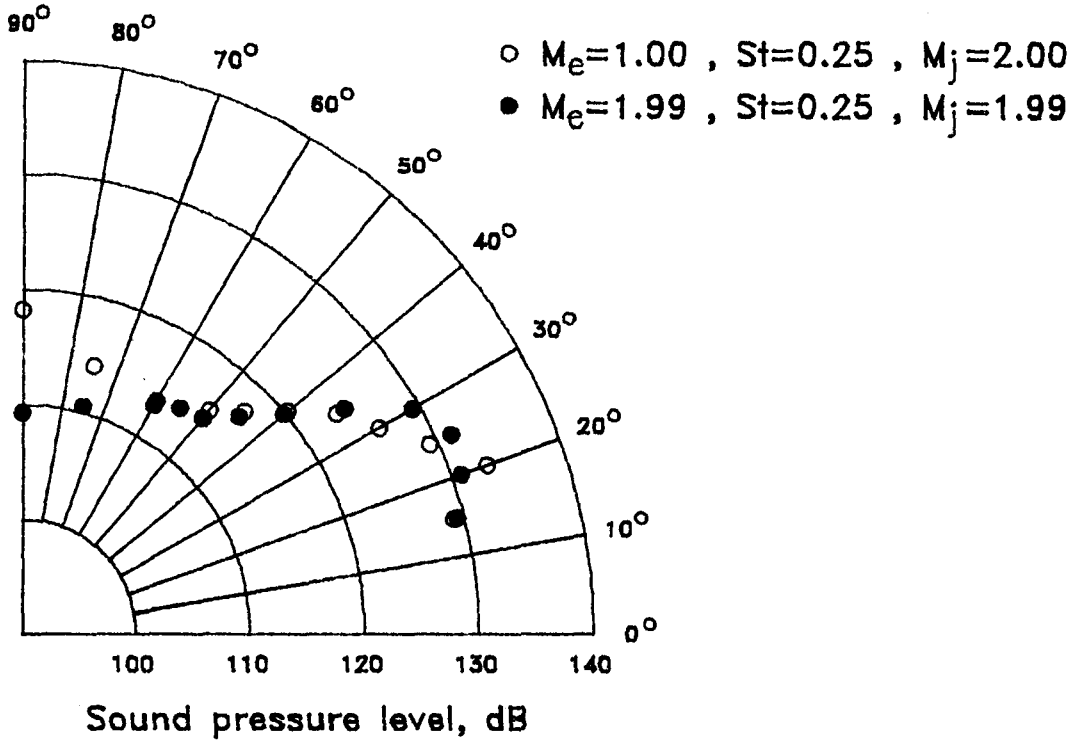

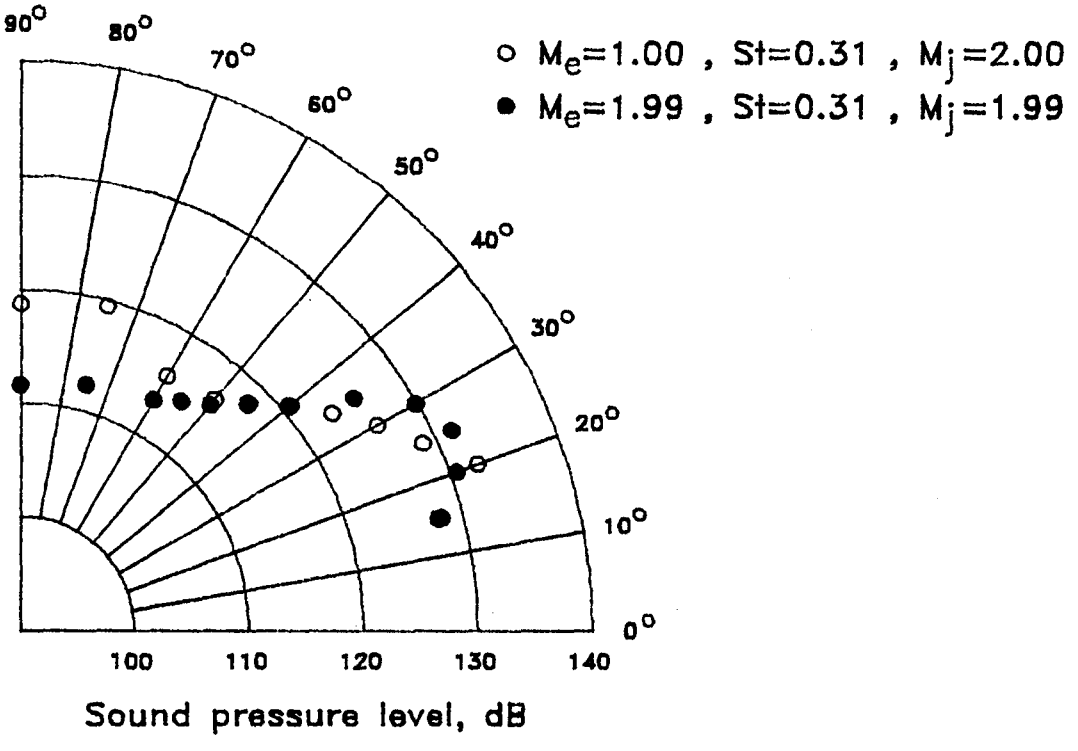

Figure 19.- Acoustic near-field directivity comparisons of underexpanded convergent nozzle plume with shocks with M_d = 2.0 shock-free plume.

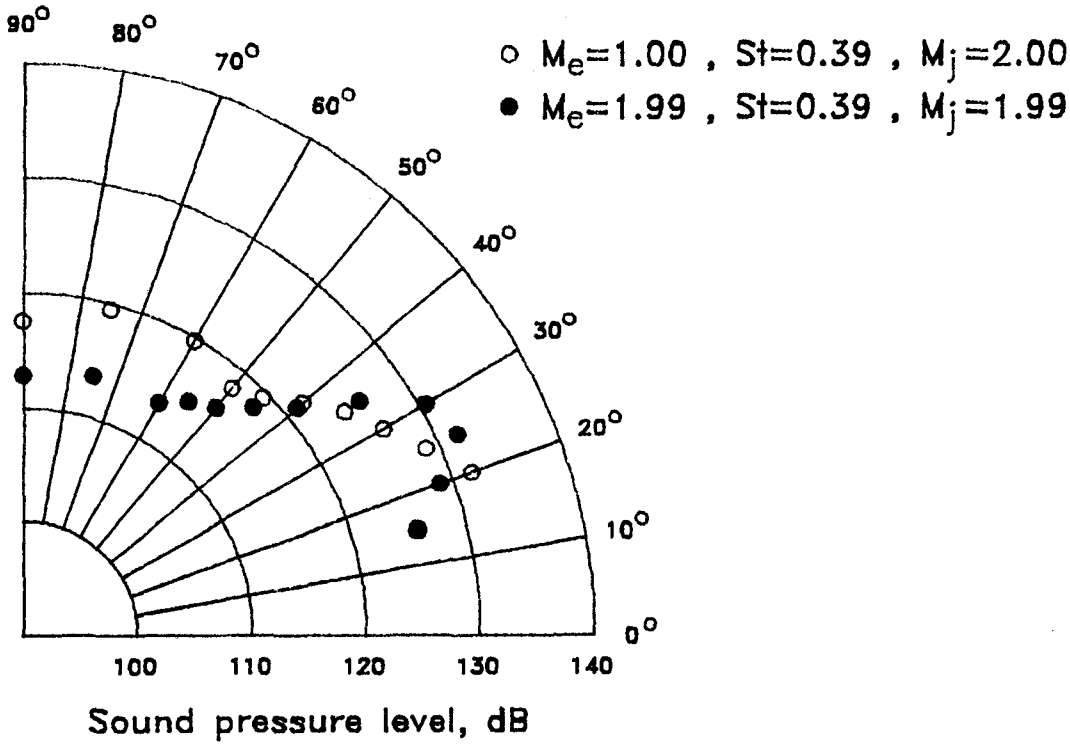

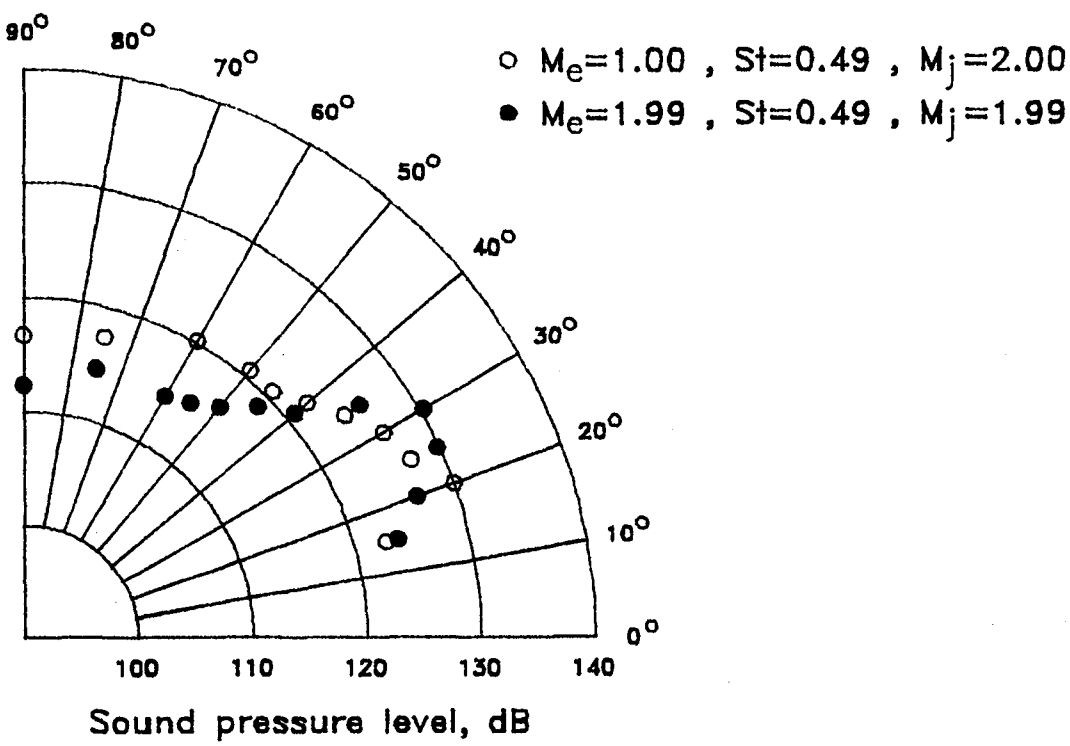

Figure 19.- Continued.

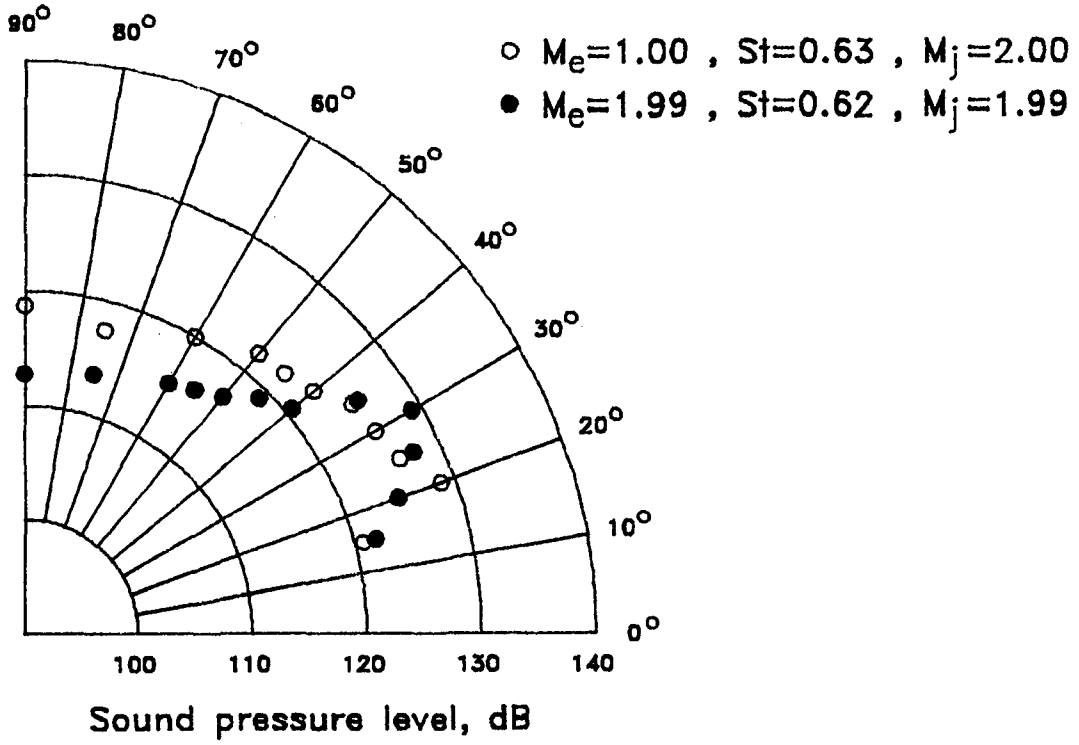

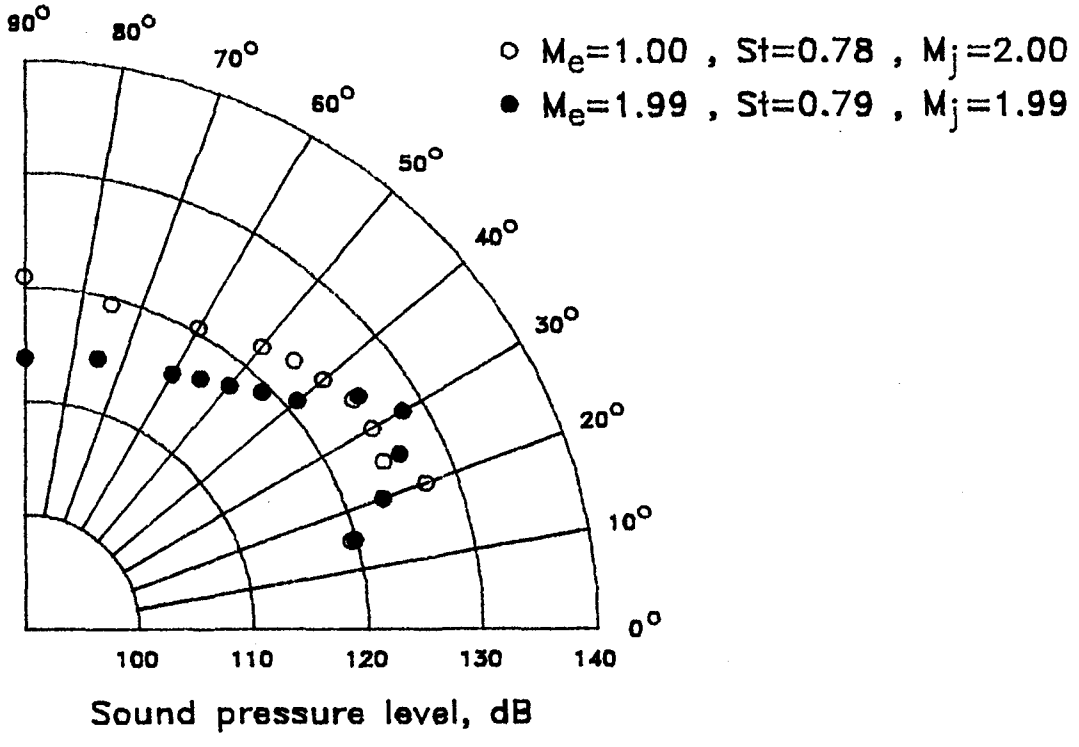

Figure 19.- Continued.

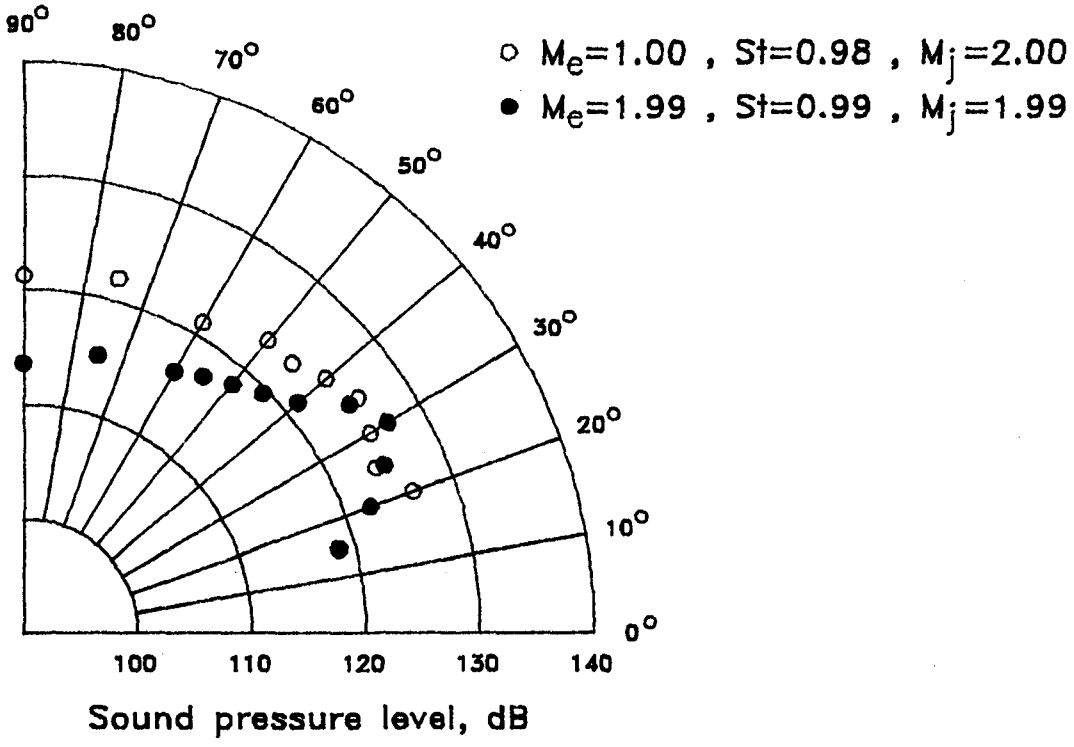

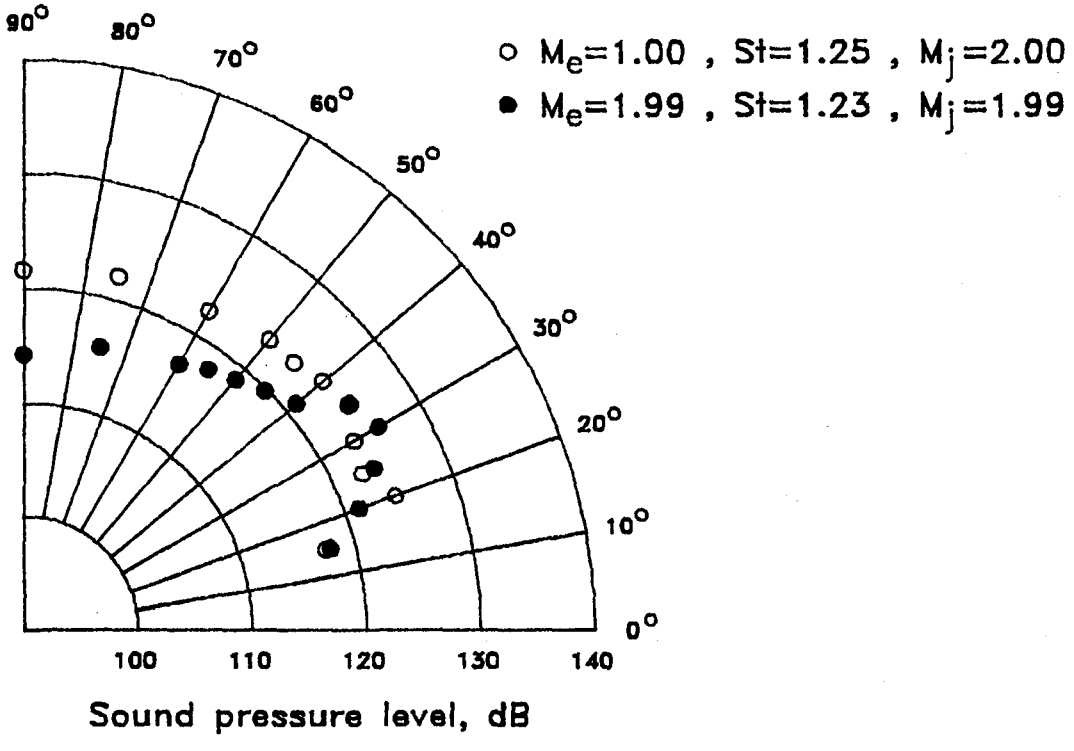

Figure 19.- Concluded.

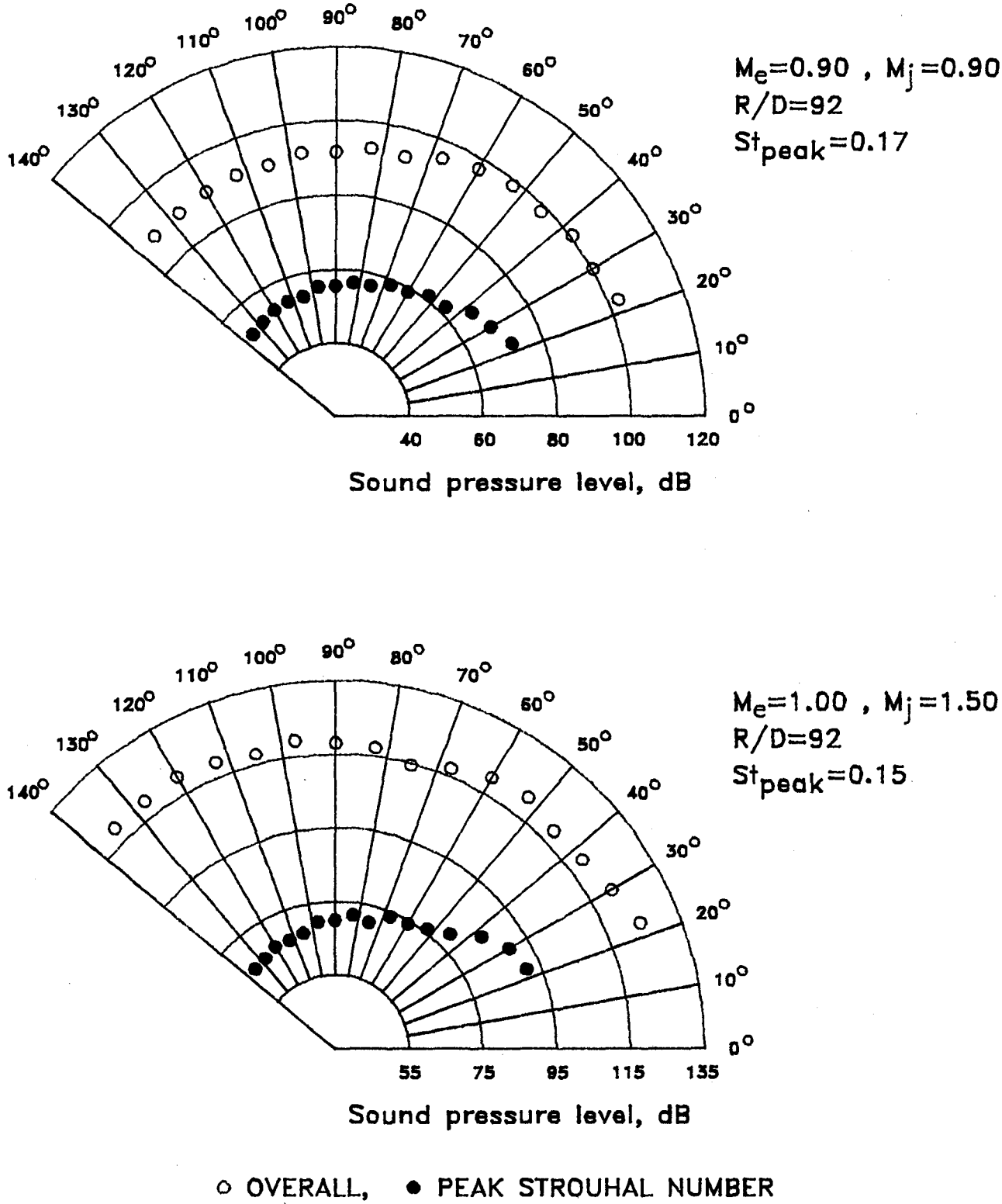

Figure 20.- Far-field directivities.

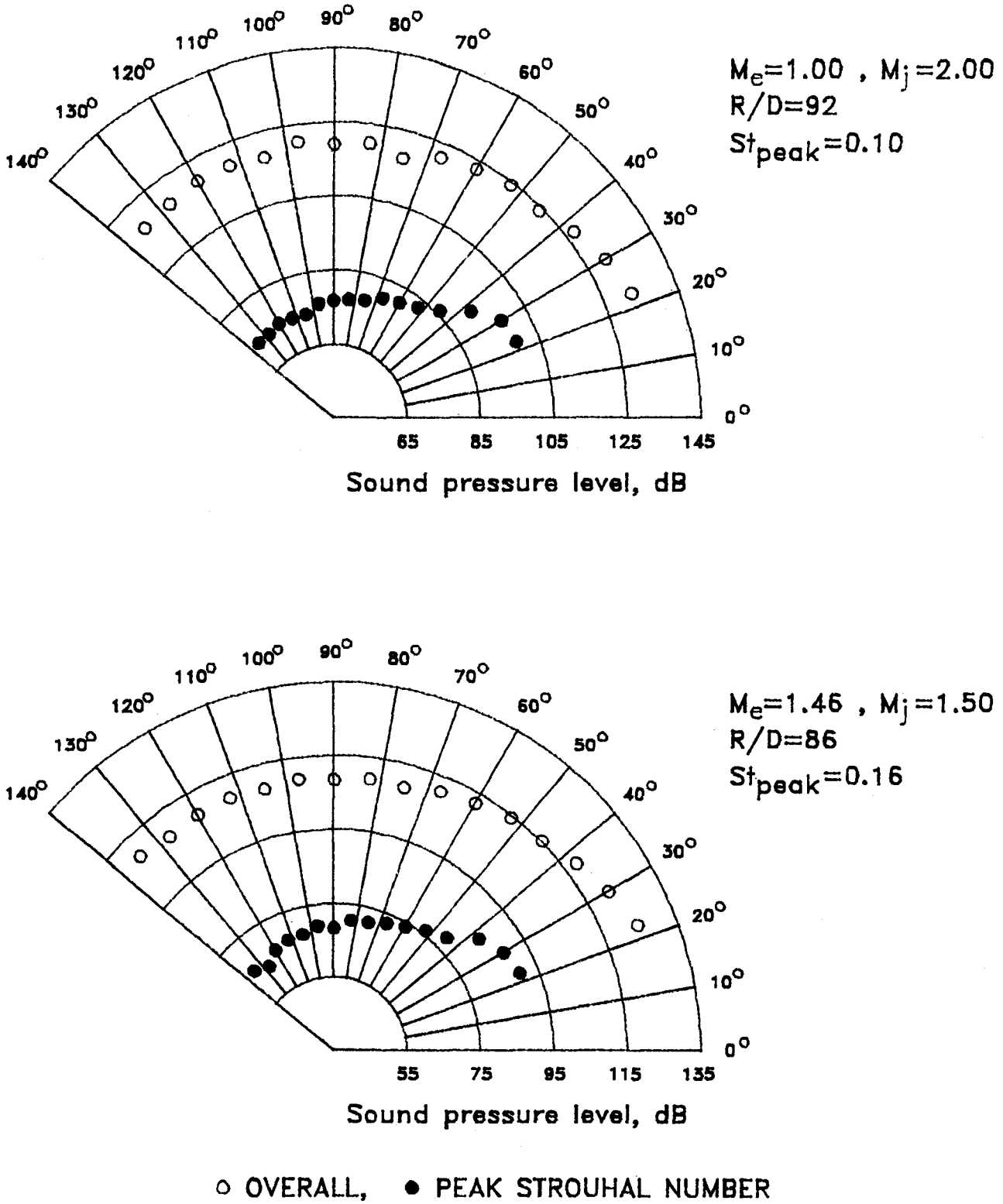

Figure 20.- Continued.

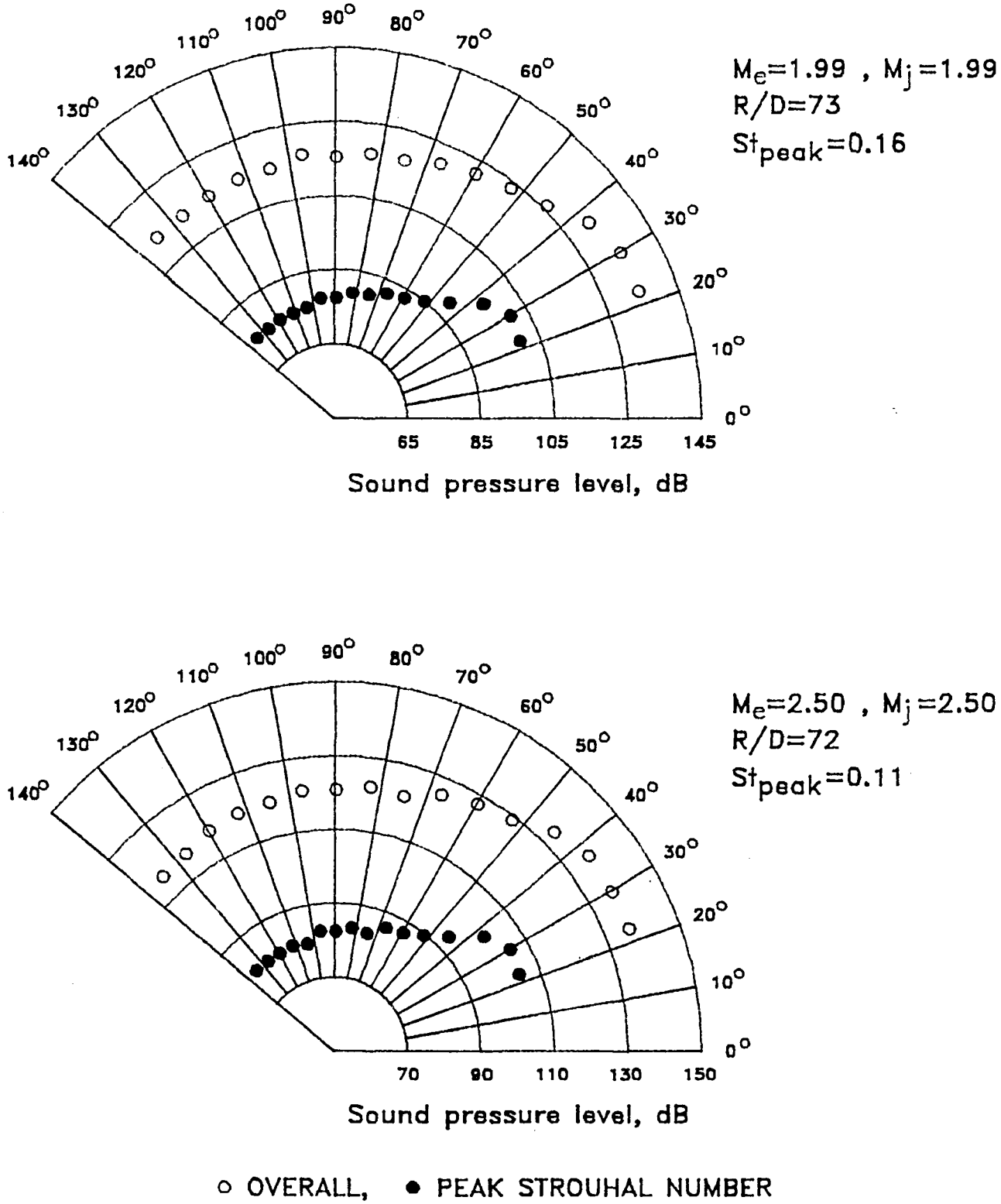

Figure 20.- Concluded.

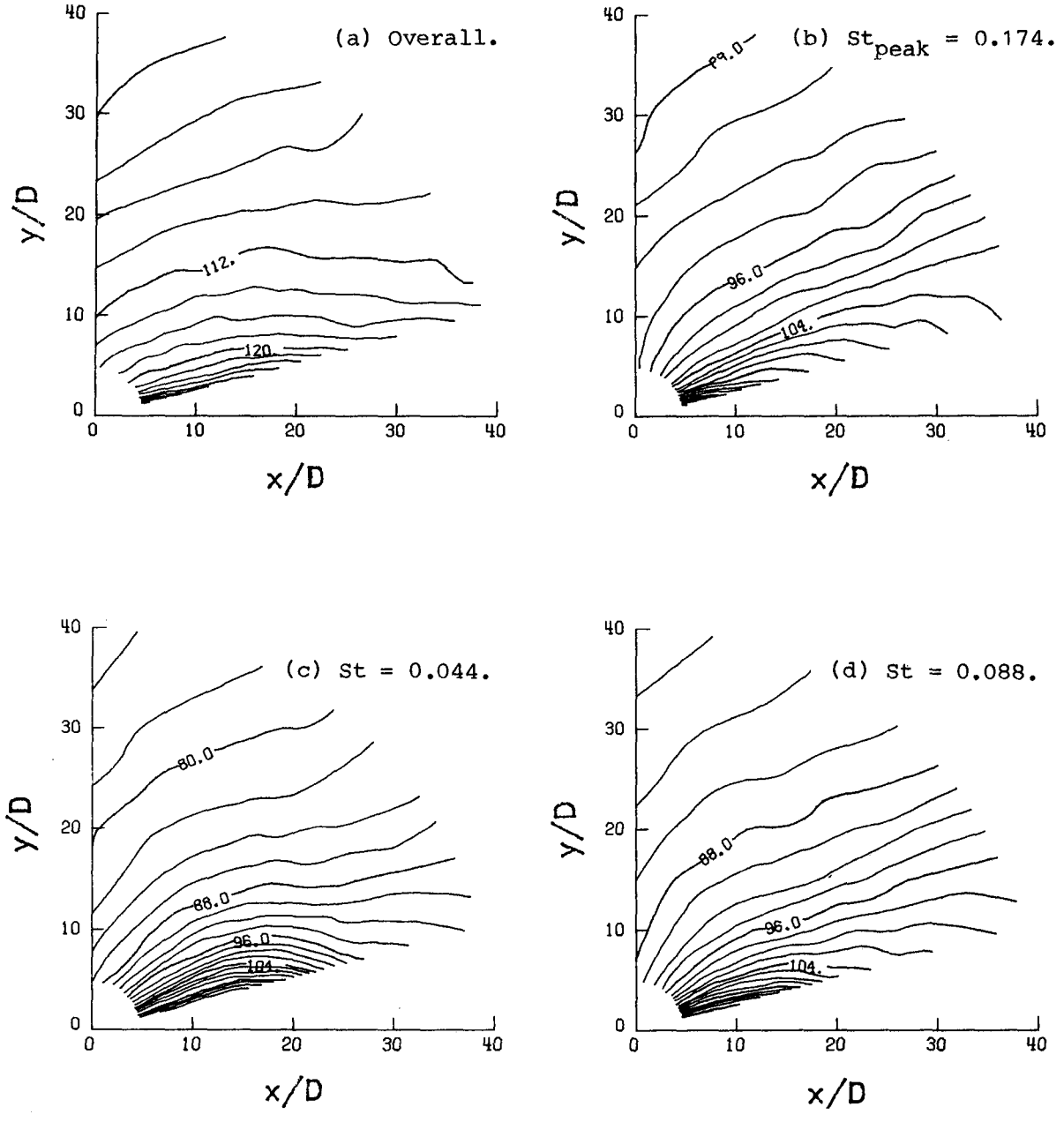

Figure 21.- Acoustic near-field contours of convergent nozzle at M_j = 0.9.

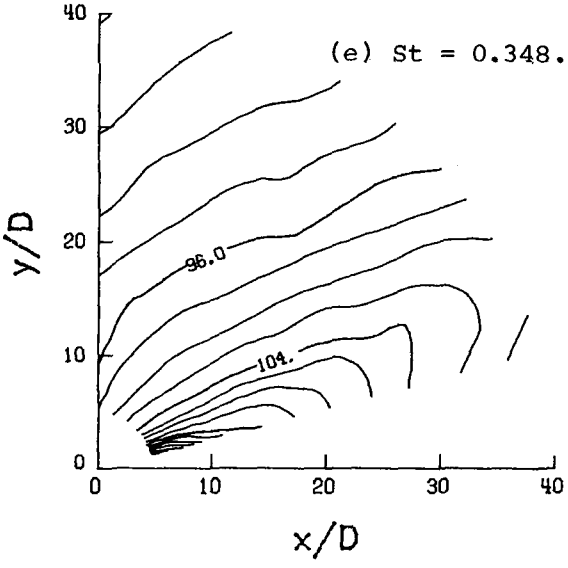

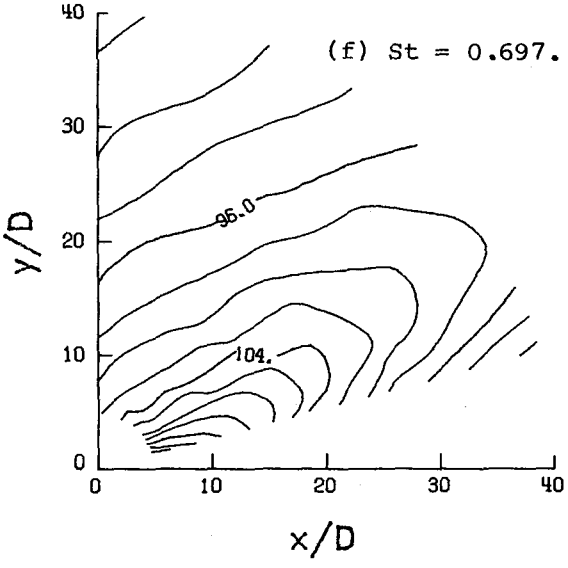

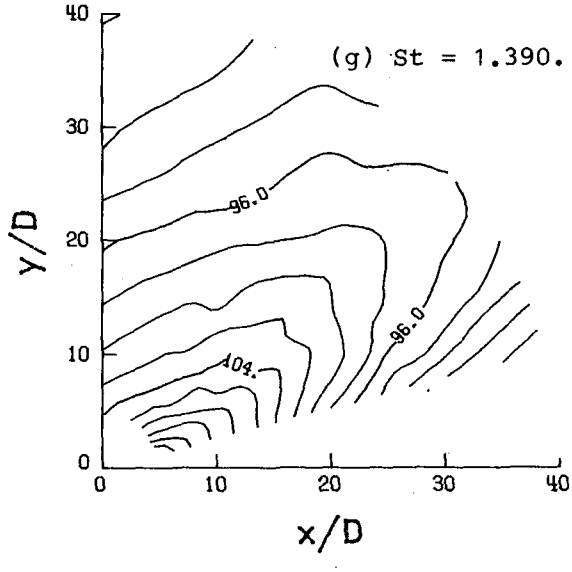

Figure 21.- Concluded.

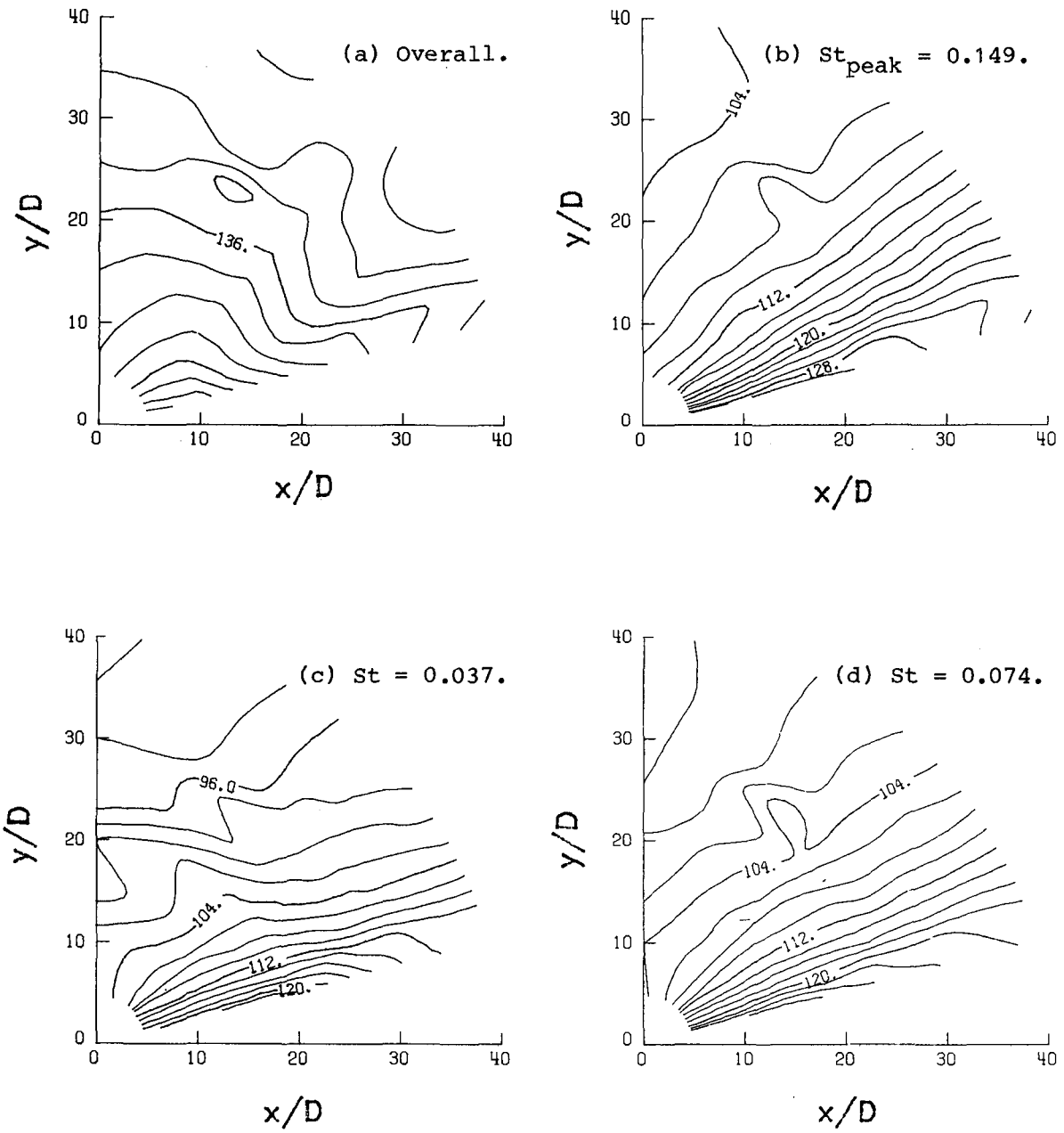

Figure 22.- Acoustic near-field contours of convergent nozzle at M_j = 1.5.

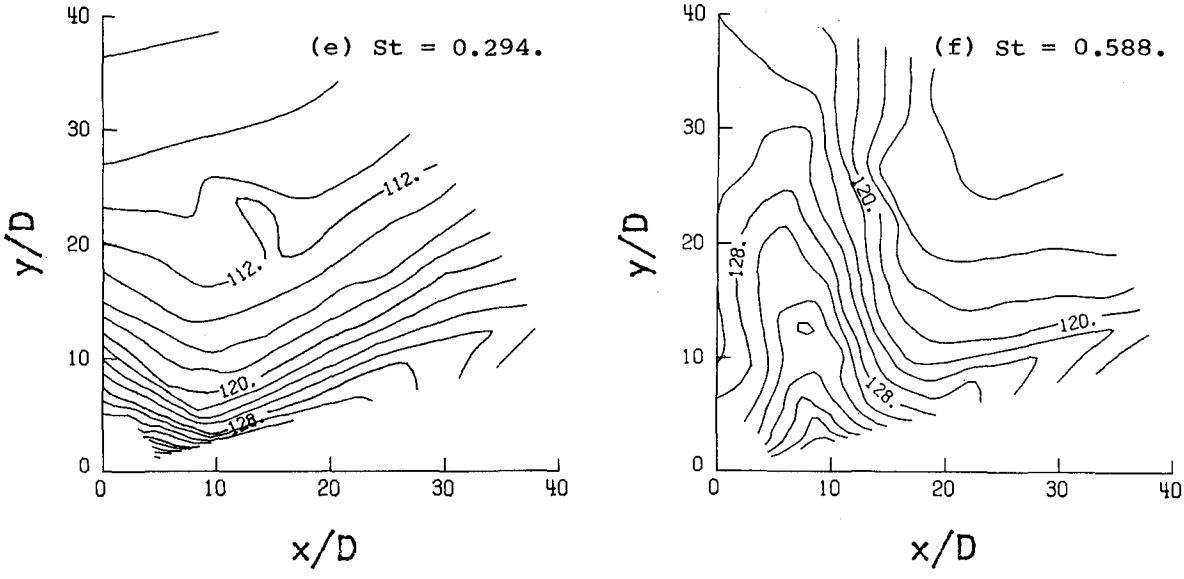

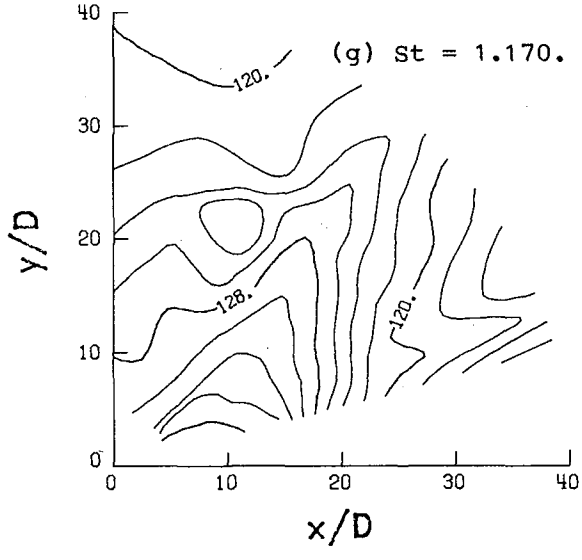

Figure 22.- Concluded.

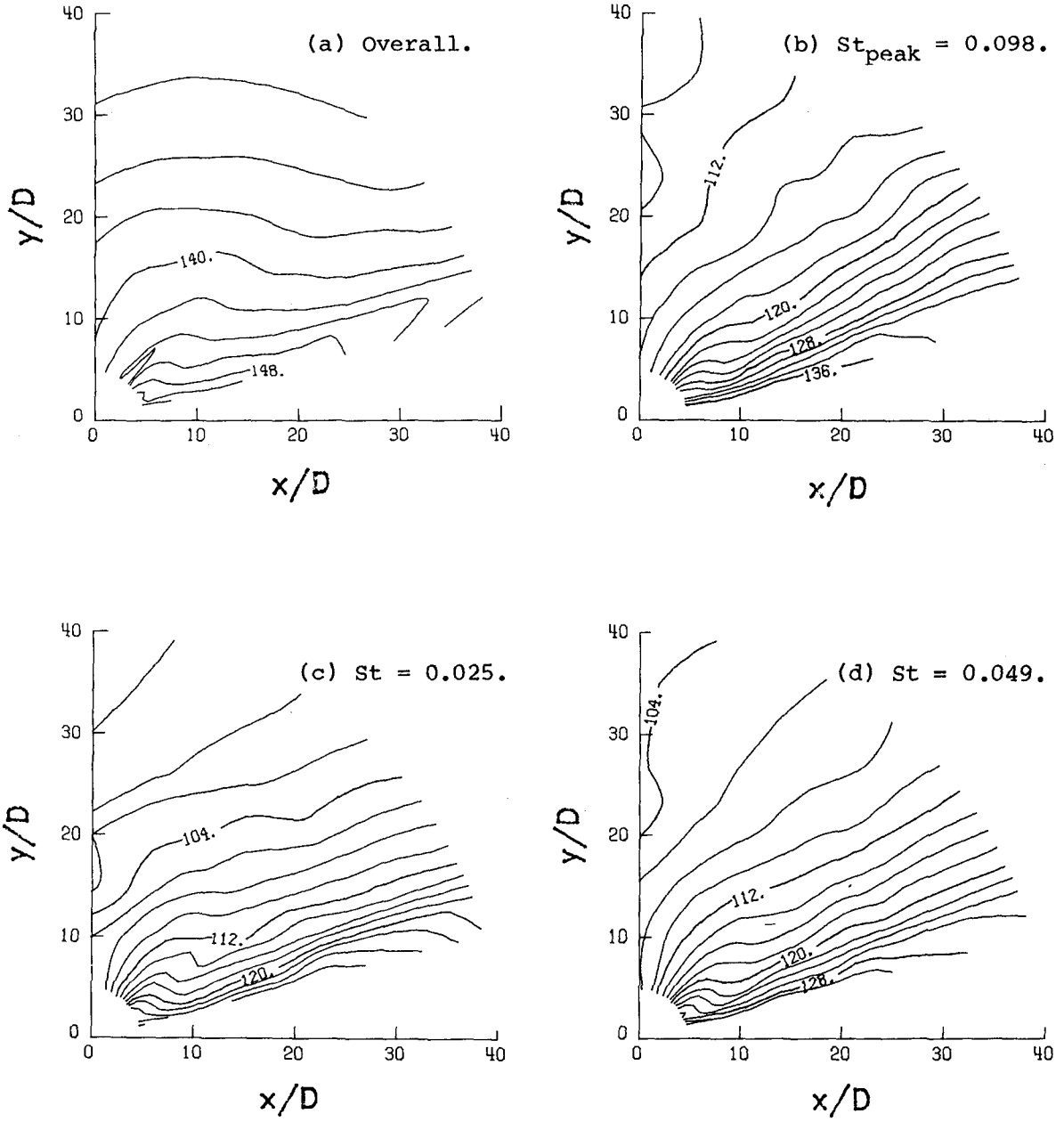

Figure 23.- Acoustic near-field contours of convergent nozzle at M_j = 2.0.

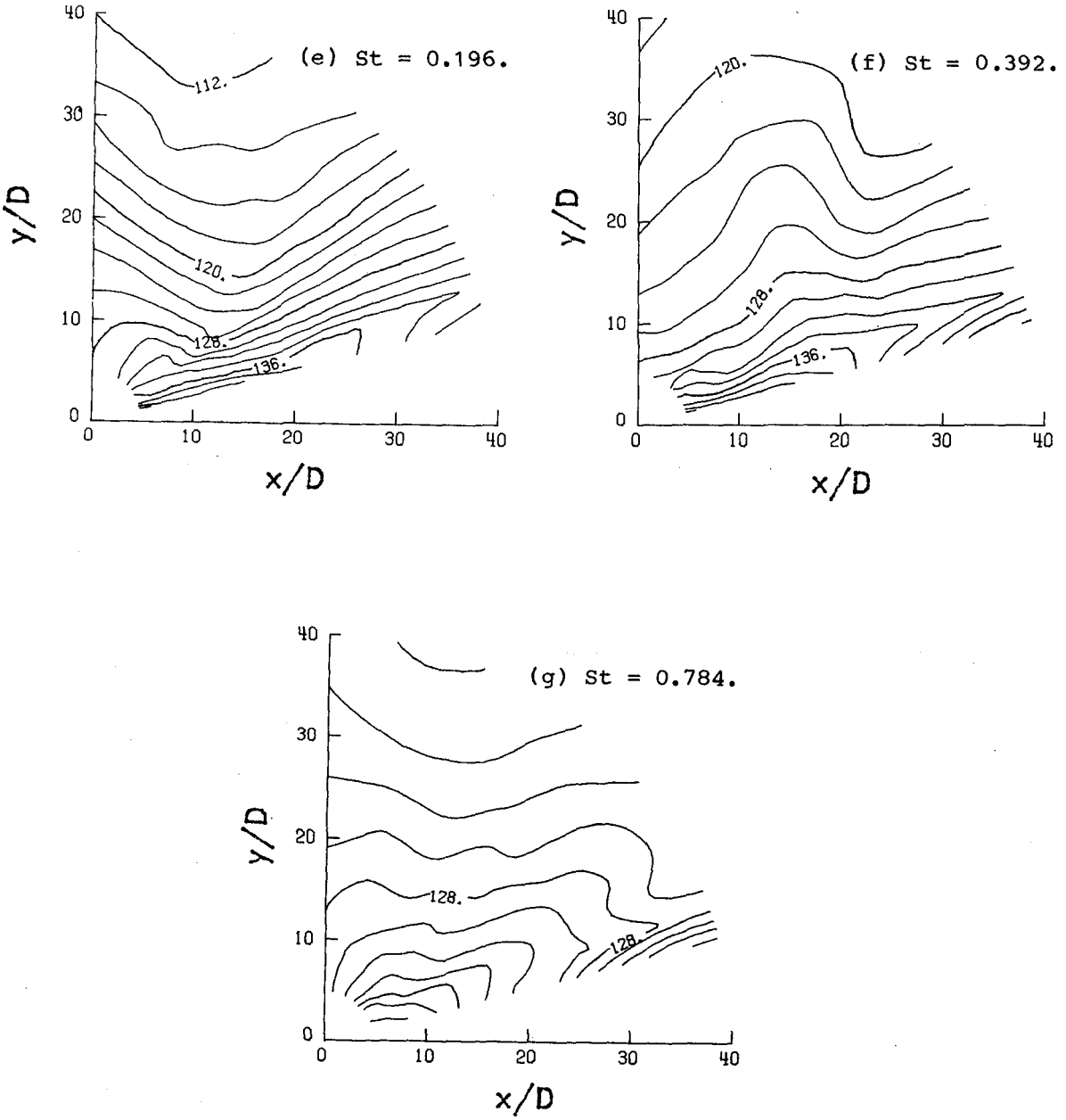

Figure 23.- Concluded.

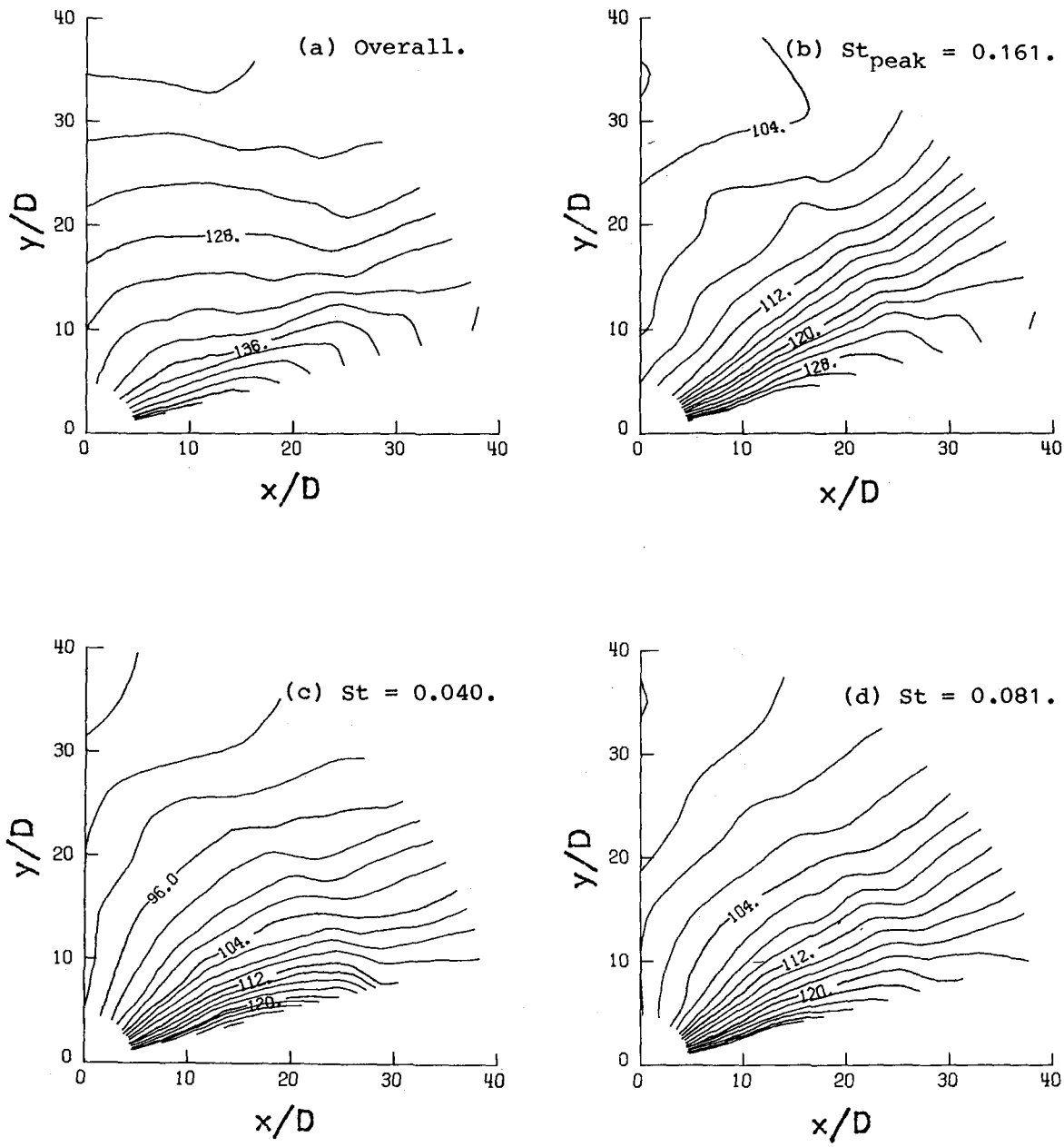

Figure 24.- Acoustic near-field contours of M_d = 1.5 nozzle near its design point.

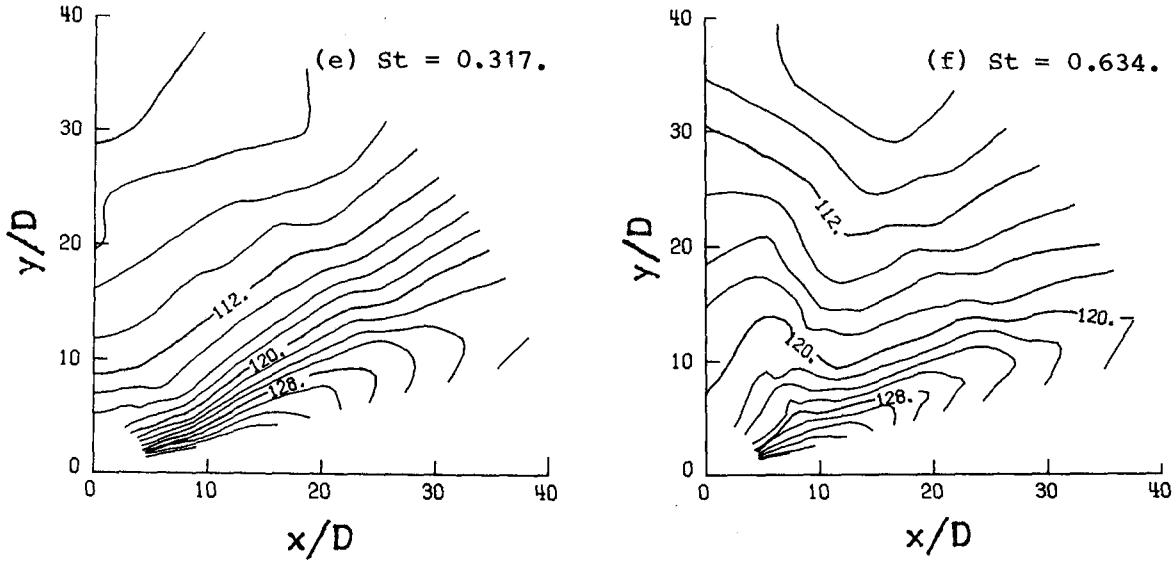

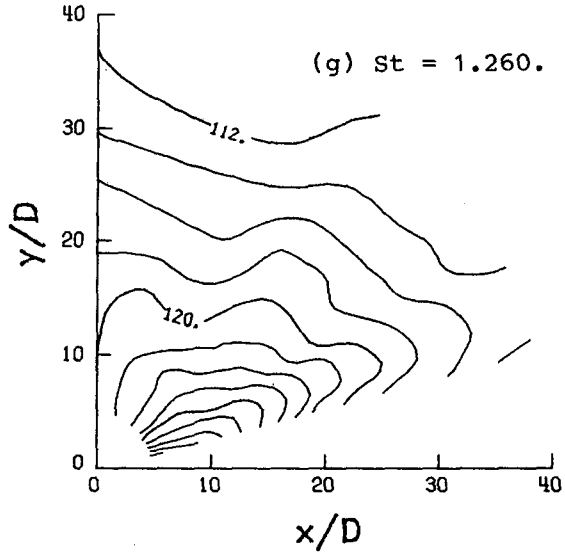

Figure 24.- Concluded.

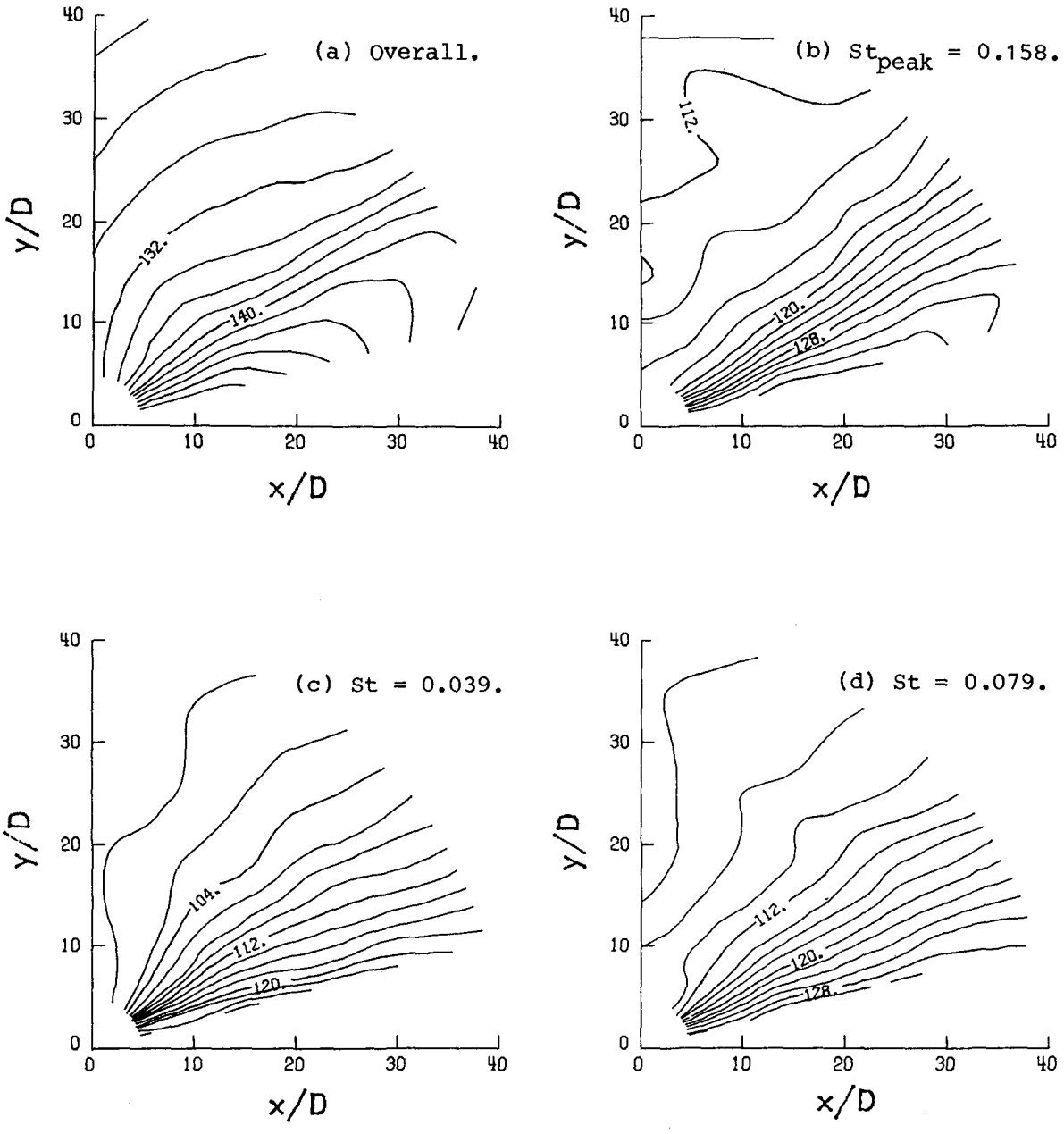

Figure 25.- Acoustic near-field contours of M_d = 2.0 nozzle at its design point.

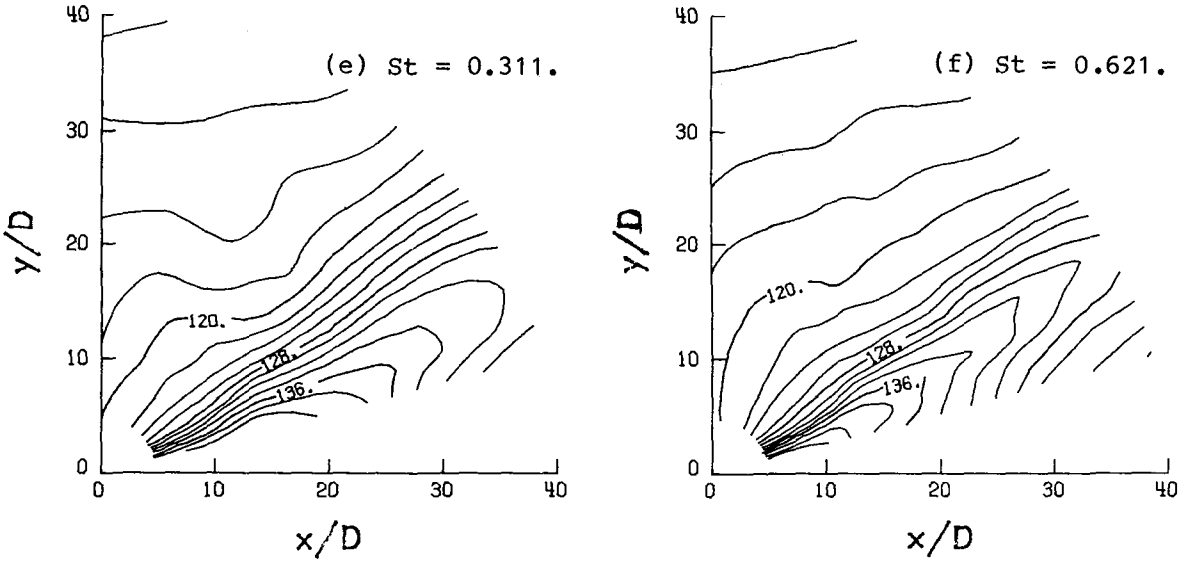

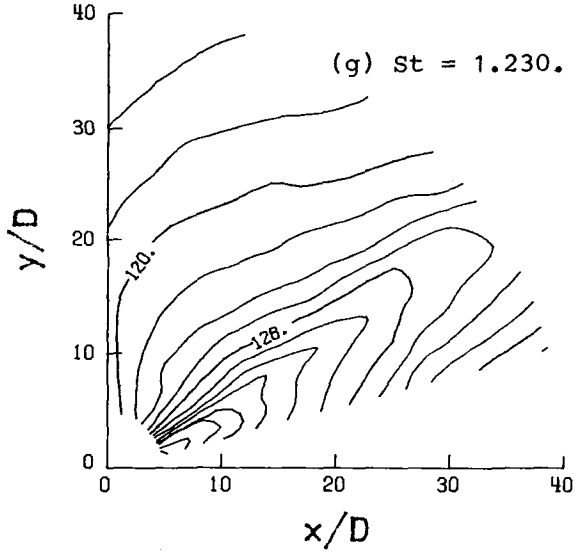

Figure 25.- Concluded.

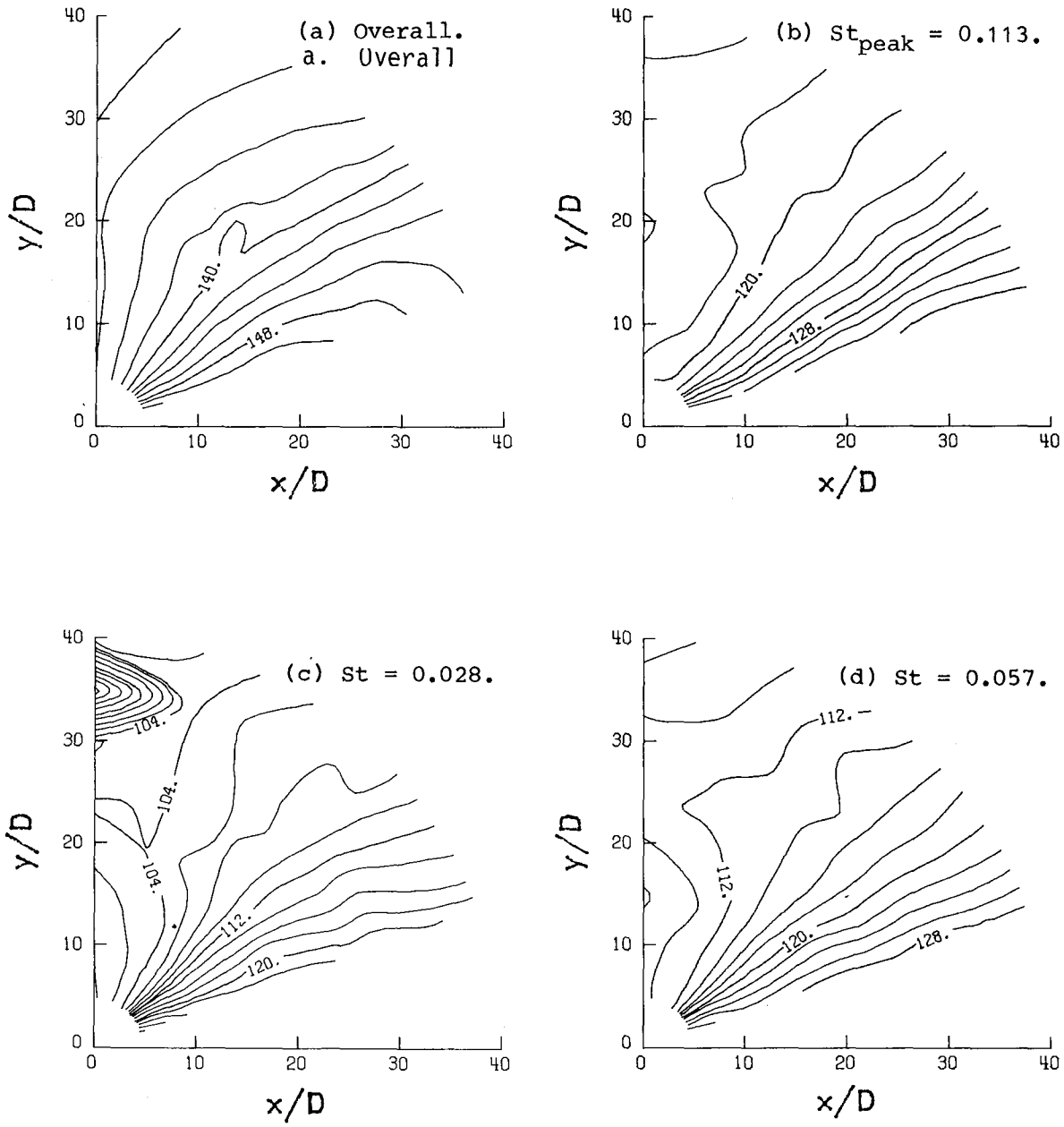

Figure 26.- Acoustic near-field contours of M_d = 2.5 nozzle at its design point.

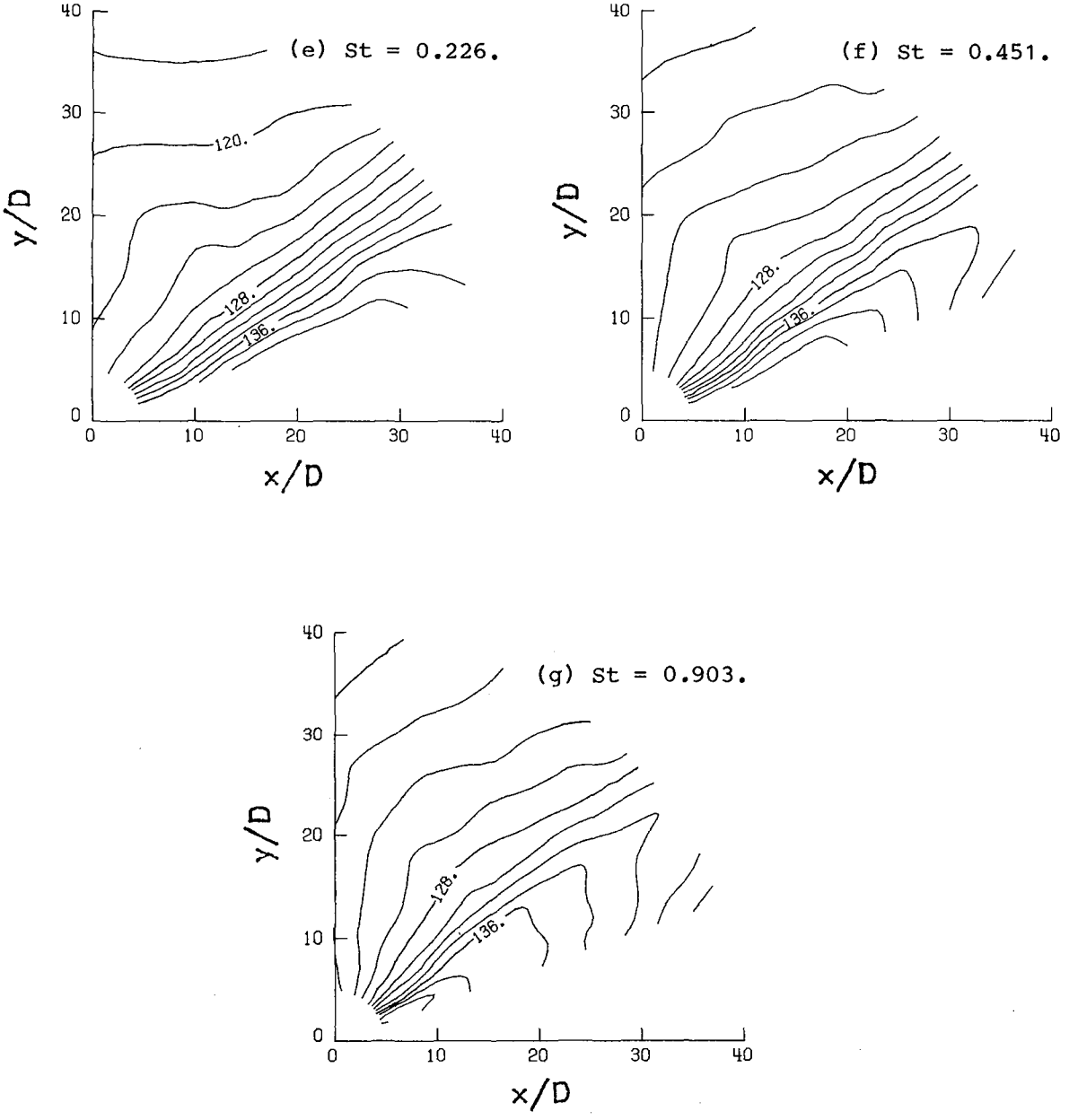

Figure 26.- Concluded.

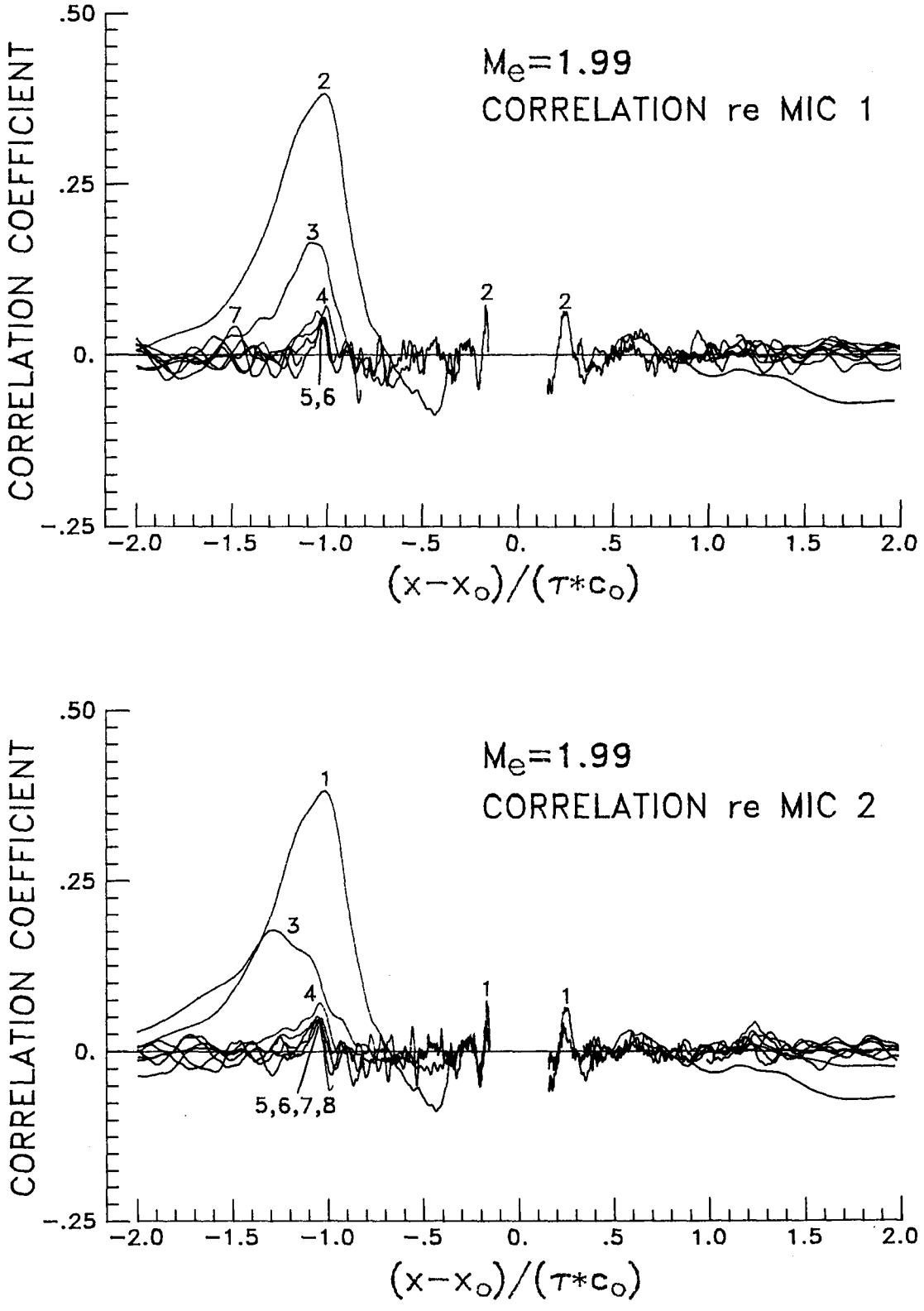

Figure 27.- Near-field microphone covariance from linear array for M_d = 2 shock-free plume.

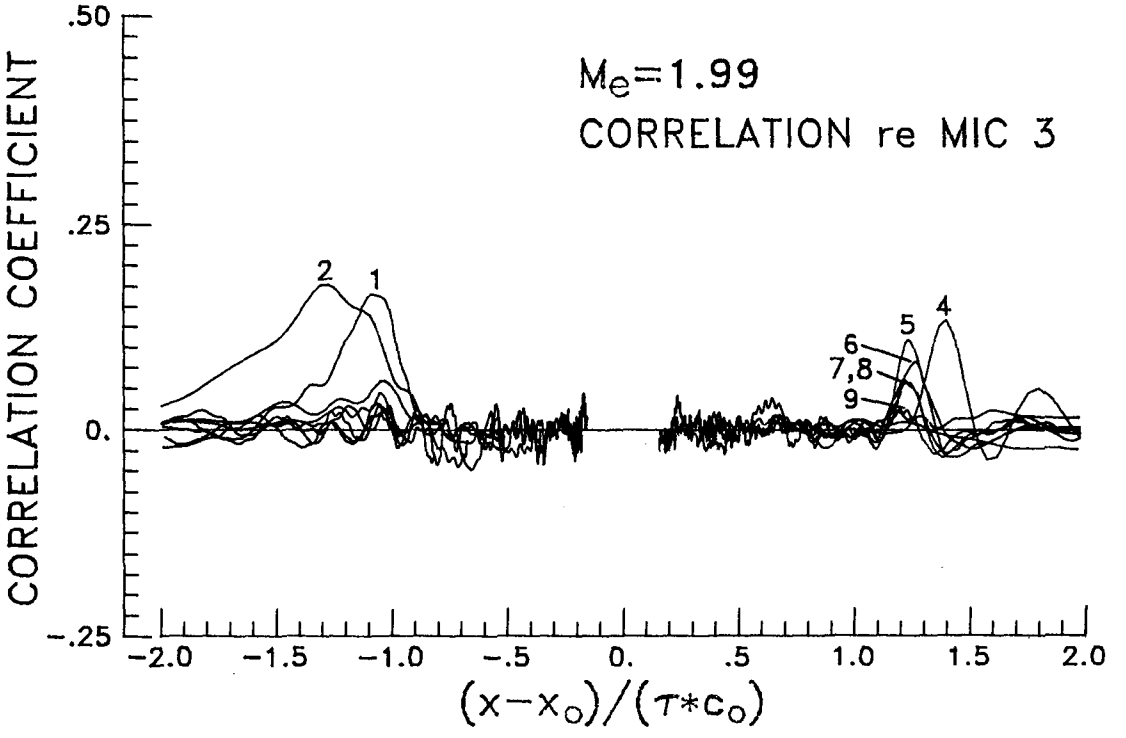

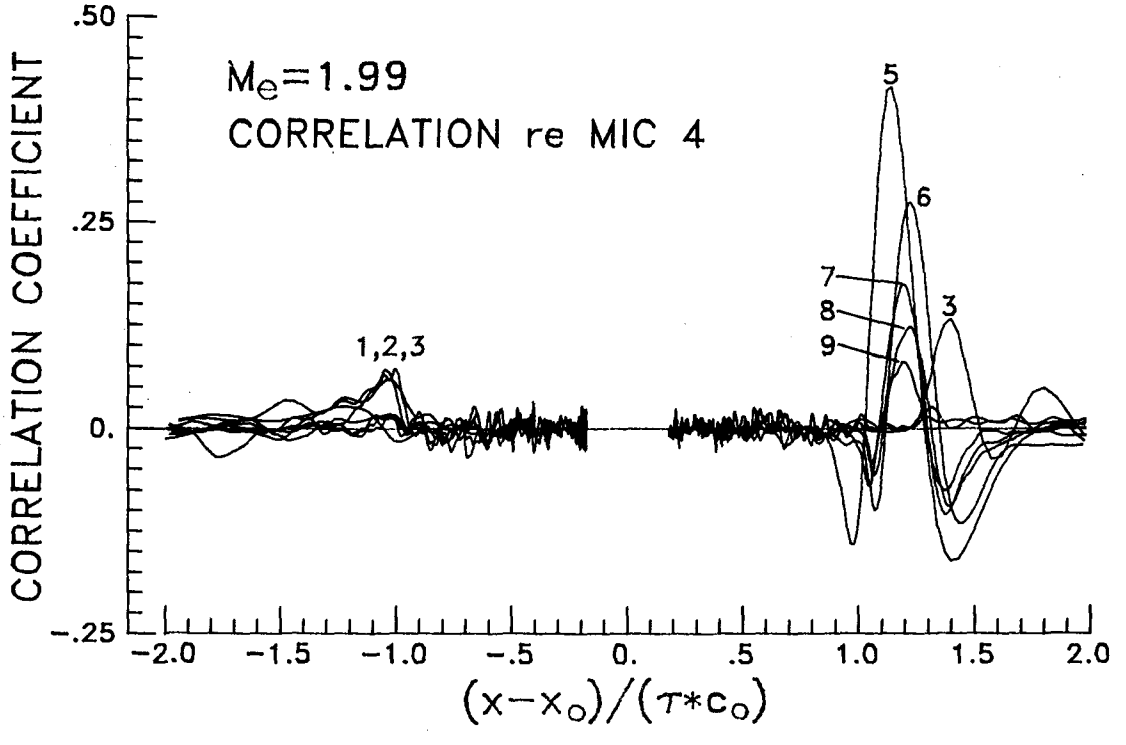

Figure 27.- Continued.

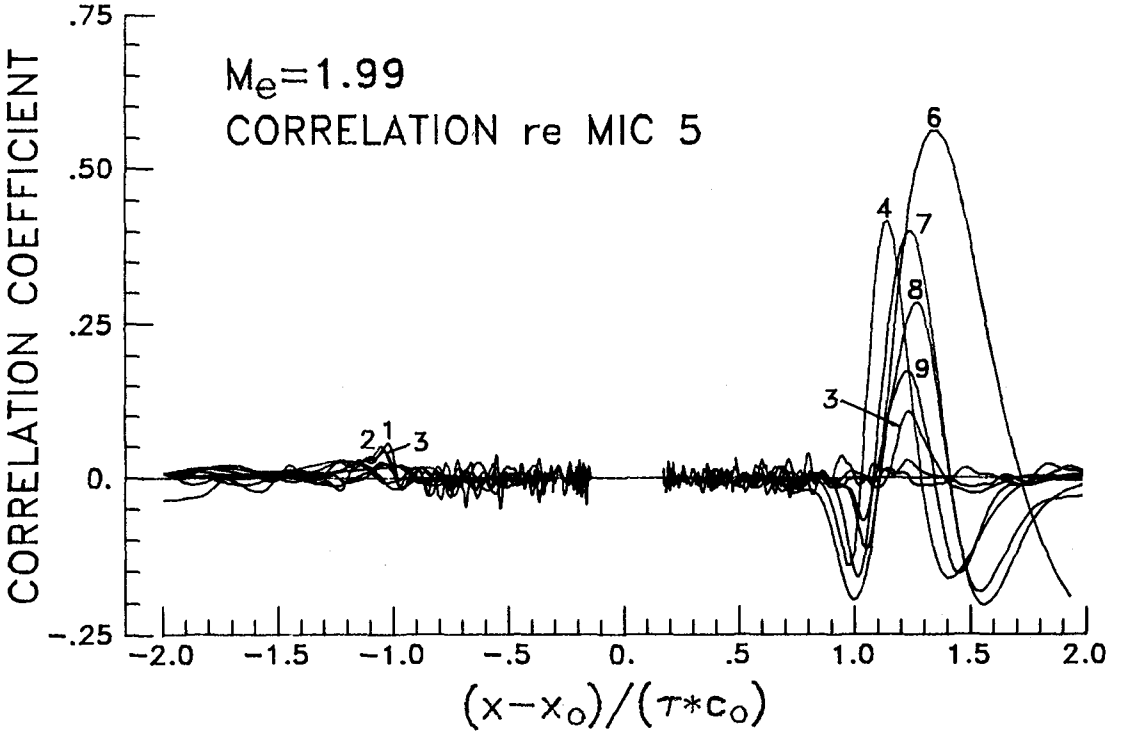

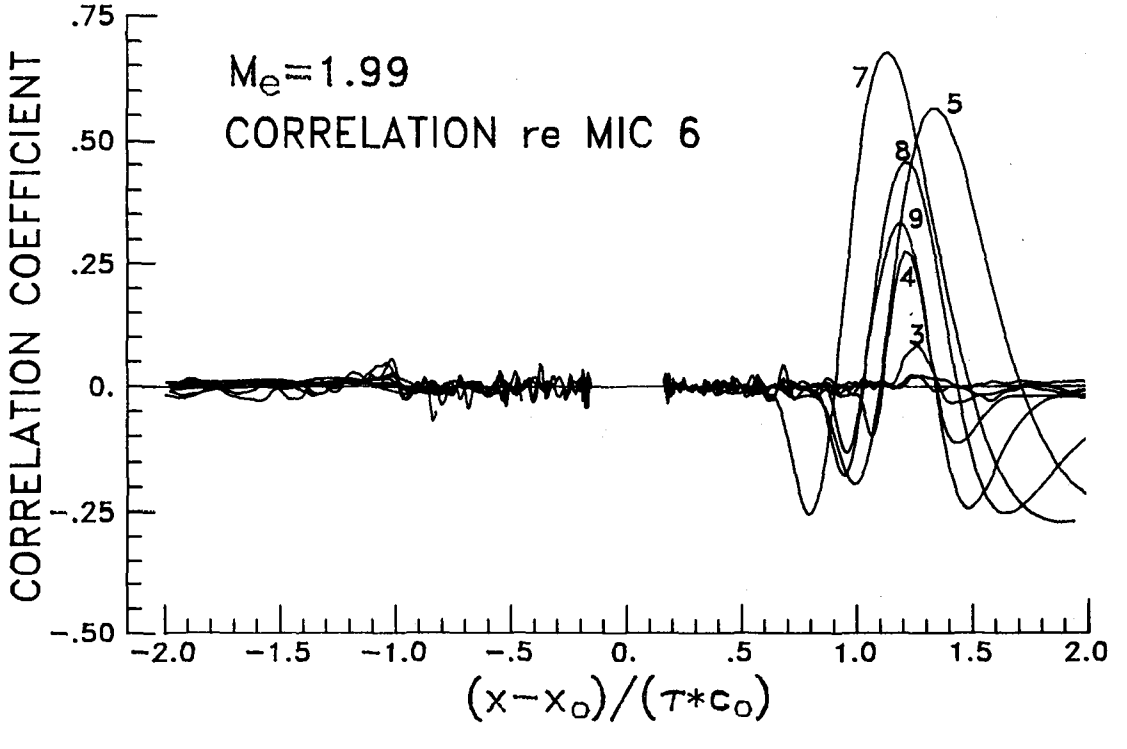

Figure 27.- Continued.

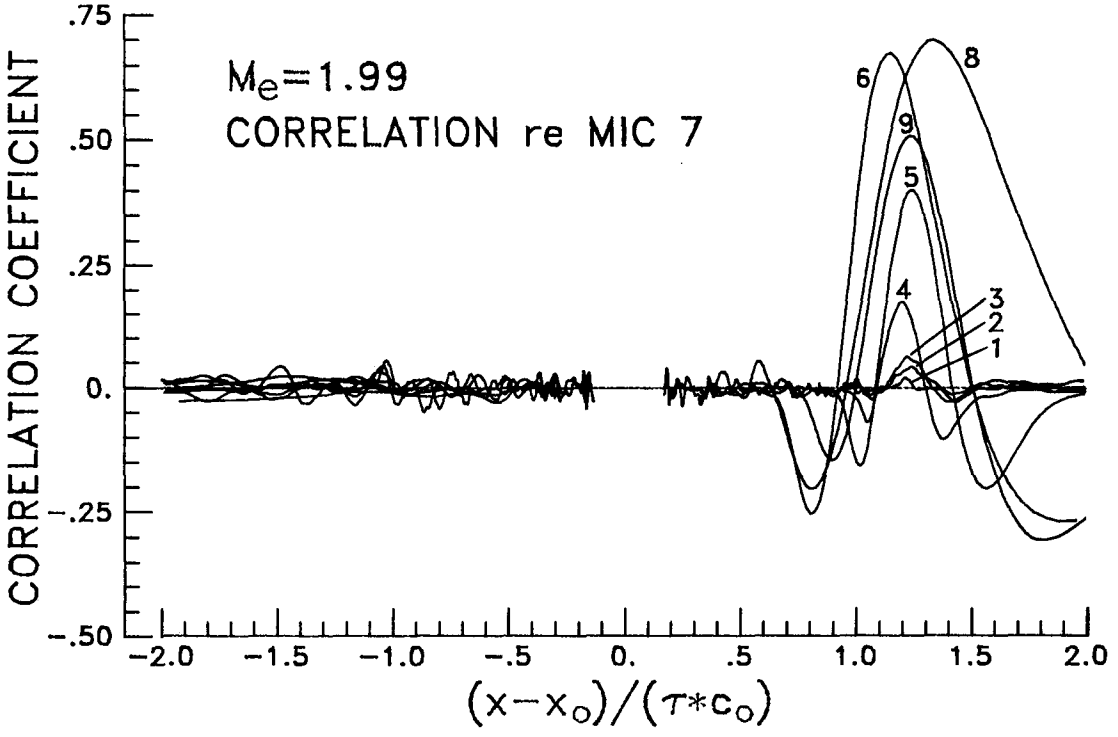

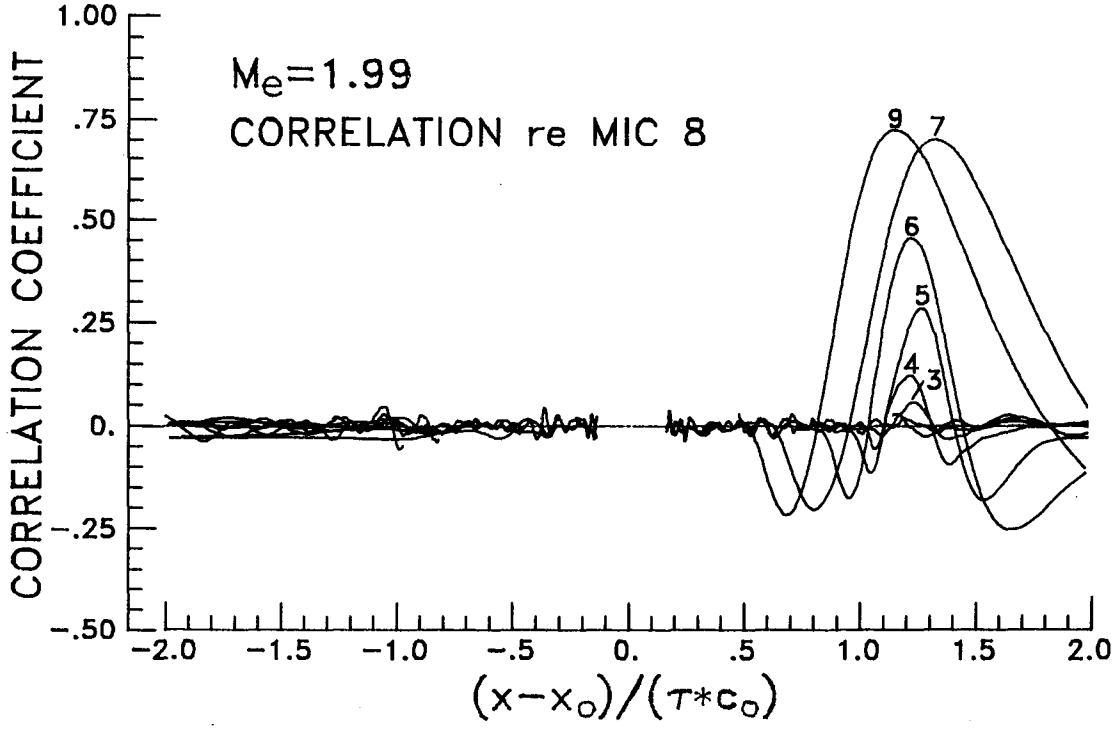

Figure 27.- Continued.

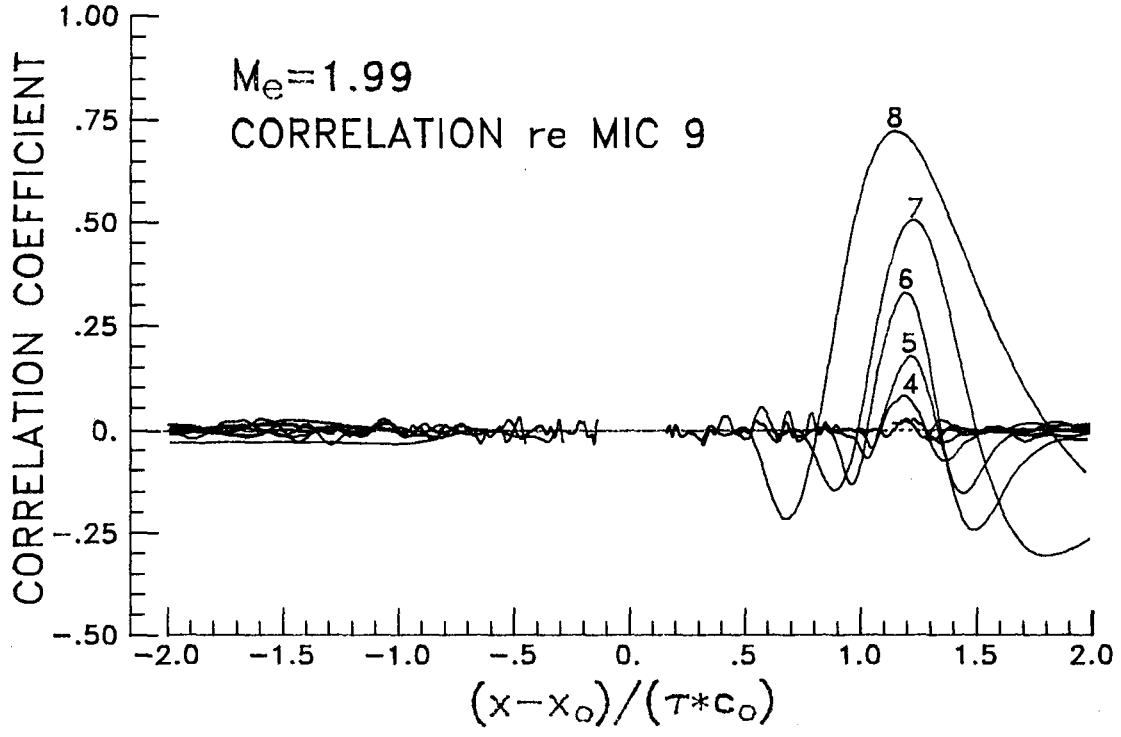

Figure 27.- Concluded.

1. Report No.	2. Government Accession No.	3. Recipient's Catalog No.
NASA TM-86296		

4. Title and Subtitle	5. Report Date
AEROACOUSTIC DATA FOR HIGH REYNOLDS NUMBER SUPERSONIC AXISYMMETRIC JETS	January 1985
	6. Performing Organization Code: 505-31-33-12
7. Author(s): John M. Seiner and Michael K. Ponton	8. Performing Organization Report No.: L-15846
	10. Work Unit No.
9. Performing Organization Name and Address: NASA Langley Research Center, Hampton, VA 23665	11. Contract or Grant No.
	13. Type of Report and Period Covered: Technical Memorandum
12. Sponsoring Agency Name and Address: National Aeronautics and Space Administration, Washington, DC 20546	14. Sponsoring Agency Code

15. Supplementary Notes

John M. Seiner: Langley Research Center, Hampton, Virginia.
Michael K. Ponton: Kentron International, Inc., Hampton, Virginia.

16. Abstract

Both aerodynamic and near-field acoustic behavior of several unheated axisymmetric shock-free and shock-containing high-speed jet plumes are reported. The exit Mach number range for these data is from 0.9 to 2.5. The aerodynamic measurements include both mean and turbulence quantities for a shock-free jet plume produced by a convergent-divergent nozzle designed to have an exit Mach number of 2. The near-field acoustic measurements presented include narrow-band spectra, directivity and contour plots of select one-third-octave-band data, and near-field microphone correlations from a linear array. Shock noise results are also included as obtained by operating an underexpanded convergent nozzle at the design point of two supersonic exit Mach number convergent-divergent nozzles.

17. Key Words (Suggested by Author(s))	18. Distribution Statement
Acoustics Supersonic Turbulance	Unclassified - Unlimited Subject Category 71

19. Security Classif. (of this report)	20. Security Classif. (of this page)	21. No. of Pages	22. Price
Unclassified	Unclassified	68	A04

For sale by the National Technical Information Service, Springfield, Virginia 22161 NASA-Langley, 1985

National Aeronautics and
Space Administration

Washington, D.C.
20546

Official Business
Penalty for Private Use, $300

THIRD-CLASS BULK RATE

Postage and Fees Paid
National Aeronautics and
Space Administration
NASA-451

POSTMASTER: If Undeliverable (Section 158 Postal Manual) Do Not Return